DTIC FILE COPY

AD-A218 477

FROM: AFIT/CI

11 July 1989

SUBJECT: Review of Thesis/Disseration for Public Release

TO: PA

1. Request you review the attached for public release prior to being sent to DTIC.

2. Reply by indorsement to CI NLT _____.

Ernest A. Haygood

ERNEST A. HAYGOOD, 1st Lt, USAF
Executive Officer
Civilian Institution Programs

1 Atch.
THESIS 89-072
PANTLEY

1st Ind, AFIT/PA

TO: CI

08 FEB 1990

Approved/~~Disapproved~~ for public release.
Log Number: 89-10-113

Harriet D Moultrie

HARRIET D. MOULTRIE, Capt, USAF
Director, Office of Public Affairs

DTIC
ELECTE
FEB 22 1990
S E D

SECURITY CLASSIFICATION OF THIS PAGE

REPORT DOCUMENTATION PAGE

Form Approved OMB No. 0704-0188

1a. REPORT SECURITY CLASSIFICATION UNCLASSIFIED	1b. RESTRICTIVE MARKINGS NONE
2a. SECURITY CLASSIFICATION AUTHORITY	3. DISTRIBUTION/AVAILABILITY OF REPORT APPROVED FOR PUBLIC RELEASE; DISTRIBUTION UNLIMITED.
2b. DECLASSIFICATION/DOWNGRADING SCHEDULE	
4. PERFORMING ORGANIZATION REPORT NUMBER(S)	5. MONITORING ORGANIZATION REPORT NUMBER(S) AFIT/CI/CIA-89-072
6a. NAME OF PERFORMING ORGANIZATION AFIT STUDENT AT SAN JOSE STATE UNIVERSITY 6b. OFFICE SYMBOL (If applicable)	7a. NAME OF MONITORING ORGANIZATION AFIT/CIA
6c. ADDRESS (City, State, and ZIP Code)	7b. ADDRESS (City, State, and ZIP Code) Wright-Patterson AFB OH 45433-6583
8a. NAME OF FUNDING/SPONSORING ORGANIZATION 8b. OFFICE SYMBOL (If applicable)	9. PROCUREMENT INSTRUMENT IDENTIFICATION NUMBER
8c. ADDRESS (City, State, and ZIP Code)	10. SOURCE OF FUNDING NUMBERS PROGRAM ELEMENT NO. / PROJECT NO. / TASK NO. / WORK UNIT ACCESSION NO.

11. TITLE (Include Security Classification) (UNCLASSIFIED)
A Study of Turbulence Near Thunderstorm Tops

12. PERSONAL AUTHOR(S)
Kim Christine Pantley

13a. TYPE OF REPORT	13b. TIME COVERED	14. DATE OF REPORT (Year, Month, Day)	15. PAGE COUNT
THESIS/~~DISSERTATION~~	FROM _____ TO _____	1989 May	132

16. SUPPLEMENTARY NOTATION
APPROVED FOR PUBLIC RELEASE IAW AFR 190-1
ERNEST A. HAYGOOD, 1st Lt, USAF
Executive Officer, Civilian Institution Programs

17. COSATI CODES			18. SUBJECT TERMS (Continue on reverse if necessary and identify by block number)
FIELD	GROUP	SUB-GROUP	

19. ABSTRACT (Continue on reverse if necessary and identify by block number)

20. DISTRIBUTION/AVAILABILITY OF ABSTRACT ☒ UNCLASSIFIED/UNLIMITED ☐ SAME AS RPT. ☐ DTIC USERS	21. ABSTRACT SECURITY CLASSIFICATION UNCLASSIFIED
22a. NAME OF RESPONSIBLE INDIVIDUAL ERNEST A. HAYGOOD, 1st Lt, USAF	22b. TELEPHONE (Include Area Code) (513) 255-2259 22c. OFFICE SYMBOL AFIT/CI

DD Form 1473, JUN 86 Previous editions are obsolete. SECURITY CLASSIFICATION OF THIS PAGE

AFIT/CI "OVERPRINT"

72

A STUDY OF TURBULENCE NEAR THUNDERSTORM TOPS

a Thesis

Presented to

the Faculty of the Department of Meteorology

San Jose State University

in Partial Fulfillment

of the Requirements for the Degree

Master of Science

DTIC COPY INSPECTED 8

Accession For	
NTIS GRA&I	☒
DTIC TAB	☐
Unannounced	☐
Justification	
By	
Distribution/	
Availability Codes	
Dist	Avail and/or Special
A-1	

By

Kim Christine Pantley

May, 1989

90 02 20 153

Approved for the Department of Meteorology

Douglas M. Sinton

Ralph E. Lieth

Approved for the University

Serena H. Stanford

ABSTRACT

It has been known for many years that turbulence significant for aviation often occurs near thunderstorm tops. However, that turbulence is not well-predicted because of an incomplete understanding of the processes which generate it and because of inadequate observations. The current study seeks to alleviate these problems via: 1) a comprehensive review of recent theoretical and experimental studies related to turbulence near thunderstorm tops (TNTT), and 2) three case studies designed to examine the feasibility of using data derived from commercial aircraft to study TNTT.

The literature review revealed extensive evidence which showed that convection often produces significant barrier effects; several mesoscale phenomena capable of producing turbulence may occur, depending on wind and stability conditions near the thunderstorm tops. These include two- and three-dimensional lee waves, rotors, Kelvin-Helmholtz instabilities, and Karman vortices.

Conventional meteorological data were combined with data derived from the aircraft flight tapes to produce quantitative descriptions of the turbulence ~~and its~~ Theses (jhd) mesoscale environment for the three cases. One of the turbulence incidents was caused by flight through gravity waves in the lee of a squall line. The second was also located downwind of a squall line, but appeared to occur in a strongly three-dimensional wake. The third case was caused by flight through a thunderstorm updraft. The latter unambiguous determination could not have been possible with only conventional meteorological data and ordinary pilot reports.

The results of this study indicate that efforts should be made to tap the rich data source of available Digital Flight Data Record (DFDR) information for more analyses and, ultimately, a better understanding of TNTT.

ACKNOWLEDGMENTS

I greatly appreciate the efforts of my advisor, Dr. Peter F. Lester, on my behalf during this project. His insight, patience, and support, as well as his occasional threats, were critical in enabling me to successfully complete this study.

Special thanks go to Ralph Bach, Jr. and Rod Wingrove at NASA-Ames Research Center for their aid and support. They provided untiring assistance, especially with explanations of the aeronautical aspects of the study and the usage of SMACK.

Finally, a note of thanks must go to all my friends and co-workers whose encouragement and support kept me working on this project. Their continual interest and concern in my progress helped keep me motivated.

This research was sponsored in part by NASA-Ames Cooperative Agreement NCC 2-315. The computations were performed using the facilities at NASA-Ames Research Center.

TABLE OF CONTENTS

	Page
ABSTRACT	iii
ACKNOWLEDGMENTS	iv
LIST OF FIGURES	vii
LIST OF TABLES	x
Chapter	
1. INTRODUCTION	1
a. Objectives	2
2. LITERATURE REVIEW	4
a. General	4
b. Turbulence Defined	4
c. Causes of Turbulence Significant to Aircraft	5
(1) Mechanical Turbulence	7
(2) Turbulence Associated with Convection	7
(3) Turbulence Associated with Gravity Waves	10
d. Observations of Waves and TNTT	16
e. Causes of TNTT	20
(1) Penetrative Convection	21
(2) Latent Heat Release	21
(3) Kelvin-Helmholtz Instability	22
(4) The Thunderstorm as a Barrier	22
f. External Mesoscale Circulations Produced by Flow Over and Around Thunderstorms	27
g. Current Capabilities to Observe and Forecast TNTT	39

TABLE OF CONTENTS (continued)

Chapter		Page
3.	CASE STUDIES OF TNTT: METHODOLOGY	42
	a. General	42
	b. The NASA-Ames Turbulence Study	42
	c. TNTT Case Selection Criteria	44
	d. Aircraft Data Processing	44
	e. Meteorological Data Analysis	53
4.	CASE STUDIES OF TNTT: ANALYSIS	60
	a. Hannibal	60
	b. Bermuda	82
	c. South Carolina	93
	d. Case Comparison	109
5.	SUMMARY, CONCLUSIONS, AND RECOMMENDATIONS	115
REFERENCES		118
APPENDIX A.1		131
APPENDIX A.2		132

LIST OF FIGURES

Figure		Page
2.1	Typical location of thunderstorm turbulence . .	9
2.2	Schematic of gravity or K-H wave breakdown (two-dimensional)	12
2.3	Schematic diagram of the crest lines of a ship wake type pattern	29
2.4	Schematic diagram of atmospheric vortices to the lee of an isolated obstacle	30
2.5	Three-dimensional sketch of the most prominent features of strongly stratified flow past a bluff body	31
2.6	Isentropes generated at model time 2000 s	33
2.7	(A) Composite 500 mb relative wind field around a thunderstorm. (B) Synthesized streamline and isotach pattern based on winds in (A).	35
2.8	Mechanism for development and shedding of vortex eddy behind a stationary rotating cylinder embedded in a uniform water flow . . .	35
2.9	Relative winds, streamlines, and isotachs around an isolated cumulonimbus	36
2.10	Generalized three-dimensional circulation patterns around an isolated cumulonimbus . . .	37
2.11	Large amplitude "mountain" waves formed by forcing flow over the top of a thunderstorm or line of thunderstorms	38
3.1	Procedure used to estimate winds from airline operating records	47
4.1	Large-scale view of the meteorological conditions in the vicinity of Hannibal, MO on 4 April 1981	72
4.2	IR satellite images for the Hannibal, MO case of 4 April 1981	73

LIST OF FIGURES (continued)

Figure		Page
4.3	Sounding plot for Peoria, Illinois valid at 0000 GMT on 4 April 1981	74
4.4	Distribution of radar echoes at 0130 GMT on 4 April 1981	75
4.5	Flight data: Vertical acceleration and altitude along the flight path for the Hannibal, MO case	[illegible]
4.6	Flight data: Vertical velocity and potential temperature along the flight path for the Hannibal, MO case	77
4.7	Flight data: Potential temperature and altitude along the flight path for the Hannibal, MO case	78
4.8	Flight data: Horizontal wind direction along the flight path for the Hannibal, MO case . . .	79
4.9	Flight data: Horizontal wind speed and vertical velocity along the flight path for the Hannibal, MO case	80
4.10	Plan view of the Hannibal, MO case	81
4.11	Large-scale view of the meteorological conditions in the vicinity of the Bermuda case on 12 October 1983	88
4.12	Enhanced IR satellite image for the Bermuda case valid at 0400 GMT on 12 October 1983 . . .	89
4.13	Flight data: Vertical acceleration and altitude along the flight path for the Bermuda case	90
4.14	Flight data: Potential temperature and altitude along the flight path for the Bermuda case	91
4.15	Flight data: Vertical velocity and potential temperature along the flight path for the Bermuda case	92

LIST OF FIGURES (continued)

Figure		Page
4.16	Large-scale view of the meteorological conditions near Charleston, SC on 25 November 1983	99
4.17	IR satellite images for the South Carolina case of 25 November 1983	100
4.18	Sounding plot for Charleston, SC at 2300 GMT on 24 November 1983	101
4.19	Distribution of radar echoes at 0026 GMT on 25 November 1983	102
4.20	Flight data: Vertical acceleration and altitude along the flight path for the South Carolina case	103
4.21	Flight data: Potential temperature and altitude along the flight path for the South Carolina case	104
4.22	Flight data: Vertical velocity and potential temperature along the flight path for the South Carolina case	105
4.23	Flight data: Horizontal wind direction along the flight path for the South Carolina case	106
4.24	Flight data: Horizontal wind speed and vertical velocity along the flight path for the South Carolina case	107
4.25	Plan view of the South Carolina case	108

LIST OF TABLES

Table		Page
2.1	Turbulence reporting criteria	6
2.2	Derived gust velocity and typical response of most aircraft	7
2.3	TNTT forecasting rules of thumb	40
3.1	Cases selected for study	45
3.2	Initial sampling rates for the two aircraft types involved in the incidents studied	46
3.3	RMS errors from DFDR plus radar track calculations	51
3.4	Observed, derived, and computed turbulence parameters	57
4.1	Aircraft track and mean meteorological conditions	109
4.2	Turbulence statistics	110
4.3	Turbulent Kinetic Energy (TKE)	112
4.4	Mesoscale conditions	113

Chapter 1

INTRODUCTION

It has been known for many years that regions over and immediately downwind of thunderstorm tops have a potential for significant aircraft turbulence (Burnham, 1970). The state of the knowledge of the processes that produce this turbulence (TNTT*) is reflected in the inability of forecasters and pilots to predict it with much accuracy. Forecast methods are primarily rules of thumb (e.g., Chandler, 1987) which generally lead to "over-forecasts" of both turbulence areas and intensities. The results of such errors are longer and more costly flights to avoid TNTT.

Similarly, pilots and air traffic controllers have little guidance in determining the exact location of TNTT from visual or radar observations of thunderstorms (e.g., see FAA, 1977; USAF, 1982). This has led to flights into unanticipated severe or extreme TNTT. The latter incidents have occasionally resulted in passenger or crew injuries and/or aircraft damage (e.g., NTSB, 1984).

The problems described above are common to the predictions of all types of turbulence significant to aviation. They are aggravated by inadequate observations. Furthermore, the transfer of useful information from researcher to

---

*TNTT - Turbulence Near Thunderstorm Tops

forecaster in the past fifteen years has also been limited. As a result, turbulence forecast techniques have benefited little from either improved measurements of turbulence or from a better understanding of its causes (Camp and Frost, 1987).

In the last few years, Digital Flight Data Recorder (DFDR) information from commercial aircraft has become available to the scientific community. These data are much more quantitative and less subjective than the more common Pilot Reports (PIREPS). A few investigators have taken advantage of their detail to study turbulence (e.g., Nastrom and Gage, 1983; Lilly and Petersen, 1983). At NASA-Ames Research Center, Wingrove and Bach (1986; also see Lester et al, 1988) have combined DFDR and ATC radar information to reconstruct detailed wind and turbulence conditions for a number of severe turbulence enccunters by commercial aircraft. Three of the cases that they have collected occurred in the vicinity of thunderstorm tops, i.e., they were the result of TNTT. Given the availability of these data, a systematic analysis is in order, considering the needs for better understanding and better forecasts of TNTT as described above.

a. Objectives

The purposes of the current research are: i) to complete a comprehensive review of the literature relevant to the diagnosis and prediction of TNTT, and ii) to

investigate the use of DFDR information from commercial aircraft in the study of TNTT.

In the following, the literature review is presented in Chapter Two, analysis procedures for TNTT cases are presented in Chapter Three, and the results of the case analyses are given in Chapter Four.

Chapter 2

LITERATURE REVIEW

a. General

In the present chapter, turbulence significant to aircraft in flight is defined and turbulence-producing phenomena including generic mesoscale structures and circulations which are conducive to the production of those phenomena are discussed. Subsequently, the current knowledge of the role of thunderstorms in the production of similar structures and circulations is reviewed and present capabilities for the observation and prediction of turbulence near thunderstorms are documented.

b. Turbulence Defined

Common definitions of atmospheric turbulence are normally based on characteristics of the airflow. For example, Panofsky and Dutton (1984) defines turbulence as: i) a fluid velocity which is chaotic and a random function in space and time, ii) a strongly rotational and three-dimensional flow with gradients occurring in all directions, iii) a nonlinear process which causes energy to be distributed smoothly with wavelength, iv) a process where gradients are created by the stretching of vortices causing kinetic energy to move to smaller wavelengths, and v) a diffusive and intermittent process.

In contrast, the term "turbulence" when used with respect to aviation is often defined according to its effects on the aircraft and passengers, e.g., "bumpiness in flight" (FAA, 1977). This convention will be used in the current study.

Several categorical definitions based on the intensity of turbulence effects are in common use. Examples of standard semi-quantitative and quantitative classifications are given in Tables 2.1 and 2.2, respectively. In the latter table, U_{de} is the derived gust velocity given by

$$U_{de} = \frac{2}{\rho_o} \frac{\Delta n \; W/S}{m \; K_g \; V_e} \qquad (2.1)$$

where Δn is the incremental departure of the vertical component of aircraft acceleration from the normal acceleration (1 g), W is aircraft weight, ρ_o is air density, m is wing lift curve slope, K_g is gust alleviation factor, V_e is equivalent airspeed, and S is wing area (Pratt and Walker, 1954).

c. <u>Causes of Turbulence Significant to Aviation</u>

Since the "turbulence" considered here is defined on the basis of its effects on aircraft, it includes not only the chaotic, nearly random, small-scale motions described by the classical definition of turbulence, but also coherent, quasi-periodic motions with characteristic scales within the critical response range of the aircraft. Thus

Table 2.1 - Turbulence reporting criteria (Kessler, 1981).

INTENSITY	AIRCRAFT REACTION	REACTION INSIDE AIRCRAFT
Light	Momentary slight, erratic changes in altitude and/or attitude (pitch, roll, yaw).	Occupants may feel slight strain against seat belts or shoulder straps. Unsecured objects may be displaced slightly. Food service may be conducted and little or no difficulty is encountered in walking.
Moderate	Changes in altitude and/or attitude occur but aircraft remains in positive control at all times. It usually causes variations in indicated airspeed.	Occupants feel definite strains against seat belts or shoulder straps. Unsecured objects are dislodged. Food service and walking are difficult.
Severe	Large, abrupt changes in altitude and/or attitude. It usually causes large variations in indicated airspeed. Aircraft may be momentarily out of control.	Occupants are forced violently against seat belts or shoulder straps. Unsecured objects are tossed about. Food service and walking are impossible.
Extreme	Aircraft is violently tossed about and is practically impossible to control. It may cause structural damage.	

Table 2.2 - Derived gust velocity and typical response of most aircraft (Holcomb, 1976; Kessler, 1981).

INTENSITY	U_{de} (ms^{-1})	Δn		TAS VARIATIONS (ms^{-1})
		ROOT MEAN SQUARE (g)	PEAK (g)	
Light	1.5-6.1	<0.2	±>0.2-0.5	<7.7
Moderate	>6.1-10.7	0.2-0.3	±>0.5-1.0	7.7-12.9
Severe	>10.7-15.2	>0.3-0.6	±>1.0-2.0	>12.9
Extreme	>15.2	>0.6	±>2.0	

there are three general causes of bumpiness in flight: (i) mechanically induced turbulence, (ii) thermally induced turbulence (cellular convection), and (iii) the formation and breakdown of gravity waves (Vinnechencho et al, 1980).

(1) Mechanical Turbulence

Near the surface of the earth, mechanically produced eddies are significant turbulent sources, especially in strong winds. These eddies are simply due to strong vertical shear over flat terrain or to flow separation over complex terrain (Scorer, 1978). Their scales are proportional to the height above the ground and to the scale of the terrain roughness elements (Lester and Burton, 1988).

(2) Turbulence Associated with Convection

Discrete convective cells result when air becomes statically unstable due to one or more of a variety of causes. These include surface heating, cooling aloft, and the release of latent heat (Miller et al, 1983). The structure of convective cells has been well documented

(e.g., Scorer, 1978) and need only be treated generally here.

In the surface boundary layer, convection often takes the form of dry "thermals", i.e., toroidal circulations with a narrow jet-like updraft in the center and more gentle sinking along the sides. These buoyant features rise and expand, entraining environmental air. Turbulence is particularly noticeable at the interface between the up and down drafts and on the leading edge ("cap") of the thermal. If the thermal passes through the convective condensation level (CCL), a cumulus cloud forms, with characteristic cauliflower-shaped protuberances which highlight turbulence areas on the periphery of the updraft.

The size of an individual thermal is proportional to its height above the ground. Its intensity will decrease due to entrainment and loss of buoyancy. However, an added vertical acceleration occurs at the CCL due to the release of latent heat. Under conditions of great static instability, continued growth of the cumulus cloud may occur resulting in cumulus congestus and, finally, cumulonimbus (i.e., a thunderstorm; Wallace and Hobbs, 1977), which typically extends from the lower troposphere to the lower stratosphere.

Aircraft turbulence associated with thunderstorm cells commonly occurs in the areas indicated in Figure 2.1 (USAF,

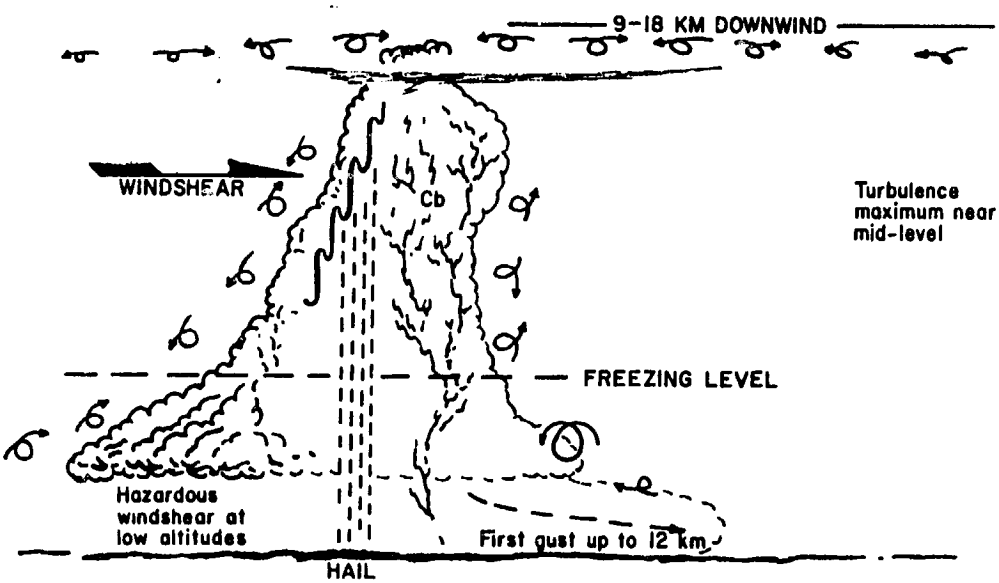

Figure 2.1 - Typical location of thunderstorm turbulence (redrawn from USAF, 1982).

1982). The nature of that turbulence, especially within and below the thunderstorm cell, has been well-documented.

For example, in the boundary layer, turbulence producing phenomena such as downbursts, strong horizontal shears, and gust fronts have been documented thoroughly by Fujita (1978), Kessler (1982), and others. Within the cloud, strong turbulence due to updrafts, downdrafts, and shears between the two are well known (e.g., Byers and Braham, 1949). It is also known that significant turbulence often occurs in association with thunderstorms, but outside the convective area. The latter turbulence is less well documented and is of particular interest in the present study. This will be discussed in detail later.

(3) Turbulence Associated with Gravity Waves

Gravity waves are formed when a parcel of air with some horizontal velocity is displaced vertically in a stable environment. Once the displacing force is removed, the parcel will oscillate vertically, often with a wave length (λ) dictated by the mean horizontal wind-speed and the local Brunt-Väisäliä frequency (N); i.e.,

$$\lambda \simeq \frac{2\pi\bar{u}}{N} \qquad (2.2)$$

where $N = \left(\frac{g}{\theta}\frac{\partial\theta}{\partial z}\right)^{1/2}$, where g is acceleration due to gravity and θ is potential temperature (Gossard and Hooke, 1975).

Typical environmental values of $\bar{u}$ and N yield wave lengths in the range of a few to a few tens of kilometers. Larger waves (a few 100 kilometers) are possible as a function of the scale of the forcing (displacement) process. Gravity waves are commonly forced by mountains, especially during the winter in mid-latitudes, when both wind speeds and stabilities are high. Standing gravity waves develop in the lee of mountains and, under certain conditions, may propagate to very high levels in the atmosphere, carrying wave energy upward and momentum downward (Alaka, 1960; Nicholls, 1973). It will also be seen that waves in stable airflow may be perturbed by convective activity at lower levels. This will be discussed in detail in a later section. A summary of measurements of the characteristics of

gravity waves and their environment is presented in Appendix A.1.

Shearing gravity waves, also known as Kelvin-Helmholtz (K-H) waves are a related gravity wave phenomena. In the simplest example, they form when the stable interface between two layers of air which have different temperatures and different velocities is displaced vertically. Waves with typical scales of a few hundred meters to a few kilometers form at the interface. A summary of measurements of the characteristics of K-H waves and their environment is presented in Appendix A.2. Because K-H waves fall into the scale range of aircraft response, they are more likely to be associated with aviation turbulence than the larger gravity waves, at least prior to wave breakdown. When the latter occurs, both types of waves are likely to produce significant turbulence.

Wave breakdown is the transition from coherent wave motion to turbulence. It occurs when the gravity or K-H wave amplitude in a sheared environment grows to the point that the wave overturns, i.e., the wave crest overruns the wave trough. The two-dimensional case is shown in Figure 2.2.

Vertical wind shear, then, plays a critical role for turbulence production by either gravity wave or K-H wave breakdown. Gravity waves may propagate into an area of

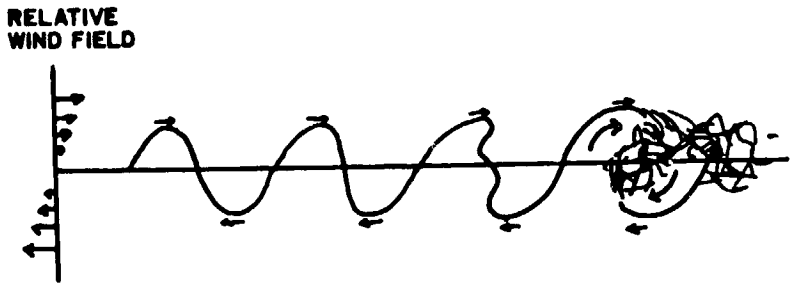

Figure 2.2 - Schematic of gravity or K-H wave breakdown (two-dimensional). Fluid interface of a disturbance in a sheared environment is depicted. Small arrows indicate relative wind experienced at wave crests and troughs. As wave moves downstream, the wave crest gradually overruns the trough and the wave overturns, resulting in turbulence.

strong shear, while, of course, K-H waves already exist in a sheared environment.

For both types of waves, the value of the local gradient Richardson number (Ri) is an indicator of the regions of the wave most likely to break down into turbulence. Defined as

$$Ri = \frac{\frac{g}{\theta}\frac{\partial\theta}{\partial z}}{\left(\frac{\partial u}{\partial z}\right)^2} \qquad (2.3)$$

its value has been noted by some to be a good indicator of the likelihood of clear air turbulence (CAT; Reiter and Lester, 1968; Dutton, 1971; Gossard and Hooke, 1975). As noted by Delay and Dutton (1971) in their study of severe CAT incidents, favorable conditions are a combination of

strong vertical wind shear, a mesoscale perturbation in the potential temperature field, and Ri less than 0.25. A critical Ri value of 0.25 has also been deduced from many theoretical studies (Browning, 1971; Bekofske and Liu, 1972; Reiss and Corona, 1977; Stobie et al, 1983).

When gravity waves break, eddies with typical dimensions of 0.5 to 1.0 km and with horizontal axes often form. The associated turbulence results from overturning which reduces the local Ri to negative values (Bekofske and Liu, 1972; Keller, 1975; and Keller et al, 1983). For example, when standing gravity waves (lee waves) form downstream of topographic barriers, a well-documented rotor circulation often forms under the lee wave crests near mountaintop level. This phenomena, which is typically 0.5 to 1.0 km in diameter is well known for its extreme turbulence (Kuettner, 1958; Lester and Fingerhut, 1974). Theory also indicates that such overturning for a standing wave will occur in any atmospheric layer where the mean horizontal velocity and the phase velocity are equal (Scorer, 1978). Of course, in a standing mountain wave, this occurs where $u=0$. It has been suggested that such "critical layers" may be found in the lower stratosphere (Klemp and Lilly, 1975; Clark and Peltier, 1977).

Many observational studies have identified K-H waves with billow clouds in the atmosphere. Relatively short-lived, large-amplitude billows usually last less than 30

minutes and often occur in well-defined rows of 2-8 (Browning, 1971). They are oriented perpendicular to the wind shear and travel at the velocity of the winds in the middle of the shear layer (Browning and Watkins, 1970a). The associated K-H waves usually start on the edge of a stable layer but, once initiated, can extend vertically over a substantial depth (Browning and Watkins, 1970b). Browning et al (1973) found that the minimum potential temperature occurs at the crest of the billow and that the vertical winds are 90° out of phase with the potential temperature field, the vertical motion is negative ahead of the billows, zero at their center, and positive behind them. K-H waves are often observed in other cloud formations, such as cumulus; however, they preferentially form in regions devoid of cloud particles (Hicks and Angell, 1968).

K-H waves break down due to the instability that arises because of an accumulation of the vorticity of the layer at the alternate nodes of the wave. They eventually "roll up" and break, in a phenomenon known as Kelvin-Helmholtz instability (KHI; Atkinson, 1981). Chaotic motions, initiated when fully three-dimensional small-scale motions are introduced into the core of the billow, gradually spread throughout the shear layer, resulting in the billow's collapse (Thorpe, 1983; Klaassen and Peltier, 1985). Later, when the layer is well mixed, it is replaced

by two thinner strongly sheared stable layers at the top and bottom of the mixed layer. The instability process can then repeat itself in those layers, resulting in billows of different wave lengths and orientations being formed at almost the same level (Scorer, 1971).

When a K-H wave breaks down, the intensity of the turbulence associated with it depends on the wave amplitude and the vertical wind shear across the wave (Browning, 1971). In fact, Browning et al (1970) specifically noted that large amplitude K-H waves (amplitude $\geq$ 500 m) are not sufficient to produce severe turbulence unless strong vertical wind shear is also present. Browning (1971), however, also found that as a large-amplitude K-H wave grows, the wind shear and small-scale turbulence associated with it are locally increased.

Flights through K-H billows to investigate the turbulence intensity have found that the most severe turbulence is encountered within the troughs of the waves (Mather and Hardy, 1970), within the crests of the waves (Browning et al, 1973), and within the parts of the waves where small-scale (secondary) waves grew on the back of amplifying (primary) waves inclined in the same sense as the vertical shear vector (James and Browning, 1981). James and Browning also noted that secondary billows often formed in the areas of the most intense turbulence.

Theoretical considerations and observations in the laboratory, in the ocean, and in the free atmosphere suggest that KHI is probably responsible for most occurrences of clear air turbulence (CAT; Browning, 1971).

Since the two major components in the occurrence, growth, and breakdown of gravity waves into turbulence are stability and shear, it is not surprising that aside from mechanical boundary layer turbulence and convection, most of the atmospheric structures identified with types of turbulence significant to aviation are those associated with strongly sheared stable layers, i.e., fronts and tropopauses (Reiter, 1963; Endlich, 1964). Also, it is well known that mountain lee waves enhance vertical shears near the tropopause level causing the production of KHI (e.g., see Lester and Bach, 1986).

d. Observations of Waves and TNTT

The fact that thunderstorms generate secondary (i.e., external) disturbances, especially near and above the tropopause, has been known for many years. For example, Davies and Jones (1971) determined that certain ionospheric disturbances were the result of acoustic waves generated by thunderstorms. Taylor (1983) concluded that vertically propagating gravity waves generated by thunderstorms were the cause of the mesospheric heating he was investigating. Gravity waves attributed to thunderstorms were detected by pressure pulsations measured at ground level by Brunk

(1949). Curry and Murty (1974) definitely identified three cases of gravity waves generated by thunderstorms by tracing the waves back to their source along the track of storms. Erickson and Whitney (1973) and Stobie et al (1983) have used satellite observations to identify wave clouds radiating from overshooting thunderstorms. Balachandran (1980) has shown that, in the presence of an intense and persistent mean wind near the thunderstorm top, the storm-generated waves prefer the downwind direction.

Balachandran (1980) also suggested that although thunderstorm-generated gravity waves occur in a broad range of scales, they are not completely random, i.e., they appear to be related to the different scales of motion associated with the storm itself. Lu et al (1984) found a similar result in terms of wave period. Although the spectrum of waves was broad, the maximum spectral power exhibited a distinct preference for periods of 30-60 min, close to the lifetime of a typical thunderstorm cell (Byers and Braham, 1949).

Uccellini (1975) has pointed out that thunderstorm-generated waves are common. They are often associated with synoptic-scale systems in the area, making them hard to detect.

In addition to the gravity wave activity described above, smaller scale turbulence significant to aviation is found over and downwind of thunderstorms. Over the years,

aircraft have reported the following, concerning the location and intensity of turbulence encountered in the vicinity of thunderstorms: moderate to severe turbulence in the clear air may extend as high as 3.0 km above any visible cloud tops and as far as 12.4 km around it (often in the anvil cirrus shield downwind). Current turbulence forecast procedures crudely relate the occurrence of TNTT to the strength of the wind near tropopause level (Burnham, 1970; Prophet, 1970; NWS, 1974; FAA, 1977; USAF, 1982; Chandler, 1987).

An example of TNTT was documented during Project Roughrider, an investigation conducted specifically to investigate atmospheric turbulence in the upper troposphere and lower stratosphere in the vicinity of thunderstorms (Burns and Harrold, 1966; Burns, 1972). Observations were taken flying over and around the storm tops, in and around the anvil cloud, and along the sides of the storm buildups. Very little significant turbulence was found at lower altitudes, but moderate intensities were not unusual at and above the level of the cirrus sheet. The one incident of severe turbulence occurred without warning downwind of a thunderstorm complex where overshooting tops extended more than 3.6 km above the anvil cirrus. The turbulence was encountered immediately above the anvil where winds were 36 ms^{-1} (70 knots) and decreasing with height.

Roach (1969) examined five incidents where aircraft encountered severe TNTT. In all cases the aircraft were flying in extremely stable air with large negative wind shear (similar to the case previously described). In addition, in one incident, Roach noted that there was a sudden decrease in air temperature just prior to the turbulence occurrence, leading him to assume that a new air mass had been entered. In fact, temperature fluctuations as a whole have been found to increase markedly over storm areas (5C versus 1-2C away from storm areas; Roach, 1967) possibly as a result of turbulent mixing in a stably-stratified environment (Brandes et al, 1986).

More recently, Detwiler and Heymsfield (1987) examined the observations of the lower anvil region of a large cumulonimbus in Montana taken by an instrumented aircraft. Five cross-wind passes through the anvil were made, 5-7 core diameters downstream of the active updraft region. They found that the winds relative to the moving anvil were 15 ms^{-1}. The horizontal wind field indicated the storm blocked the wind as a single cell, forming a sharp "shadow." Winds there were depleted by about 10 ms^{-1} with a broader shadow found at higher levels than at lower ones. The vertical wind field consisted of many small-scale fluctuations but revealed a transition from upward to downward motion as the aircraft entered the anvil at all altitudes. These downdraft regions were 10-20 km wide and were

characterized by a drop in vertical speed of 1-2 ms^{-1} and a rise in potential temperature of 3-5 degrees. Also, variations in the horizontal winds were noted to be on a scale ten times greater than those in the vertical. Overall, Detwiler and Heymsfield found the flow downstream of the core to resemble the near-wake region of a bluff object embedded in flow which is uniform except for an increase in winds with height. Although little evidence of the coherent eddies or wave-like motions often found in wake regions was observed, they noted that it would be very difficult to detect them with the cross-anvil penetrations used. Finally, while the variability of the anvil was three-dimensional on a smaller scale, its large-scale appearance was quasi-two-dimensional.

e. Causes of TNTT

The observations of TNTT in stable, vertically-sheared environments where gravity waves are common has led most investigators to the conclusion that TNTT is not caused directly by cellular convection, but rather is the result of unstable gravity waves or K-H waves excited by the convection. Four possible interactions have been proposed: 1) penetrative convection (Pierce and Coroniti, 1966; Townsend, 1966; Bradbury, 1973; Stull, 1976), 2) release of latent heat (Lindzen, 1974; Lindzen and Tung, 1976; Ley and Peltier, 1981), 3) KHI associated with strong shear (Balachandran, 1980; Lilly, 1983; Stobie et al, 1983), 4)

flow over and/or around the thunderstorm which acts as an obstacle (Burnham, 1970; Burns, 1972; Kuettner, 1972; Bradbury, 1973; Curry and Murty, 1974; Seitter and Kuo, 1983; Keller et al, 1983).

(1) Penetrative Convection

In this process, the convection overshoots into a stable layer (e.g., the lower stratosphere), displacing a portion of the stable layer, and then collapses due to strong negative buoyancy. As this process repeats itself the interface between the stable and convective layer is disturbed and a pattern of waves arises from the superposition of many ripples (Townsend, 1966; Stull, 1976). Kuettner et al (1987) have extended the work by Jaeckisch (1970) and Kuettner (1972), based on glider observations, to show that relatively weak penetrative convection may induce significant gravity wave motions in the overlying stable layer.

(2) Latent Heat Release

In this case, waves result from the liberation of latent heat in the intense convection. This heating constitutes a forcing mechanism which excites a broad-band spectrum of normal modes of the ambient atmosphere. The result is an energy transfer which initiates and drives the waves. The total disturbance is described by the superposition of the many excited modes (Lindzen and Tung, 1976; Ley and Peltier, 1981).

(3) Kelvin-Helmholtz Instability

KHI arises when thunderstorms penetrate a region of very strong winds near the tropopause. Strong vertical shears in the lower stratosphere are enhanced, reducing Ri to less than 0.25. Even when the background wind over thunderstorms lacks adequate shear to generate a wave in this manner, Balachandran (1980) notes that the shear present in thunderstorm outflows is often sufficiently strong.

(4) The Thunderstorm as a Barrier

The interpretation of a cumulonimbus cloud as a "solid" obstacle has far reaching ramifications with respect to TNTT occurrence. For this reason, a detailed review of the appropriate evidence is in order.

It has long been accepted that thunderstorms (or cumulus type clouds) are not just parcels of undiluted boundary-layer air adiabatically lifted without mixing (Palmén and Newton, 1969; Raymond and Wilkening, 1982). Due to temperature and liquid water content considerations, mixing from above the boundary-layer must occur. Entrainment of outside air uniformly from all sides as the cumulus cell rises is consistent with these observations and has long been the accepted hypothesis. However, actual observational evidence of this entrainment process is very sparse. As noted by Raymond and Wilkening it is possible to explain this process without entrainment. For example, Fraser (1968) developed a consistent cumulus cloud model with

inflow at the top and bottom and net outflow around the sides.

To check the entrainment hypothesis, Raymond and Wilkening flew an instrumented aircraft around developing and mature thunderstorms over the mountains in New Mexico and measured the convergence or divergence occurring at several levels around the sides of the storm cells. Based on their investigation, they came to the following conclusions: 1) convergence occurs only below mountaintop level (at or below the base of the cloud), 2) divergence dominates aloft, and 3) when significant clouds are present, a secondary divergence maximum is found near 500 mb with weak divergence occurring between the cloud base and this 500 mb outflow.

Other investigations into the entrainment question have given similar results. In 1976, as part of the National Hail Research Experiment, the NCAR/NOAA Explorer sailplane flew in and around developing cumuli in northeast Colorado. Upon examination of the data, Paluch (1979) concluded that the laterally entraining plume model (where environmental air is entrained from the sides and carried along in the updraft) was inconsistent with his results. Also, in a field experiment conducted by Telford and Wagner (1974) specifically designed to measure the air motion around typical small fair weather cumulus and looking for inflow due to entrainment, they found the airflow to be

outward at the sides of the clouds they examined. The net effect being "entrainment through the sides of almost zero" (Telford and Wagner, 1980).

As early as 1959, Newton and Newton postulated that the thunderstorm updraft tends to behave like an obstacle causing the environmental air to divert around it. While the updraft is not a solid obstacle to the flow, further work by Kessler (1982) and Rotunno and Klemp (1982), as well as data collected by Lemon (1976) and by Johnson and Brandes (1986) supports the existence of a barrier type effect around thunderstorms. Recent research using Doppler radar shows the blocking effect is most pronounced around the updraft regions (Brewster and Zrnic, 1986; Heymsfield and Schotz, 1986).

The blocking nature of thunderstorm tops is supported by observations of a warm spot accompanied by an enhanced-V signature over severe storms on infrared satellite images. Mills and Astling (1977) hypothesized an overshooting top to explain it. This theory was expanded by Fujita (1978) and Lin (1986) who noted that the overshooting top tends to block the winds, diverting the ambient flow around it, and resulting in streamlines similar to those of turbulent flow past a cylinder. The situation appears to be analogous to airflow over mountains since an air parcel experiences an upward and downward motion when passing over the cloud dome (Heymsfield et al, 1983a and 1983b). However, it was not

clear whether the warm spot resulted from rising or sinking motion in its lee (McCann, 1981). In either event, the stationary nature of a thunderstorm is also important since it affects the severity of the downstream effect. Visual and radar observations have shown that cumulus clouds move at a speed different from the velocity of the ambient wind at their level. As the cloud grows, a transfer of momentum takes place mainly in an upward direction. Since the transfer is from layers with lower wind velocities, the velocity of the cloud at higher levels becomes less than the velocity of the air outside of it (Pinus, 1962). As a result, the air at cloud top level will overtake the thunderstorm. However, the strength of this relative wind is less than if the thunderstorm were completely stationary and thus the blocking effect is less. If the thunderstorm grows to supercell class, though, it can remain stationary for thirty minutes or more (Browning and Ludlam, 1962; Fankhauser, 1971; Miller and Fankhauser, 1983). Considering the very strong upper winds often associated with supercells, it is expected that they commonly produce the strongest blocking effects.

On the basis of the foregoing evidence, it is concluded that thunderstorms (as a whole or in part) may act as an obstacle to the horizontal wind. Flow will, therefore, go around and/or over the cloud much like the flow around and/or over hills. Hence, a wake will form

downstream and/or above the thunderstorm cell. The characteristics of the thunderstorm wake at tropopause level, therefore, depend to some extent on the shape of the top of the thunderstorm and on the relative movement of the thunderstorm with respect to the ambient winds.

Shape characteristics of thunderstorm tops have been documented by Roach (1967). Observations were collected by aircraft in the summit areas of severe storms (usually associated with squall lines) in Oklahoma. He found that the anvil cirrus sheet generated by the storms occurs at the equilibrium level predicted by parcel theory, i.e., somewhat above the environmental tropopause. Storm tops protruded through the cirrus sheet and were confined mainly to a belt about 50 km wide extending along the upstream edge of the cirrus with a density of about 1 top per 600 km^2 (or about 1 top per 20 km along the squall line). Most of the tops appeared as isolated cumuliform protrusions 3-8 km in diameter extending up to 2.4 km above the surrounding cirrus deck. However, in the regions with the highest development, clusters of cells appeared to produce a vast heap or a rough cone with a shallow slope consisting of cumuliform cloud. Thirty to forty miles in diameter, the centers of these heaps attained heights of 4.5-6.0 km above the surrounding cirrus deck.

More recently, Heymsfield et al (1986) and Poellot and Heymsfield (1986) have observed that the tops of multicell

and supercell thunderstorm complexes have a pulsating nature as a discrete cloud tower associated with each updraft rises above the anvil cirrus. Fujita (1978) has related the subsequent collapse of these towers in severe thunderstorms to tornado occurrence at lower layers.

f. Excernal Mesoscale Circulations Produced by Flow Over and Around Thunderstorms

It is obvious from the preceding descriptions that flow over thunderstorm tops bear many similarities to flow over rugged terrain. Although the interaction between the thunderstorm and its environment is complicated by the growth, motion, and dissipation of the thunderstorm, the qualitative comparison is strong enough to warrant a review of mesoscale circulations induced by stable flow over complex terrain. These then offer potential explanations of observed motions around thunderstorms and, ultimately, of the circulations which produce TNTT.

The formation of mesoscale circulations downwind of terrain obstacles are determined by the stability of the air and, in the stable case (our main concern here), whether the air flows over or around the obstacle. The latter determination is usually based on the kinetic energy of the parcels of air impinging on the obstacle and the potential energy which must be supplied to surmount the barrier. One example is the ratio between the two energies, i.e., the nondimensional Froude Number (Fr),

$$Fr = \frac{U}{\left(g \frac{\Delta\rho}{\bar{\rho}} D\right)^{1/2}} \tag{2.4}$$

where U is current speed, $\bar{\rho}$ is mean density, $\Delta\rho$ is the density difference between layers, and D is the total depth of the fluids (Atkinson, 1981). If:

$$Fr \begin{Bmatrix} > \\ = \\ < \end{Bmatrix} 1 \quad \text{flow goes} \begin{cases} \text{over} \\ \text{both} \\ \text{around (or is blocked).} \end{cases}$$

If the stable air primarily goes over an isolated terrain feature, a three-dimensional lee wave pattern results. Noticed originally in low clouds on satellite images (Scorer, 1978), the pattern is analogous to an internal ship wave. Two types of waves are produced, diverging and transverse as illustrated in Figure 2.3. Scorer (1978) notes that the shape of the obstacle determines the wave type generated. For a long narrow obstacle (length parallel to mean wind) only diverging waves are produced. On the other hand, for a squat flat obstacle only transverse waves are generated. Of course, an obstacle with a shape which falls somewhere between those two will produce a combination of diverging and transverse waves. Study has also shown that although an infinite number of wave modes is possible in a given situation, each mode is contained within a characteristic wedge angle, θ (Sharman and Wurtele, 1983). In the simplest case, θ equals 19°28′ (Scorer, 1978). In the atmosphere, Gjevik and Marthinsen (1978)

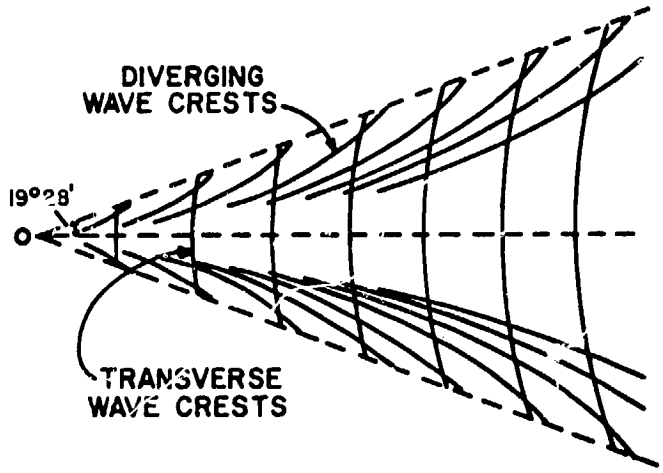

Figure 2.3 - Schematic diagram of the crest lines of a ship wake type pattern. Wake is confined to a 19°28′ (measured from center line) wedge area in the lee of the obstacle. The maximum wave amplitude occurs where the diverging phase lines cross the transverse ones (after Scorer, 1978).

note that θ can approach 90° for a stable layer embedded between two neutrally stable layers; however, its value will decrease when the stability above is increased. In their four cases they found $10.7° \leq \theta \leq 17.8°$ for the cases where diverging waves were present, and $\theta = 21.7°$ for the case where both diverging and transverse waves were evident.

If the stable air goes around an individual peak, a mesoscale lee vortex pattern (Figure 2.4) results. First noticed in the atmosphere on satellite images in the lee of islands (Hubert and Krueger, 1962; Chopra and Hubert, 1965), its properties appear to be consistent with classical Karman vortex streets (Zimmerman, 1969).

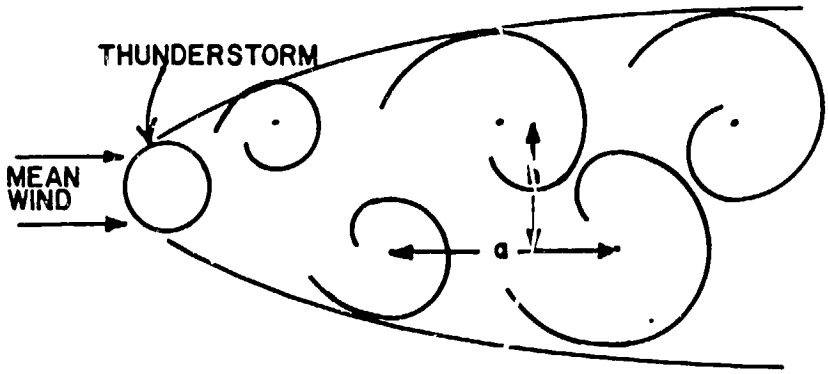

Figure 2.4 - Schematic diagram of atmospheric vortices to the lee of an isolated obstacle (after Atkinson, 1981).

Horizontal vortices (i.e., with vertical axes) are alternately shed in two parallel rows. This relationship is maintained as the vortices are carried downstream, although Zimmerman (1969) noted a case where this orientation was modified by wind shear. When shed, the vortices are comparable in diameter to the obstacle (Lyons and Fujita, 1968) but diverge and become larger farther downstream (Atkinson, 1981). Theoretical investigations by Tsuchiya (1969) noted

$$\left.\begin{aligned} U_* &= 0.76\, U_o \\ U_o \tau &= a \\ 0.3 < h/a &< 0.4 \end{aligned}\right\} \qquad (2.5)$$

where U_o is the mean wind, U_* is the displacement speed of a shed vortex, τ is the vortex shedding period, a is the distance between vortices shed in one row (see Figure 2.4), and h is the distance between rows. Typical values for

atmospheric vortices are: U^{o}, 10 ms^{-1}; U_{*}, 7-8 ms^{-1}; τ, 4-8 hours; with a vertical depth of 350-2000 m (Tsuchiya, 1969; Atkinson, 1981).

Brighton (1978) conducted a laboratory experiment to examine the three-dimensional flow patterns around an obstacle in stratified flow and was able to identify three flow types in the downstream region (Figure 2.5).

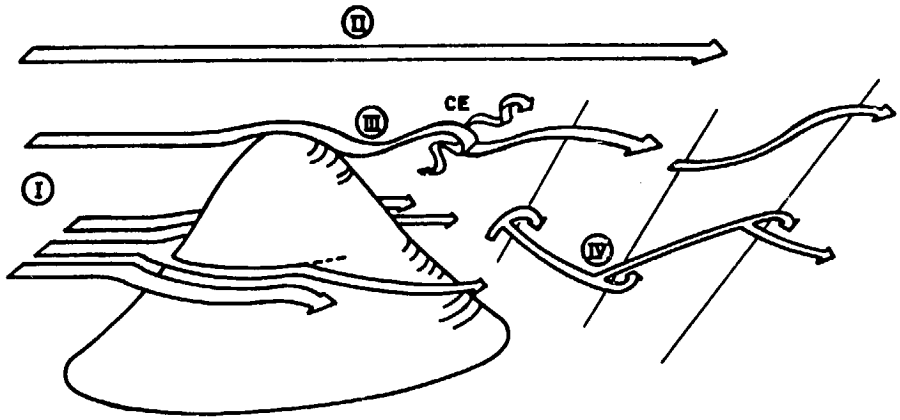

Figure 2.5 - Three-dimensional sketch of the most prominent features of strongly stratified flow past a bluff body. The flows at three different levels are illustrated. The lowest sheet of fluid approaches the obstacle in the almost horizontal layer-wise potential flow described by inviscid flow theory (region I). The flow separates from the sides of the obstacle and in the wake region (region IV) vortices may be shed. The motion is still nearly horizontal. The shedding frequency is the same at all levels and the axes of the vortices lean downstream. The second level from the bottom is very near the summit (region III) and fluid passes over the top. Downstream lee waves are formed and also sometimes a cowhorn eddy (CE). Further downstream, the influence of the vortices propagates up from region IV. Fluid at the topmost level illustrated, well above the top of the obstacle (region II), is little affected by its presence (after Brighton, 1978).

At the level of the top of the obstacle, the fluid flowed over the top, generating lee-type waves in the downstream region (region III). Very likely these waves were three-dimensional as discussed above, but the investigation only described the pattern along the center line of the experiment (Figure 2.5). At the same level a pattern called a "cowhorn eddy" by Brighton (labeled CE) is generated. Similar rotor-like patterns have been noted in the laboratory studies of Mumford (1982 and 1983) and could be analogous to the rotors which form to the lee of mountains at mountaintop level (Vinnichenko et al, 1980). Burns (1972) concluded that similar rotors which developed in the lee of thunderstorms were the cause of turbulence encountered there.

The third type of pattern found by Brighton (1978) was vortex eddies, which occur at lower altitudes (region IV in Figure 2.5) where the flow is around the obstacle rather than over the top (also, Mason and Sykes, 1979a and 1979b). As noted earlier, satellite pictures have revealed both cloud formations with this type of pattern in the lee of islands visible up to 600 km downwind (Chopra and Hubert, 1965; Tsuchiya, 1969), as well as an alternate pattern more similar to a ship wake (Gjevik and Marthinsen, 1978; Sharman and Wurtele, 1983).

Due to his laboratory setup, Brighton's study does not provide any details concerning the vertical pattern of the

turbulent wake above and behind the obstacle (his upper boundary was too close to the top). An example of what could be happening there is given by Keller et al (1983). They have developed a two-dimensional model with a thunderstorm simulated as a rigid obstacle at the lower boundary. Results show that the obstacle generates gravity waves through a deep vertical section in a stable atmosphere. Turbulence is apparent because there are several places where the gravity waves downstream from the obstacle have steepened and overturned (Figure 2.6).

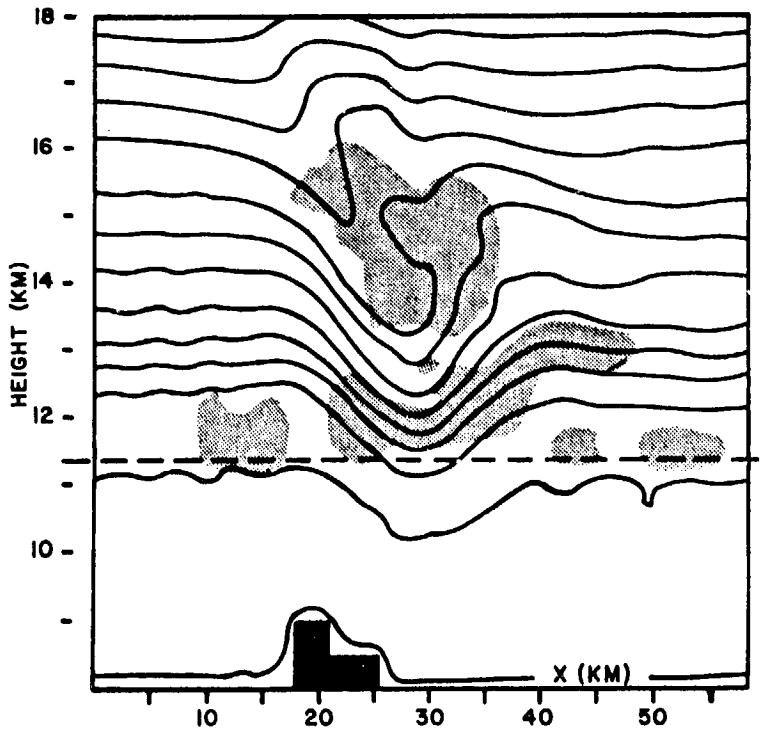

Figure 2.6 - Isentropes generated at model time 2000 s. Flight level of aircraft is shown by the horizontal dashed line. Regions of subcritical Ri are indicated by shading (Keller et al, 1983).

Fankhauser (1971) conducted two field experiments designed to investigate the dynamic and kinematic properties of low and middle level air surrounding isolated cumulonimbus clouds. He combined aircraft and chaff tracer winds, radar profiles, nearby rawinsondes, and surface recordings to piece together what happened. At 500 mb (the highest level he analyzed in detail) he found that some of the features were analogous to those in hydrodynamical experiments involving solid cylinders in quasi-potential flow. Specifically, maximum wind bands existed on both flanks of the radar echo as air flowed around a convective column in strong vertical wind shear. Since the thunderstorm moved more slowly than the winds aloft, it acted as an obstacle and forced the airstream to divide and accelerate on the cloud flanks. In addition, he found that in the lee of the storm there was a tendency for streamline confluence and light winds beneath the anvil (Figure 2.7), a condition that suggests a wave-like regime.

On further examination of the winds behind the thunderstorm, Fankhauser found the features of the circulation to be similar to those found in the laboratory behind a stationary rotating cylinder embedded in a uniform water stream. Thunderstorm rotation has been well-documented (Byers and Braham, 1949; Fujita and Grandoso, 1968). As the thunderstorm rotates, it causes the observed streamline

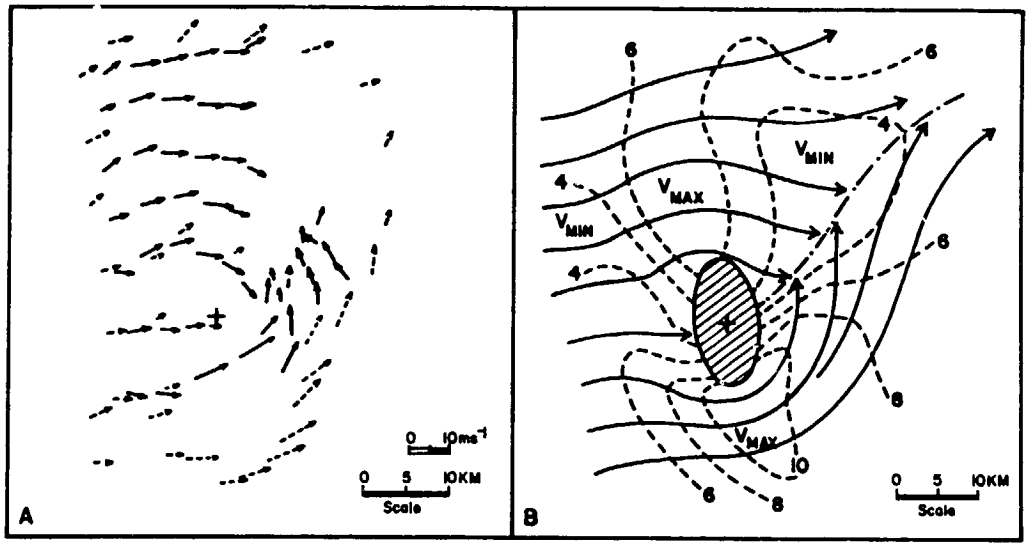

Figure 2.7 - (A) Composite 500 mb relative wind field around the thunderstorm centered on the cross, derived from aircraft measurements (dashed) and chaff displacement (solid). The vector length is proportional to its magnitude (ms^{-1}). (B) Synthesized streamline and isotach pattern based on winds in (A). The dash-dot line denotes the wake axis (after Fankhauser, 1971).

confluence in the lee of the cell to be deflected to one side and results in the generation of lee eddies (Figures 2.8 and 2.9). This same conclusion was also reached by

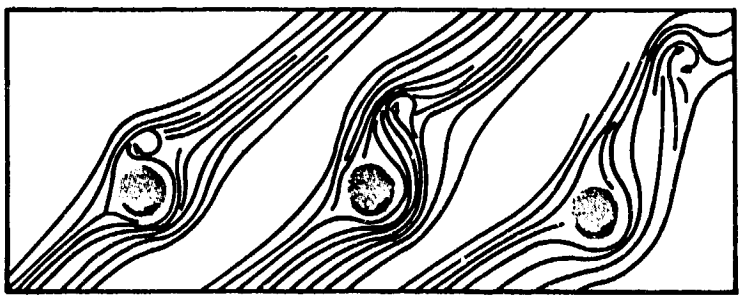

Figure 2.8 - Mechanism for development and shedding of vortex eddy behind a stationary rotating cylinder (shaded circles) embedded in a uniform water stream (after Lemon, 1976).

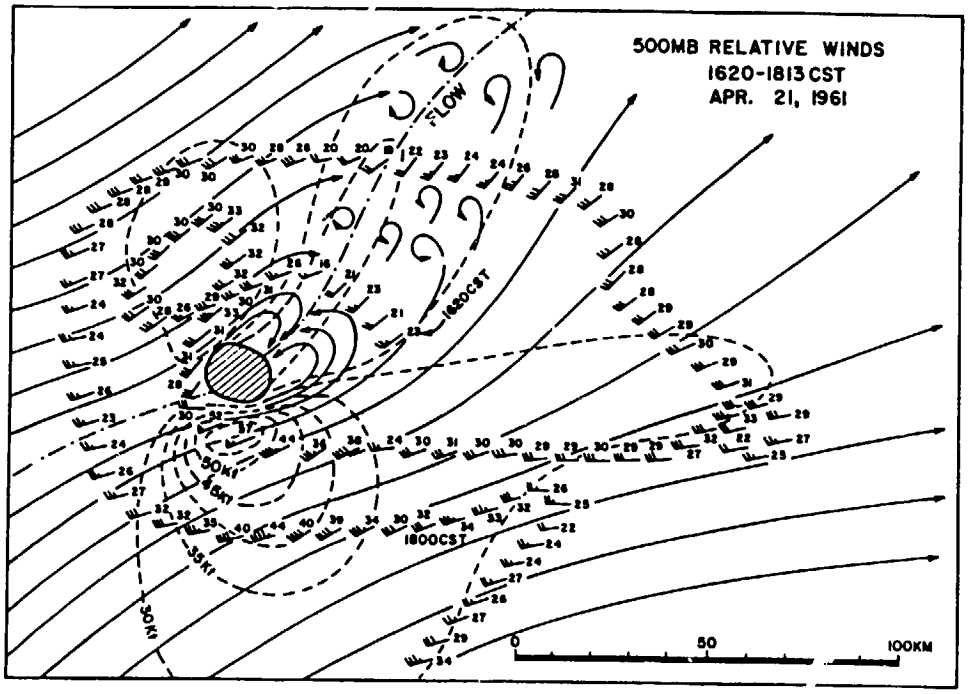

Figure 2.9 - Relative winds, streamlines, and isotachs (kt) around an isolated cumulonimbus. The relative wind was obtained by subtracting the storm's velocity from winds measured by airborne Doppler radar (after Fujita and Grandoso, 1968).

Jessup (1972) who used chaff to investigate the flow of air in the vicinity of thunderstorms and by Lemon (1976), who was examining the origin of wake vortices shed by thunderstorms.

Both Fankhauser and Lemon went on to construct a generalized three-dimensional pattern of the circulation around an isolated cumulonimbus. Their interpretations are shown in Figure 2.10. Note that neither generalization shows much, if any, detail concerning what is happening in

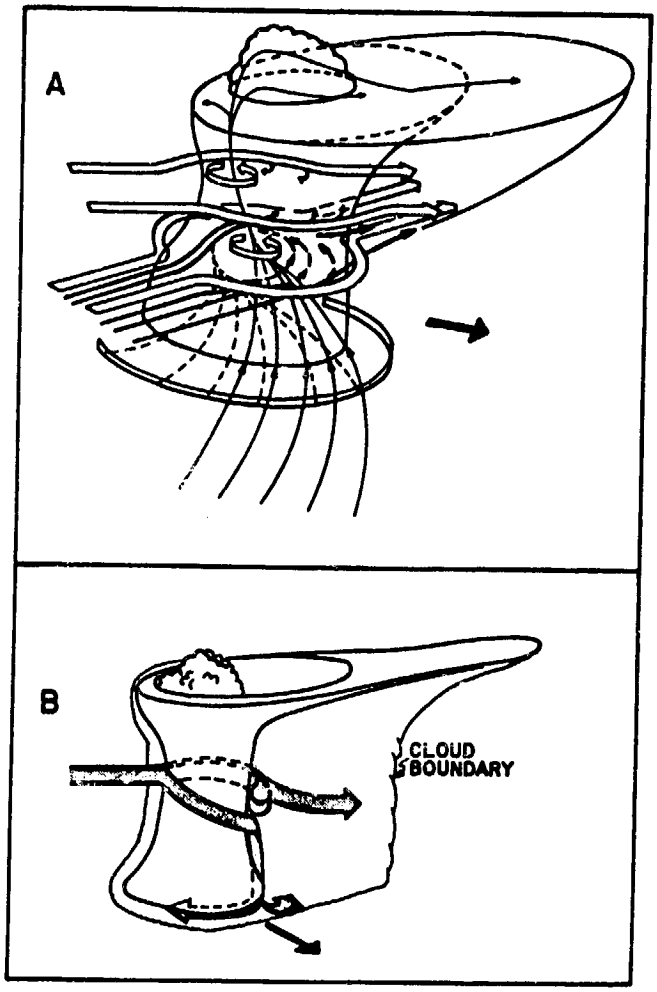

Figure 2.10 - Generalized three-dimensional circulation patterns around an isolated cumulonimbus. A: After Fankhauser (1971). B: After Lemon (1976).

the lee of the storm at the tropopause level, the primary area of interest in this study. However, their diagrams do provide some insight, especially since it has been found that if a cloud is situated under an isothermal or inversion layer, the greater part of the flow will go around rather than over the top of the cloud due to energy considerations (Vinnichenko et al, 1980).

In view of these studies, it appears that if the stable stratospheric air surmounts the thunderstorm, two- or three-dimensional "lee waves" result (Figure 2.11), TNTT occurs in associated rotor circulations and KHI, which form in regions of "lee wave" enhanced vertical shears. If the thunderstorm penetrates well into the stratosphere, the stable air r e forced to go around the thunderstorm,

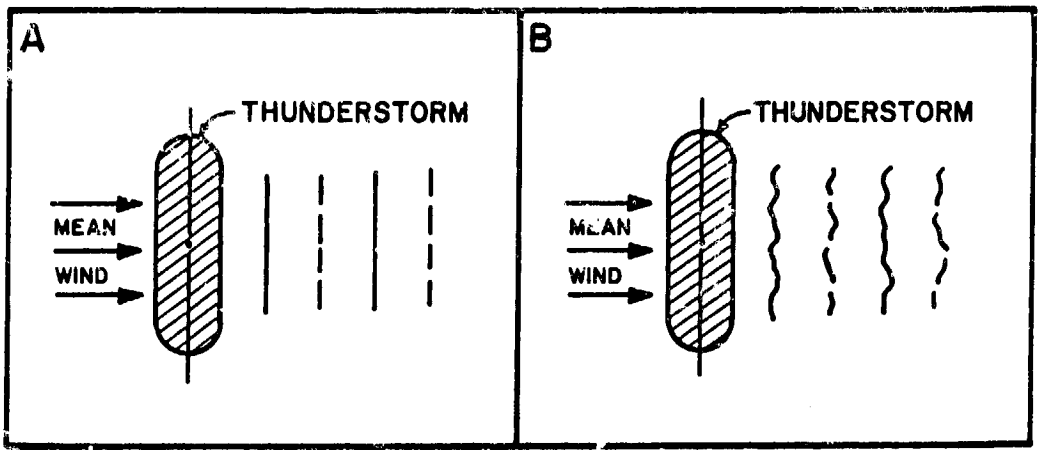

Figure 2.11 - Large amplitude "mountain" waves formed by forcing of flow over the top of a thunderstorm or line of thunderstorms. A: Two-dimensional result. B: Three-dimensional result (due to uneven cloud tops).

producing a wake similar to a Karman vortex trail. In that case, TNTT could also be due to KHI via enhanced vertical shears between horizontal eddies in shallow layers in the wake.

g. Current Capabilities to Observe and Forecast TNTT

Despite the known facts and ongoing research described above, observations of the characteristics of thunderstorm wakes are few and incomplete. Much of the problem is found with the thunderstorm itself. Because it is a moving, mesoscale entity, it is extremely difficult to establish any kind of efficient data collection effort. As a result, observations continue to consist primarily of PIREPS from the isolated aircraft which knowingly or unknowingly stray too close to the thunderstorm and encountered hazardous weather (e.g., severe turbulence which caused injuries).

Current capabilities to forecast TNTT are hampered by these observational deficiencies. Forecasting methods continue to be based primarily in rules of thumb (see Table 2.3) which rely on vague generalized terms to identify the turbulence locations. While there is good agreement that severe turbulence may extend well above the cloud tops and be encountered up to 37 km (20 nm) laterally, forecasters do not have the capability to pinpoint the exact regions where the severe turbulence will (or even may) occur. Instead, they over-forecast the area and intensity. Hence, "forecasting" TNTT often consists of nothing more than

Table 2.3 - TNTT forecasting rules of thumb.

SOURCE	RULES
FAA (1975, 1977)	Turbulence can be encountered several thousand feet above and 20 nm laterally from a severe thunderstorm (TSTM)
	Locations of probable turbulence are: moderate - near dissipating TSTMs and near towering cumuliform clouds severe - near growing and mature TSTMs
USAF (1982)	Turbulence can be encountered several thousand feet above and 20 nm laterally from a severe TSTM
	Severe turbulence is possible in the anvil 15-30 nm downwind
Army (USA, 1982)	Severe turbulence is found in anvil clouds 15-20 nm downwind from severe storm cores
	Severe turbulence is possible in the clear air on the inflow side of a severe storm
	Turbulence above cloud tops: if > 100 knot winds → significant turbulence up to 10,000 feet above cloud top decrease this value by 1000 feet for each 10 knot reduction in wind speed
Delta Air Lines (Chandler, 1987)	In cirrus associated with TSTMs: if relatively light winds → only light turbulence if moderate to strong winds → moderate turbulence near cirrus tops with most turbulence within the last 1000 feet before the top

advising aircrews to look for thunderstorms and avoid them by 37 km (20 nm) or more or, if avoidance is not possible, to minimize the effects of the turbulence (e.g., by flying the recommended turbulence penetration speed for that

aircraft, by tightening seatbelts and shoulder harnesses, etc.; USAF, 1981; USA, 1982).

However, thunderstorms cannot always be seen by the aircrew. If a thunderstorm formed under a cirrus deck and merged into i an aircraft flying in the clear air above the cirrus clouds will not be able to observe it visually. In this case, again the "forecasting" capability is limited to teaching aircrews to tilt their onboard radar downward to find these hidden thunderstorms and then to avoid flying into the area above them (Chandler, 1987).

Chapter 3

Case Studies of TNTT: Methodology

a. General

In order to investigate the utility of DFDR information for the study of TNTT, three cases were selected for analysis from the NASA-Ames archive of DFDR tapes derived from commercial aircraft turbulence encounters. In the present chapter, the NASA-Ames turbulence program and the case selection criteria are presented. Subsequently, the aircraft data processing procedures are outlined and the meteorological analyses are described.

b. The NASA-Ames Turbulence Study

Over the past few years an effort has been under way at NASA-Ames Research Center to investigate clear air turbulence (CAT). The goal of the research program is to better understand CAT-producing mechanisms and the specific influences of particular types of CAT on aircraft. Scientists there have developed a state estimation analysis technique, called SMACK (smoothing for aircraft kinematics), which combines data from several sources to determine aircraft motions along the aircraft trajectory and, usually, an estimate of the winds (Bach and Wingrove, 1985). SMACK combines knowledge of aircraft design and Air Traffic Control (ATC) radar fixes in order to maximize the

usefulness of the DFDR tapes. Specific details concerning their technique will be covered later in this chapter.

A major limiting factor in such studies is the availability of DFDR tapes. Under normal operations, data tapes are retained for later analysis only when the aircraft are involved in unusual events such as extreme turbulence which causes injuries or structural damage. The flight recorder from the aircraft is sent to the National Transportation Safety Board (NTSB) after a serious incident occurs for official investigation. NTSB then retrieves the DFDR information from the recorder, creating a tape. Scientists at NASA-Ames Research Center then obtain a copy of the tape from NTSB, radar position data from ATC en route centers, and meteorological data from other sources for the same time and location. To date, an archive containing reasonably complete data sets for several events has been compiled.

Preliminary analyses of those data sets have been successful in demonstrating the usefulness of SMACK. Cases investigated include mountain wave caused turbulence (near Calgary, Canada; near Morton, Wyoming; and over the Greenland ice cap), and a wind shear accident (at Dallas/Fort Worth). In all cases, the additional insight gained from the use of DFDR tapes and the estimated variables obtained from SMACK was extremely helpful in understanding the cause

of the accidents (e.g., see Parks et al, 1984; Lester and Bach, 1986; Lester et al, 1988).

c. TNTT Case Selection Criteria

TNTT cases were selected from the NASA-Ames archive described above on the basis of three criteria: i) turbulence appears to have been encountered in the vicinity of thunderstorm tops, ii) the turbulence was severe in intensity, iii) continuous DFDR records were available. The three cases which met this criteria are listed in Table 3.1 with dates, times, locations, intensities, and durations of the turbulence events noted.

d. Aircraft Data Processing

DFDR measurements include accelerations, Euler angles, altitude, and airspeed (Bach and Wingrove, 1985). As noted by Parks et al (1982), such records provide enough information for an accurate determination of wind velocity characteristics along the aircraft track, especially when combined with ground-based ATC radar position data.

The DFDR data were not useful immediately, however. Several steps of data manipulation were necessary to prepare it for later calculations. When the tapes were originally obtained from NTSB, formats were different for each case; therefore, the records were initially reorganized into a standard format. Subsequently, a data record "expansion" step was accomplished because the original sampling rates varied according to the parameter measured (see

Table 3.1 - Cases selected for study

	Hannibal	Bermuda	South Carolina
Aircraft	DC-10	DC-10	L-1011
Date	4 Apr 81	12 Oct 83	25 Nov 83
Time (GMT)	0125	0418	0026
Latitude (°N)	39.6	27.0	33.2
Longitude (°W)	91.8	68.7	77.8
Altitude (km)	11.3	11.3	11.3
Turbulence Extremes (g)	-1.91, +0.82	-1.50, +0.62	-2.01, +1.08
Turbulence Duration (s)	43.75	86.50	82.00
Passenger and Crew Injuries	29	12	24
Remarks	Turbulence encountered after passing over top of a line of thunderstorms.	Turbulence encountered near thunderstorms in high pressure area with light winds.	2 turbulent bursts. Aircraft just east of a line of thunderstorms.

Table 3.2). The records were expanded by interpolating all data to 64 Hz to take into account data channel offsets (Bach and Wingrove, 1989). Subsequently, the expanded record was reduced to a homogeneous sample of 4 Hz. This actually led to a data reduction in one parameter of L-1011 data. In addition, some numerical filtering was performed to eliminate high frequency noise in the data. This step first removed all obviously bad data points which exceeded

Table 3.2 - Initial sampling rates for the two aircraft types involved in the incidents studied. Rates are in samples per second.

L-1011		DC-10	
PARAMETER	RATE	PARAMETER	RATE
Roll Attitude	1.00	Roll Attitude	1.00
Pitch Attitude	1.00	Pitch Attitude	1.00
Magnetic Heading	1.00	Magnetic Heading	1.00
Longitudinal Accel.	4.00	Longitudinal Accel.	1.00
Lateral Accel.	4.00	Lateral Accel.	4.00
Vertical Accel.	8.00	Vertical Accel.	4.00
Pressure Altitude	1.00	Pressure Altitude	1.00
Indicated Airspeed	1.00	Indicated Airspeed	1.00
Left/Right Vane	2.00	Left/Right Elevator	1.00
Air Temperature	1.00	Air Temperature	0.50
Stabilator	1.00	Stabilator	0.50
Rudder Position	2.00	Lower Rudder	1.00
L/R Outside Aileron	1.00	Upper Rudder	2.00
L/R Inside Aileron	1.00	Ailerons	1.00
Engine 1/2/3	1.00	Engine 1/2/3	0.25

reasonable limits for each data type. Secondly, data were examined to determine whether any high frequency noise remained. If it did, as in the South Carolina temperature field, the unfiltered data were once again run through the filtering process. A low pass cutoff frequency of 0.1 Hz was found to be appropriate to remove the contaminating noise in that case.

With the data appropriately prepared, the next step was to apply the state estimation technique developed at NASA-Ames to determine the wind field. A schematic of the

general process is shown in Figure 3.1. There are two categories of DFDR data which are used to estimate the winds: inertial data and air data. Inertial data are measurements related to the airframe's response to external forces (e.g., roll and pitch attitudes, aileron and rudder positions), while the air data consists of details about the environment the airframe was encountering (e.g., air temperature, pressure altitude). ATC radar data are added (when available) to provide information from outside the aircraft's frame of reference. Radar information includes

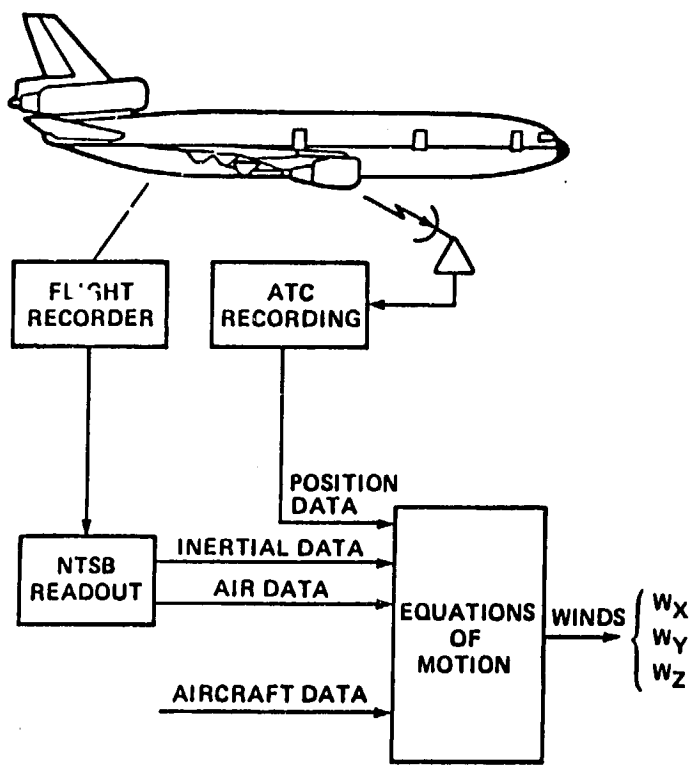

Figure 3.1 - Procedure used to estimate winds from airline operating records (from Bach and Wingrove, 1986).

slant range, bearing, and elevation angles. The final type of information shown in Figure 3.1 is "aircraft data" which includes specifications of the response of particular aircraft types to external forces. All of these data sources are combined with the equations of motion to solve for the winds along the flight trajectory. A detailed explanation of this analysis process following Bach and Parks (1987) is outlined below.

The analysis begins by expressing vehicle accelerations in the Earth frame (here considered locally flat, with the x-axis pointing north, the y-axis east, and the z-axis vertical) as

$$\left.\begin{aligned}
\ddot{x} &= a_x \cos\theta\cos\psi \\
&\quad + a_y(\sin\phi\sin\theta\cos\psi - \cos\phi\sin\psi) \\
&\quad + a_z(\cos\phi\sin\theta\cos\psi + \sin\phi\sin\psi) \\
\ddot{y} &= a_x \cos\theta\sin\psi \\
&\quad + a_y(\sin\phi\sin\theta\sin\psi + \cos\phi\cos\psi) \\
&\quad + a_z(\cos\phi\sin\theta\sin\psi - \sin\phi\cos\psi) \\
\ddot{z} &= a_x \sin\theta - (a_y \sin\phi + a_z \cos\phi)\cos\theta - g
\end{aligned}\right\} \qquad (3.1)$$

where (a_x, a_y, a_z) are on-board measurements of body-axis accelerations and (ϕ, θ, ψ) are on-board measurements of body-axis Euler angles. Integration of the differential equations (Eqn 3.1) provides estimates of inertial velocity $(\dot{x}, \dot{y}, \dot{z})$ and position (x, y, z). A set of initial conditions and bias corrections are determined by matching the

calculated x and y time-histories to radar position data and the z time-history to the measured altitude.

The wind velocity is now computed as the difference between the vehicle inertial velocity and its velocity with respect to the air mass. The wind components in the Earth frame are given by:

$$\left.\begin{aligned} w_x &= \dot{x} - V\cos\theta_w\cos\psi_w \\ w_y &= \dot{y} - V\cos\theta_w\sin\psi_w \\ w_z &= \dot{z} - V\sin\theta_w \end{aligned}\right\} \qquad (3.2)$$

where true airspeed, V, is computed from the flight records and wind-axis Euler angles (θ_w, ψ_w) are found using the identities

$$\left.\begin{aligned} \sin\theta_w &= \cos\alpha\cos\beta\sin\theta - C\cos\theta \\ \tan(\psi_w - \psi) &= \frac{\sin\beta\cos\phi - \sin\alpha\cos\beta\sin\phi}{\cos\alpha\cos\beta\cos\theta + C\sin\theta} \\ C &= \sin\alpha\cos\beta\cos\phi + \sin\beta\sin\phi \end{aligned}\right\} \qquad (3.3)$$

where α is the angle of attack and β is the sideslip angle (Parks et al, 1984; Lester et al, 1988).

The DFDR flight records for L-1011 aircraft include a vane-angle measurement from which the angle of attack may be derived. In the case of DC-10 aircraft, however, no vane measurement exists. The angle of attack must be estimated from the equation

$$C_L = C_L(\alpha,\delta_F) + C_{L_{\delta_e}}\delta_e + C_{L_q}(cq/2V) \qquad (3.4)$$

where $C_L(\alpha,\delta_F)$, $C_{L_{\delta_e}}$, and C_{L_q} are based on the aircraft's

aerodynamics. The lift coefficient, C_L, flap position, δ_F, elevator position, δ_e, and pitch rate, q, are derived from the flight recorder data, leaving the angle of attack, α, as the solved variable (Bach and Parks, 1987). In a similar manner the sideslip angle may be estimated from the equation

$$C_Y = C_{Y_\beta}\beta + C_{Y_{\delta_r}}\delta_r + C_{Y_r}(br/2V) \qquad (3.5)$$

where C_{Y_β}, $C_{Y_{\delta_r}}$, and C_{Y_r} are based on the aircraft's aerodynamics. The side-force coefficient, C_Y, rudder position, δ_r, and yaw rate, r, are derived from the flight recorder data, leaving the sideslip angle, β, as the solved variable (Bach and Parks, 1987).

Estimates of the errors involved in the air motion calculations can be made if the uncertainties in measurements are assumed to be statistically independent and α, β, ϕ, and θ are small. Under these conditions, the error in the horizontal velocity component is given by

$$\delta w_{xy} \simeq [\delta^2 V_{xy} + \delta^2 V + V^2\delta^2(\psi + \beta)]^{1/2} \qquad (3.6)$$

where δV_{xy} is the error in the horizontal-plane component of inertial velocity. Similarly, the error in the vertical velocity component is given by

$$\delta w_z \simeq [\delta^2 \dot{z} + V^2\delta^2(\theta - \alpha)]^{1/2} \qquad (3.7)$$

Table 3.3 shows typical rms errors for horizontal and vertical velocity components for the airliner encounters analyzed at NASA-Ames Research Center (Lester et al, 1988).

Table 3.3 - RMS errors from DFDR plus radar track calculations. Assumptions: level flight and $V \approx 250\ ms^{-1}$ (from Lester et al, 1988).

δw_{xy}		δw_z	
ERROR SOURCE	ERROR (ms^{-1})	ERROR SOURCE	ERROR (ms^{-1})
δV_{xy}	1.0	$\delta \dot{z}$	1.0
δV	1.0	$V\delta(\theta - \alpha)$	2.0
$V\delta(\psi + \beta)$	2.0		

When complete data sets are available, the winds are determined by following the procedure detailed above. Unfortunately, of the three cases selected for study, only Hannibal and South Carolina have complete data sets. ATC radar fixes are not available for the Bermuda case.

The lack of ATC radar data does not eliminate the possibility of determining the winds. Equations 3.1 can still be integrated to estimate the inertial velocities ($\dot{x}$, $\dot{y}$, $\dot{z}$) and positions (x, y, z). At this point, however, there are no radar positions available to compare with the calculated x and y time-histories. Initial conditions and bias corrections must be determined independently and inserted into the program, SMACK. As a result, there is a loss of accuracy in the horizontal fields with possible ambiguities introduced into the horizontal winds. It is important to note, however, that this problem has little effect on the vertical velocity calculations.

In many cases, the effects of the missing ATC radar fixes can be minimized. Since most severe turbulence incidents occur in areas with strong environmental winds, it is fairly easy to determine an accurate initial wind to start the calculation. Multiple runs can be made to fine tune this initial condition until a reasonable level of confidence is obtained. Also, as the calculated fields are compared with the observations that are available in the area, biases can be identified and corrected.

The Bermuda case, however, presented an extremely difficult problem. The incident occurred in the middle of a high pressure area where the environmental winds were essentially light and variable. This made it extremely difficult to determine an accurate initial wind to start the calculation. Furthermore, since the aircraft's position could not be determined precisely, the relationship between the aircraft track and the meteorological systems in the area also could not be determined.

Several experiments were carried out in an attempt to recover the horizontal winds for the Bermuda case. Using the reported flight track as a starting point, a best guess for an initial wind was made, and SMACK was run. The results were less than satisfactory with excessive wind speeds calculated over much of the track. Several additional attempts were made, varying the initial wind in an attempt to derive a more reasonable field when compared to

the available meteorological data. Acceptable results (i.e., agreement with the synoptic analyses) were never obtained. One of the main problems was an apparent uncorrected bias in the calculations which resulted in steadily increasing calculated wind intensities along the flight track. This intensification was consistent enough in the early runs to verify that a bias probably existed, however, even if the bias was successfully removed, the ambiguity of the meteorological observations in the area would make it impossible to derive a horizontal wind field with much confidence. Therefore, further experiments were terminated.

e. Meteorological Data Analysis

Since the turbulence measurements considered here were gathered by commercial aircraft, there was no preplanned program to collect supporting meteorological observations as one might expect in a coordinated research effort with an instrumented aircraft. Therefore, in the present study, thorough use was made of conventional meteorological data available near both the location and the time of the turbulence encounter.

The general approach to the investigation and of meteorological conditions was a "multi-scale" analysis scheme similar to that described by Lester et al (1988). In this procedure, not only are the microscale details of the turbulence examined, but the mesoscale and macroscale environments are also documented to the extent that the

available data will allow. The latter analyses aid in the identifications of larger scale meteorological phenomena which "force" the turbulence, i.e., support shear and stability conditions conducive to turbulence production. Documentation of the turbulence environment is also important since current methods of forecasting turbulence significant to aircraft are based on the more easily observed large-scale flow features.

Specific event documentation and analyses were designed to answer three questions: i) What were the turbulence characteristics? ii) What caused the turbulence? iii) Could the turbulence have been anticipated?

Eyewitness descriptions of the turbulence encounters for each of the cases were summarized from the incident reports files by the crew members and from the NTSB reports.

Macroscale ($-\beta$) conditions were documented for each case with the available constant pressure height and wind analyses nearest to flight level (250 mb) and time of the turbulence incident. Since TNTT is of interest here, surface features commonly associated with thunderstorm occurrence (e.g., fronts and squall lines) were superimposed on the upper level charts for a composite presentation.

Details of the vertical atmospheric structure in the vicinity of the TNTT were provided by nearby soundings for

the Hannibal and South Carolina cases. None were available for the Bermuda case.

Visible and Infrared (IR) data from the Geosynchronous Orbiting Earth Satellite (GOES) were used to map the extent of the thunderstorm tops. These data also allowed the estimation of cloud top heights from IR and enhanced IR images when nearly simultaneous soundings were also available. It is estimated that the positioning of the cloud boundaries from the GOES data due to the gridding error of the image and the parallax error due to cloud height and latitude are ±14 km, ±7.5 km, and ±10 km for the Hannibal, Bermuda, and South Carolina cases, respectively (NWA, 1986).

The regions of primary convective activity for the Hannibal and South Carolina cases were mapped from available weather radar reports (NOAA, 1979). None were available for the Bermuda case. Radar echo distributions were integrated with satellite data and aircraft position reports to determine the aircraft location relative to both the region of most intense convection and the anvil.

Mesoscale ($-\alpha$, $-\beta$) analyses of the horizontal winds at flight level near the TNTT incident were combined with radar echo distributions to determine whether there was any local deformation of the flow field around or over the thunderstorms. These analyses were based mainly on winds determined from the DFDR tape of the involved aircraft.

Reports (AIREPS, PIREPS) were also used when available. The confidence in the latter reports was considerably less than that in the computed DFDR winds because of the lack of precision in the aircraft positions (e.g., see Lilly, 1978), and because the aircraft were commonly at different altitudes and reported at different times. The suspected three-dimensional characteristics of the events studied here as well as the significant and rapid temporal changes in the thunderstorm structures make the use of such reports questionable for any sort of composite analysis.

Quantitative small-scale (meso-γ, micro-α, and micro-β) details of the TNTT incidents were derived solely from the DFDR information. These include the distribution of vertical accelerations, vertical motions, and potential temperatures along the aircraft track, relative to both thunderstorm locations and the known horizontal wind distribution. Further analysis included the determination of some simple statistics (i.e., means and variances) to allow a more quantitative inter-comparison of cases. Also, potential temperature and wind data acquired during large-altitude excursions during the turbulence events were used to estimate related vertical shears, stabilities, and Richardson numbers. Table 3.4 lists the observed and derived variables used in the analysis of the meso- and microscale details for each case.

Table 3.4 - Observed, derived, and computed turbulence parameters.

OBSERVED AND DERIVED PARAMETERS	
PARAMETER	SOURCE
$\ddot{z}$	DFDR vertical accelerations (measured)
w_x, w_y, w_z	Processed DFDR wind velocity components (derived)
CALCULATED PARAMETERS	
PARAMETER	COMPUTATIONAL FORMULA
DFDR Potential Temperature	$\theta_i = T_i \left(\frac{1000}{p}\right)^{.286}$
Turbulent Kinetic Energy (TKE)	$\overline{TKE} = \frac{1}{2} \overline{[(w_x)'^2 + (w_y)'^2 + (w_z)'^2]}$ Where: Average parameter along flight track $(\bar{\ }) = \frac{1}{N} \sum_{i=1}^{N} (\ )_i$ Number of data points = N Turbulence parameter $(\ )_i' = (\ )_i - (\bar{\ })$
Vertical Shear	$\frac{\partial V}{\partial z} \approx \frac{V_{ii} - V_i}{(Z_{ii} - Z_i)}$ Where: Horizontal wind vector = V
Stability	$\frac{\partial \theta}{\partial Z} \approx \frac{(\theta_{ii} - \theta_i)}{(Z_{ii} - Z_i)}$
Richardson Number	$Ri = \frac{g\left(\frac{\partial \theta}{\partial Z}\right)}{\theta\left(\frac{\partial V}{\partial Z}\right)^2}$

In addition to the observed and computed parameters listed in Table 3.4, several other analyses were considered for the high frequency DFDR samples available here. For example, Dutton (1969), Lester (1972), Lester and Fingerhut

(1974), Lilly (1978), and others have performed a wide variety of statistical analyses on high frequency turbulence data gathered by specially instrumented aircraft. These included the construction of spectra to determine the distribution of energy as a function of horizontal scale, and the computation of several terms of the budgets of momentum, temperature variance, and turbulent kinetic energy. Such analyses generally aid in the determination of those atmospheric processes which are important in the production, transport, and dissipation of turbulence.

Clearly the high frequency nature of the DFDR information presents an opportunity to extend the description of the turbulence beyond the parameters listed in Table 3.4, i.e., to spectra and energy budgets; however, to date such analyses of the NASA-Ames turbulence cases have met with mixed results at best (Lester, 1988). Certain difficulties have raised questions about the validity of some statistical analyses and, it follows, of physical interpretations based upon those analyses. The problems include: i) low signal to noise ratio in light turbulence (e.g., see Table 3.3), ii) reduction of useful information in the highest frequencies of records of derived variables is caused by mixed sampling rates (e.g., see Table 3.2), iii) highly intermittent turbulence invalidates homogeneity assumptions upon which several of the more sophisticated statistical analyses are based, iv) large vertical excursions of the

aircraft through layers which are strongly stratified causes heterogeneous samples, and v) although there is a likelihood of strong three-dimensional flow, measurements along a single flight track are often limited to two--dimensional interpretations. Some of these problems may be overcome in the future by very careful experiments, e.g., using low pass filters rather than the more common Reynolds averaging rules (Lester, 1972), however, such analyses are beyond the objectives and scope of the current study.

In summary, DFDR samples are typically short, unhomogeneous, and subject to measurement errors, especially in the highest frequencies. For these reasons, extensive statistical analyses will not be used in the current study, i.e., quantitative descriptions of the microscale turbulence in the following Chapter are limited to those listed in Table 3.4.

Chapter 4

ANALYSIS

a. Hannibal

On 4 April 1981, at 0125 GMT, a United Airlines DC-10 traveling from Los Angeles to New York encountered severe turbulence at 11.3 km AGL near Hannibal, Missouri (Figure 4.1[1]). According to the aircrew statements, just prior to the incident the aircraft was passing through thin cirrus. Lightning flashes could be seen below and to the sides; the aircraft's radar antenna had to be tilted down six to seven degrees before echoes were observed "approximately twenty miles to the right and twenty miles to the left of course." The aircraft exited the cirrus a few seconds later and entered a second "clearly formed cloud" which was illuminated "by a lightning flash off to the side and below." Subsequently, "a strong jolt followed by several others in quick succession" was experienced. Although the turbulence lasted "only a brief time," it resulted in twenty-nine injuries to passengers and crew members. The flight was diverted to Chicago, where medical attention was given to the injured (Daley, 1981; Rossiter, 1981; Taylor, 1981).

The macroscale (-β) weather conditions at the time of the incident are shown in Figure 4.1. At 0000 GMT on 4

---

[1] For clarity, all figures are located at the end of each case description.

April 1981 the axis of a southwesterly jet stream with 250 mb winds exceeding 140 knots was located just northwest of Hannibal, MO. During the previous 12 hours, the jet stream had propagated eastward at about 10 knots. Thus the southwesterly winds at the site of the turbulence incident (about 120 knots at 0000 GMT) very likely increased during the next hour and 25 minutes, i.e., up to the time of the incident.

Associated with the approaching upper level trough in Figure 4.1 is a surface frontal system well to the west. A more important surface feature, which will be shown to be closely related to the turbulence event, is the squall line located just west of Hannibal. This squall line was moving east-northeastward ahead of the front, traveling from western Missouri to just west of Hannibal in the previous 5-6 hours.

Infrared (IR) satellite imagery of the area (Figure 4.2a) shows extensive baroclinic cirrus extending from Kansas eastward across Illinois at 0100 GMT, about a half hour before the turbulence incident near Hannibal. Enhanced images at the same time and for an hour later (Figure 4.2b,c) show a band of high cloud tops (inferred from the regions of coldest temperatures) in the vicinity of the intensifying squall line shown in Figure 4.1.

The nearest upper air soundings to the incident are the two downstream stations in Illinois (Peoria, PIA, and

Salem, SLO, Figure 4.1). Considering the orientation and propagation of the jet stream, the PIA sounding is taken as the most representative of conditions at the time of the turbulence encounter near Hannibal. As shown in Figure 4.3, the sounding profile indicates a relatively dry layer extends from 2 km to 6.5 km, indicating the squall line is still approaching the station. A calculation of the Showalter stability index results in a value of -2°C so thunderstorms are likely. The wind profile indicates southwesterly directions throughout the entire depth of the atmosphere with speeds gradually increasing with altitude to a peak value of 128 knots at 12 km.

Comparing cloud top temperatures determined from the enhanced IR satellite images (Figure 4.2) with the PIA temperature profile, cloud tops near Hannibal appear to be near 11.4 km. This may be compared to 0000 GMT tropopause heights of 11.7 and 12.3 at PIA and SLO, respectively. Thus, the aircraft flight level appears to be very close to both the tropopause and the cloud tops.

Figure 4.4 is an enlargement of the area within the rectangle shown in Figure 4.1. The radar echoes associated with the squall line, as observed by the St. Louis, MO (STL) weather radar, are shown for 0125 GMT. The aircraft track and turbulence location are shown for reference purposes. The point of the turbulence occurrence is clearly over the band of echoes, just east (downstream) of the most

intense returns. Notice the echo band is oriented in a south-southwest to north-northeast line, so the prevailing 250 mb winds (Figure 4.1) intersect the band at about a 40° angle. Echo intensities show a maximum DVIP* level of 5, indicating intense precipitation at the small black dot to the southwest of the turbulence location. Comparison with the radar echoes from 15 minutes earlier (not shown) indicates maximum DVIP levels of 4, indicating rapid intensification occurred in the area.

Fine-scale details of the turbulence incident are illustrated by several DFDR parameters. For example, Figure 4.5 shows the records of vertical acceleration and aircraft altitude for a six minute (about 110 km) segment of the aircraft track which includes the turbulence event. The flight was relatively smooth for the first 200 s. Thereafter, vertical accelerations became large with a maximum deviation of -1.908 g from normal gravity (+1.0 g) occurring at an elapsed time of about 210 s in Figure 4.5 (0124 GMT). Such acceleration values correspond with extreme turbulence. Light turbulence (deviations less than 0.5 g) continued for about 80 s after that point and then smooth flight was resumed. Height excursions of as much as 152 m

---

*Digital Video Integrator and Processor (DVIP) represents reflectivities as intensity levels, which are related to rainfall rates (estimated from the reflectivities).

are a result of both controlled and uncontrolled aircraft responses to the turbulence.

Computed vertical velocities and potential temperatures along the aircraft track are shown in Figure 4.6. A bias has been removed from the vertical velocity (w_z) to ensure that the mean is zero in nonturbulent regions. Excluding the turbulent region, nodes (w_z=0) in the vertical velocity record are noted at elapsed times of 50 s, 150 s, 250 s, and 350 s. These suggest some type of wave in the w_z field with a period of 200 s. Crests are found at elapsed times of about 50 s and 250 s, and troughs near 150 s and 350 s in Figure 4.6. For a standing wave, a period of 200 s yields a wave length of 60 km assuming an aircraft speed of 300 ms^{-1}. That distance is about the width of the DVIP level 3 band in the squall line which the aircraft traversed prior to encountering the turbulence (Figure 4.4). A schematic of the suggested wave pattern is shown at the top of Figure 4.6. Actual passage of the aircraft over the midpoint of the squall line was at about 135 s into the record.

The intense turbulence in Figure 4.6 is included in the updraft region of the long (60 km, 200 s) wave described above. The turbulence itself is characterized by much shorter time scales, and very large vertical velocities (i.e., $-24\ ms^{-1} < w_z < +15\ ms^{-1}$).

If the quasi-periodic motions in the vertical velocity record (Figure 4.6) are associated with a gravity wave, a strong correlation with the potential temperature (θ) record would be expected. For example, if θ is measured in horizontal flight through the waves, it would be expected to be lower in wave crests and higher in wave troughs. However, such a relationship isn't immediately obvious in Figure 4.6, most likely due to altitude variations by the aircraft. If the stability is strong and the slope of the aircraft track is much steeper than the slopes of the streamlines, then a more obvious correlation would be expected to be found between θ and aircraft altitude rather than between θ and vertical velocity. Figure 4.7 shows the records of both θ and altitude along the aircraft track. Disregarding the approximately ± 0.67 K noise band in θ, it appears that there is indeed a correlation between θ and the primary altitude changes (see Figure 4.7), i.e., θ tends to decrease during descents and increase during ascents.

Although the information in Figure 4.7 is not useful for determining the suspected wave characteristics, it can be used to determine stability characteristics of the atmosphere in the vicinity of the turbulence encounter. In the present case, the maximum lapse rate of potential temperature is 12 K(152 m)$^{-1}$ (79 Kkm^{-1}), i.e., an extremely stable value which conclusively places the aircraft in the

lower stratosphere. Note that this computed stability value is much greater than that indicated in the PIA sounding at the same height (Figure 4.3). Such a deviation may have been due to a significant modification of the stability structure as the upper tropospheric airflow was disturbed by the squall line.

The horizontal wind direction record (Figure 4.8) also displays a sinusoidal oscillation along the flight track. With the exception of the large direction variations associated with the turbulence event, directions back gradually about ten degrees as the aircraft passes over the squall line, then veer ten degrees through the turbulence region, finally backing about twelve degrees to the end of the record.

Wind speeds (Figure 4.9) smoothly increased to a maximum of more than 150 knots as the aircraft crossed the location of the squall line. Speeds decreased to about 130 knots in the vicinity of the turbulence, jumped to more than 170 knots, then decreased irregularly thereafter.

Vertical velocities (Figure 4.6) are also superimposed on the horizontal speeds of Figure 4.9. A negative correlation, i.e., negative vertical velocities at the same location as a relative wind maxima, is apparent near elapsed times of 100 s and 300 s. Although at the latter time, the relationship is somewhat masked by turbulence, the total pattern is suggestive of the downward momentum

transport commonly found in mountain lee waves (e.g., Durran, 1986).

In a manner similar to the previously discussed stability calculations, vertical vector wind shear was determined to be 5.9×10^{-2} s^{-1} at the location of the maximum altitude deviation along the aircraft track (see Figures 4.5, 4.8, and 4.9). This value is more than six times the threshold value associated with CAT (USAF, 1982), however, its significance should be interpreted with some caution. Because of the rapid changes of aircraft attitude within the turbulent region, there is less confidence in the wind calculations at that location. Also, turbulent regions are commonly characterized by large horizontal as well as vertical shears (e.g., Lester, 1972). It is not possible to discriminate between those gradients on the basis of the available data.

The data discussed above suggest that the intense convective activity associated with the squall line (Figure 4.4), is acting as a barrier to the relative flow, resulting in "mountain wave"-like disturbances in the lee. Furthermore, the turbulence is associated with the updraft region of the primary wave. The suggested mesoscale flow pattern is inherently two-dimensional and has led to some prior, related analyses.

The preliminary analysis of the incident was accomplished by NTSB (1981). On the basis of the available, raw

DFDR records and crew descriptions, it was concluded that the cloud which the aircraft entered just prior to the turbulence was a lenticular (wave) type, produced by flow over the thunderstorm; furthermore, the severe turbulence occurred when "the aircraft transversed the updrafts that were producing the cloud."

Keller et al (1983), used a two-dimensional, nonlinear primitive equation model of the atmosphere to further investigate the possibility that the turbulence was related to gravity waves generated by the squall line. When the model was initialized with available upstream wind and temperature data and suitable lower boundary conditions, it produced a large amplitude "mountain wave" disturbance near the "obstacle" at, and above, flight level. Regions of low Ri within this disturbance were interpreted as localized turbulence zones, i.e., KHI produced by enhanced vertical shears in the gravity waves.

In the current study, the stability and vertical wind shear calculations presented earlier were combined to estimate Ri from the actual aircraft data in the primary turbulence region. The Ri value was determined to be 0.4. Since the calculation was conducted over a depth of 152 m, it is possible that regions of Ri less than the critical value for turbulence breakdown ($Ri \leq 0.25$) were embedded within the layer. However, as noted by Wallace and Hobbs (1977), once turbulence has been established within a shear

layer (e.g., in the current case), energy considerations indicate that it will be maintained as long as Ri does not exceed 1.0.

The small-scale structure of the turbulence zone in the Hannibal case was considered by Mehta (1984) and Parks et al (1984) at NASA-Ames Research Center. They noted that the vertical velocity profiles along the aircraft track (especially in the immediate vicinity of the turbulence) exhibited patterns suggestive of the so-called "cat's eye" vortex pattern which is produced by KHI (e.g., Scorer, 1978). A simple analytic vortex model was constructed to simulate the horizontal and vertical wind fields which would be experienced by the passage of an aircraft through, or near, such vortices. The comparison between model results and the DFDR estimate from the Hannibal case was good, albeit not perfect.

The analysis by NTSB (1982), Keller et al (1983), and Mehta (1984), as described above, are similar in that all interpret the flow disturbances two-dimensionally. These are reasonable first approximations because of the two-dimensional character of the squall line which appears to have forced the event. However a closer examination of both the topography of the squall line (Figure 4.4) and the variation of the wind along the flight track (Figures 4.8 and 4.9) reveals potentially important three-dimensional features.

An expanded view of the radar echo distribution near the aircraft track (the area within the rectangle on figure 4.4) is shown in figure 4.10. Flight level winds determined from the DFDR data are shown at 15 s intervals (about 4.5 km). The wind vectors are approximately parallel except immediately downstream of the turbulence location (Figure 4.10). East of that point the winds veer and increase over a distance of about 30 km (see also figures 4.8 and 4.9).

The dashed lines in figure 4.10 are drawn from the boundaries of the disturbed region along the aircraft track, upwind to an isolated area of high intensity radar returns (DVIP $\geq$ 5 indicated by the black dot in Figure 4.10). The lines enclose an apparent wake, with a wedge angle, θ, similar to those noted in ship wake patterns discussed in Chapter 2. Here θ equals 6-7°, an angle somewhat less than, but similar to, those measured by Gjevik and Marthinsen (1978) in their diverging wave-type cases.

In addition to the circumstantial evidence presented in Figures 4.10, several other characteristics favorable to three-dimensional wake production are also present. These include strong stability, strong vertical wind shear, and, for turbulence, low Richardson number. These necessary (but not sufficient) conditions suggest that the disturbed area is a three-dimensional lee wave, specifically of the ship wake variety. The obstacle generating the wake then

would be a growing convective cell indicated by the higher DVIP region located 14 km to the south of the flight path (Figure 4.10).

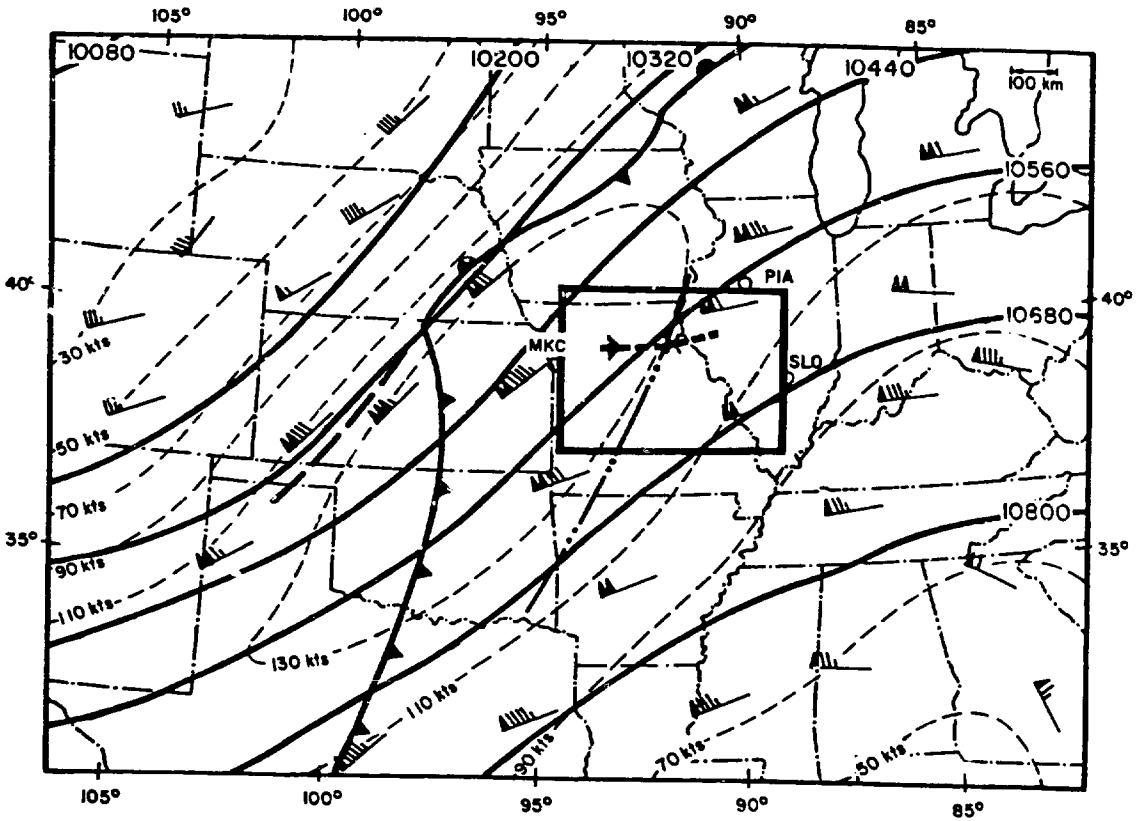

Figure 4.1 - Large-scale view of meteorological conditions in the vicinity of Hannibal, MO on 4 April 1981. NMC surface frontal positions for 0000 GMT are superimposed with NMC 250 mb winds, isotachs, and contour lines. The dashed line within the rectangle shows the flight path. The X indicates the severe turbulence location near Hannibal. Isotachs are shown with thin dashed lines.

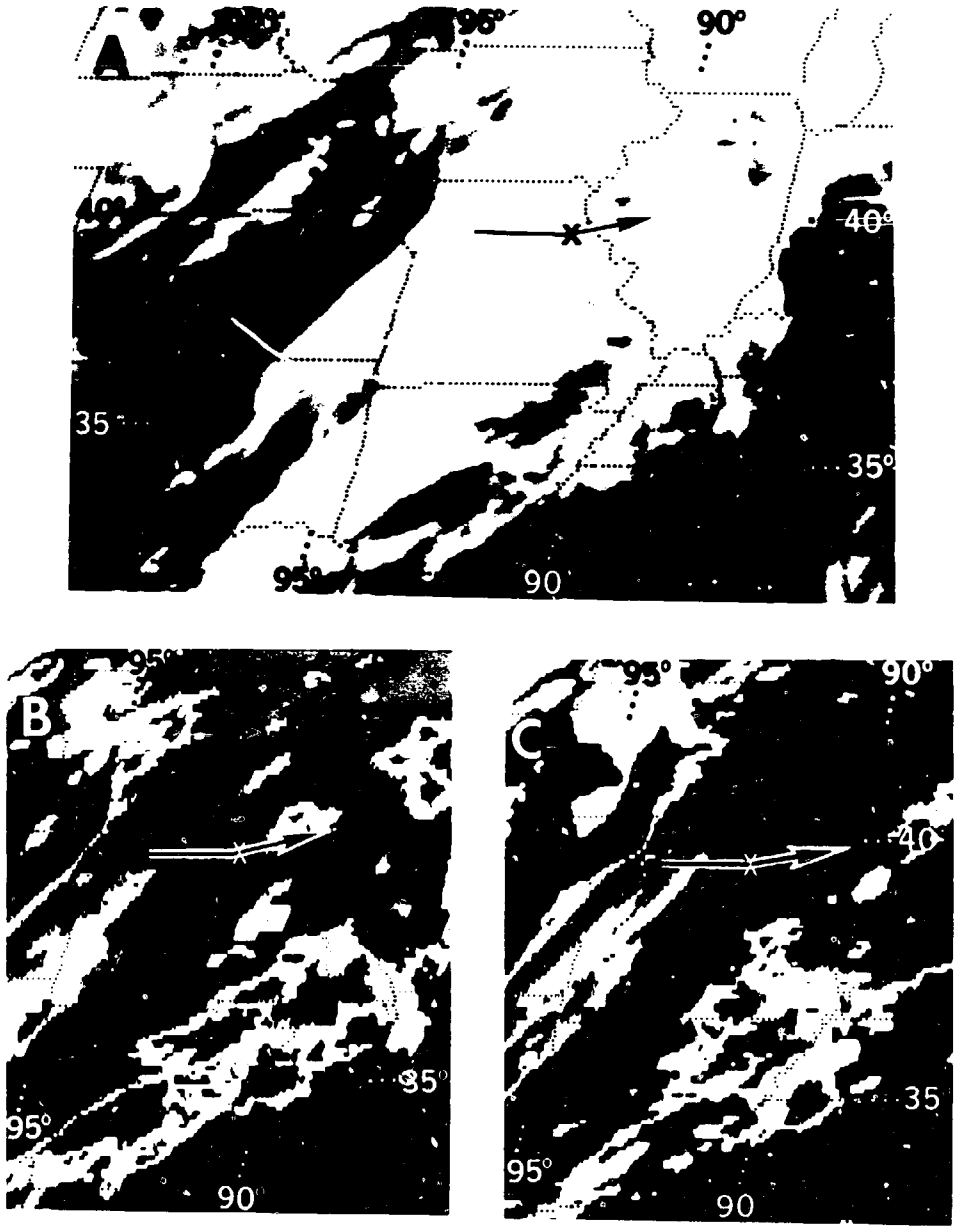

Figure 4.2 - IR satellite images for the Hannibal, MO case of 4 April 1981. (A) IR at 0100 GMT. (B) Enhanced IR at 0101 GMT. (C) Enhanced IR at 0200 GMT. On all images the black and white line and the "X" indicate flight track and incident location, respectively. On the enhanced images the dot-dot-dash line indicates the squall line. The enhancement is research curve 61 with gray scale temperatures within the images: normal IR curve (>-20°C), white (-20 to -34°C), dark gray (-34 to -44°C), light gray (-44 to -54°C), black (-54 to -59°C), repeat white (-59 to -64°C).

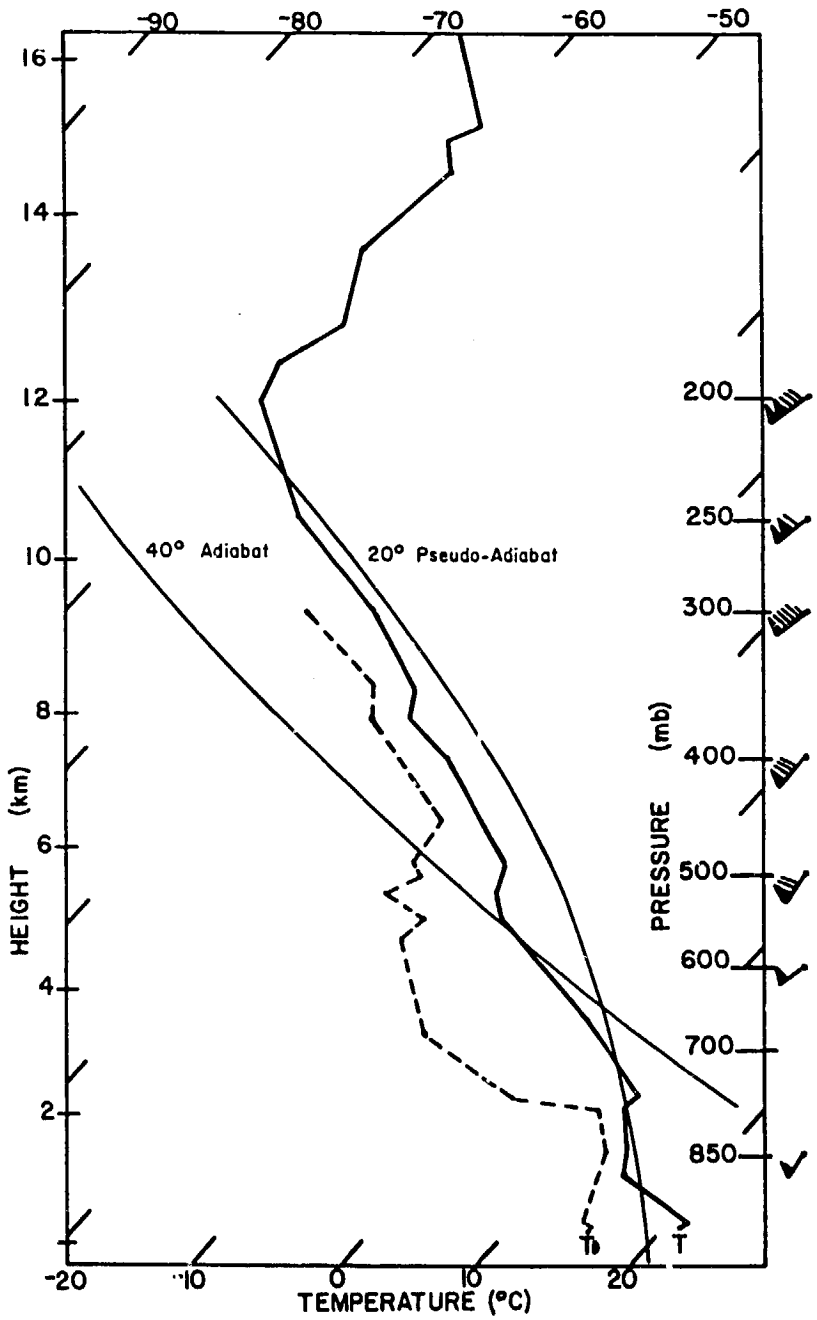

Figure 4.3 - Sounding plot for Peoria, Illinois valid at 0000 GMT on 4 April 1981. Height scale is based on reported height surfaces in geopotential meters.

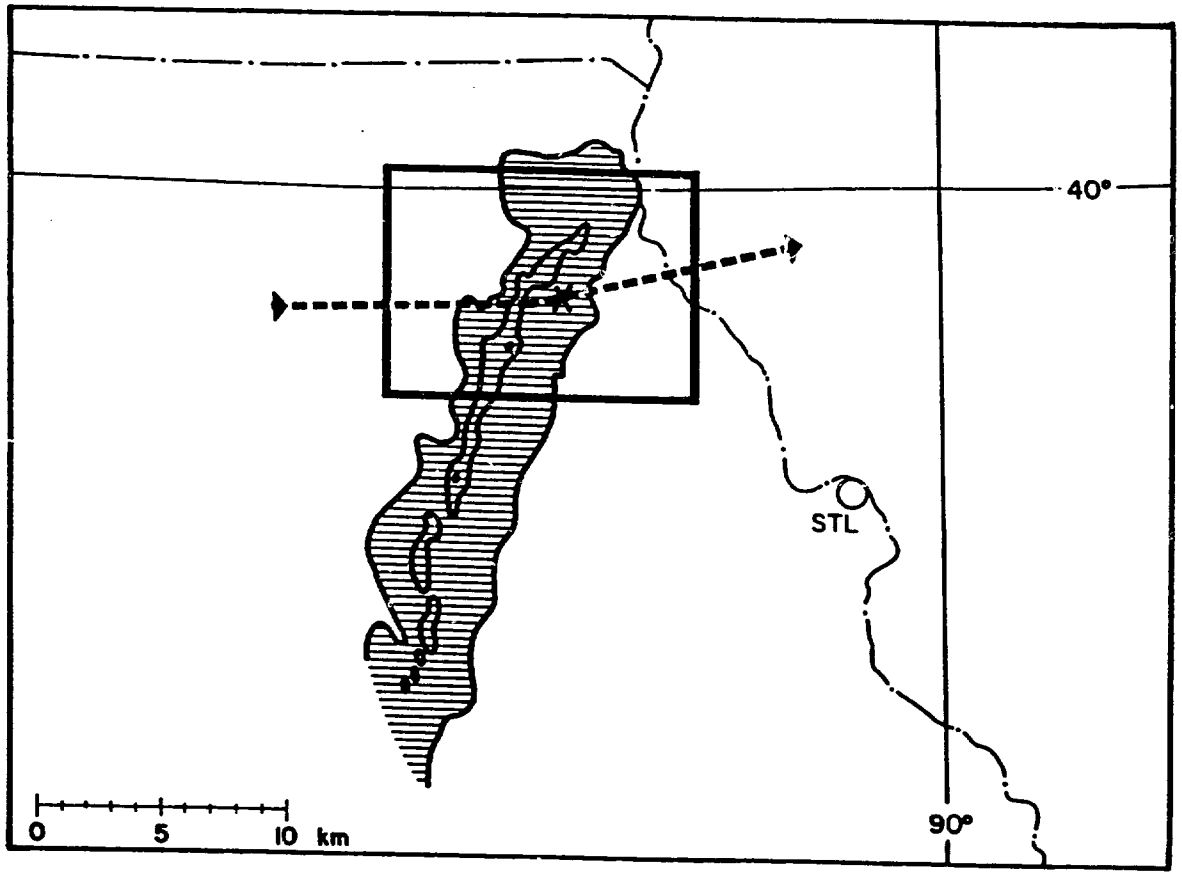

Figure 4.4 - Distribution of radar echoes at 0130 GMT on 4 April 1981. The STL radar returns are shown for the region enclosed by the rectangle in figure 4.1. DVIP 1 and 3 levels are hatched, DVIP 5 levels are solid. A dashed line and X indicate the flight path and incident location, respectively.

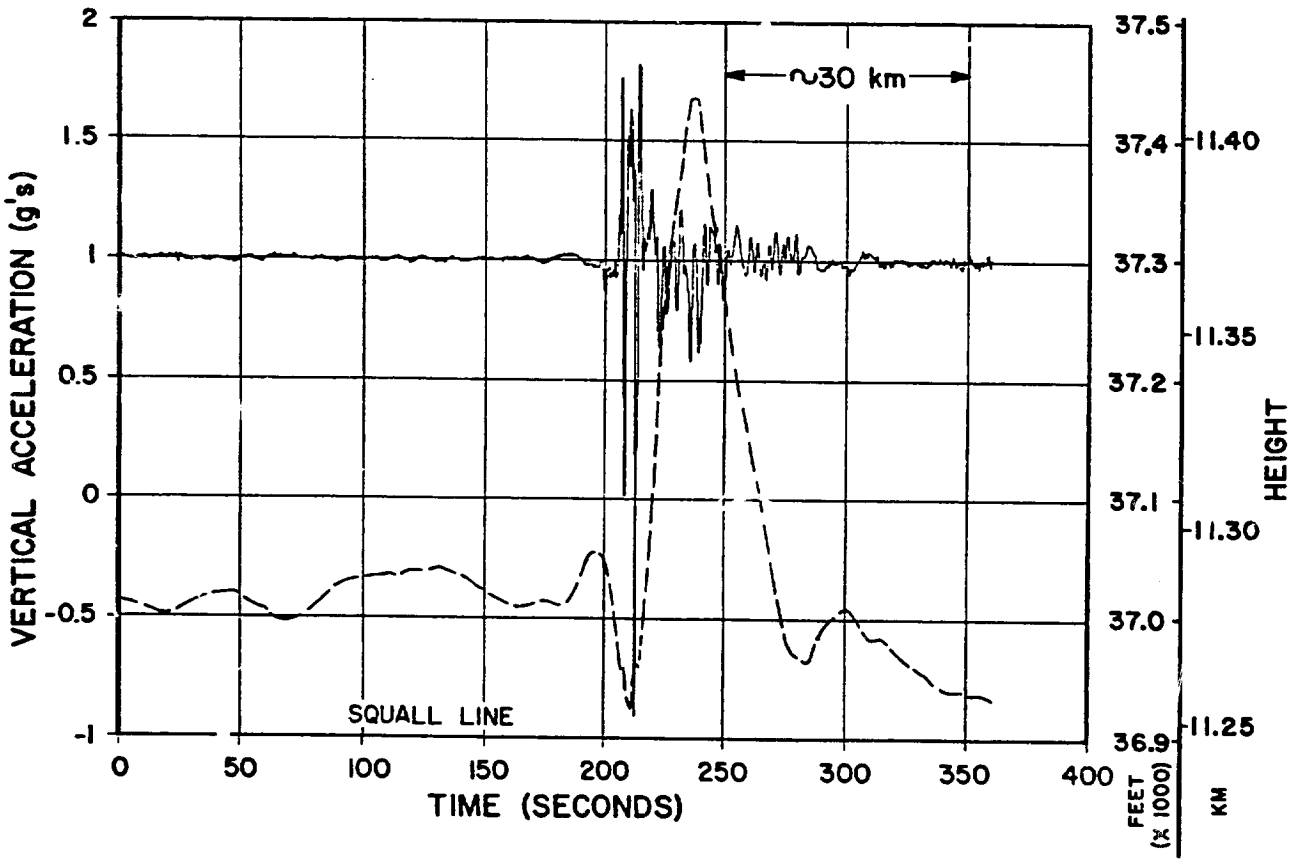

Figure 4.5 - Flight data: Vertical acceleration (solid) and altitude (dashed) along the flight path for the Hannibal, MO case from 0121 to 0127 GMT on 4 April 1981. "Squall line" indicates the approximate time the squall line was passed.

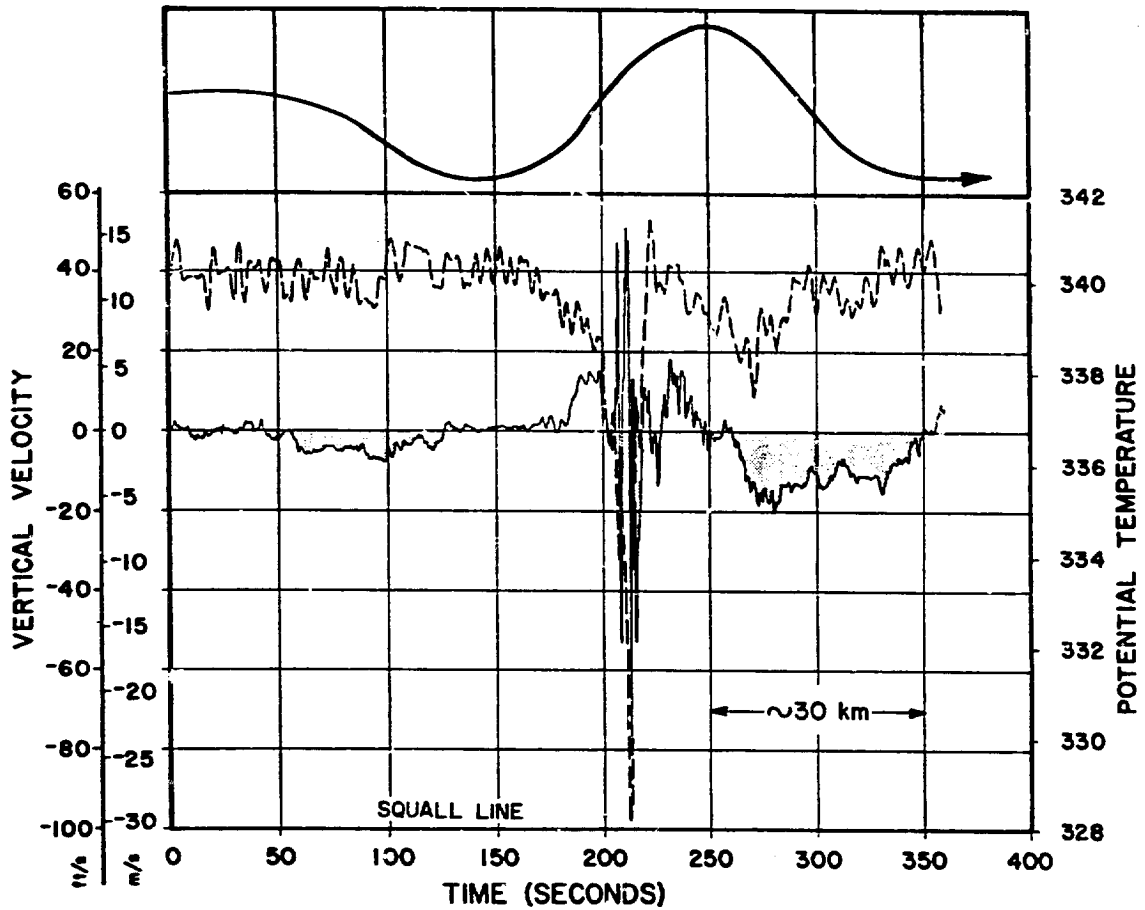

Figure 4.6 - Flight data: Vertical velocity (solid) and potential temperature (dashed) along the flight path for the Hannibal, MO case from 0121 to 0127 GMT on 4 April 1981. A schematic streamline of the phase relationships is presented at the top. Negative values of vertical velocity are shaded. "Squall line" indicates the approximate time the squall line was passed.

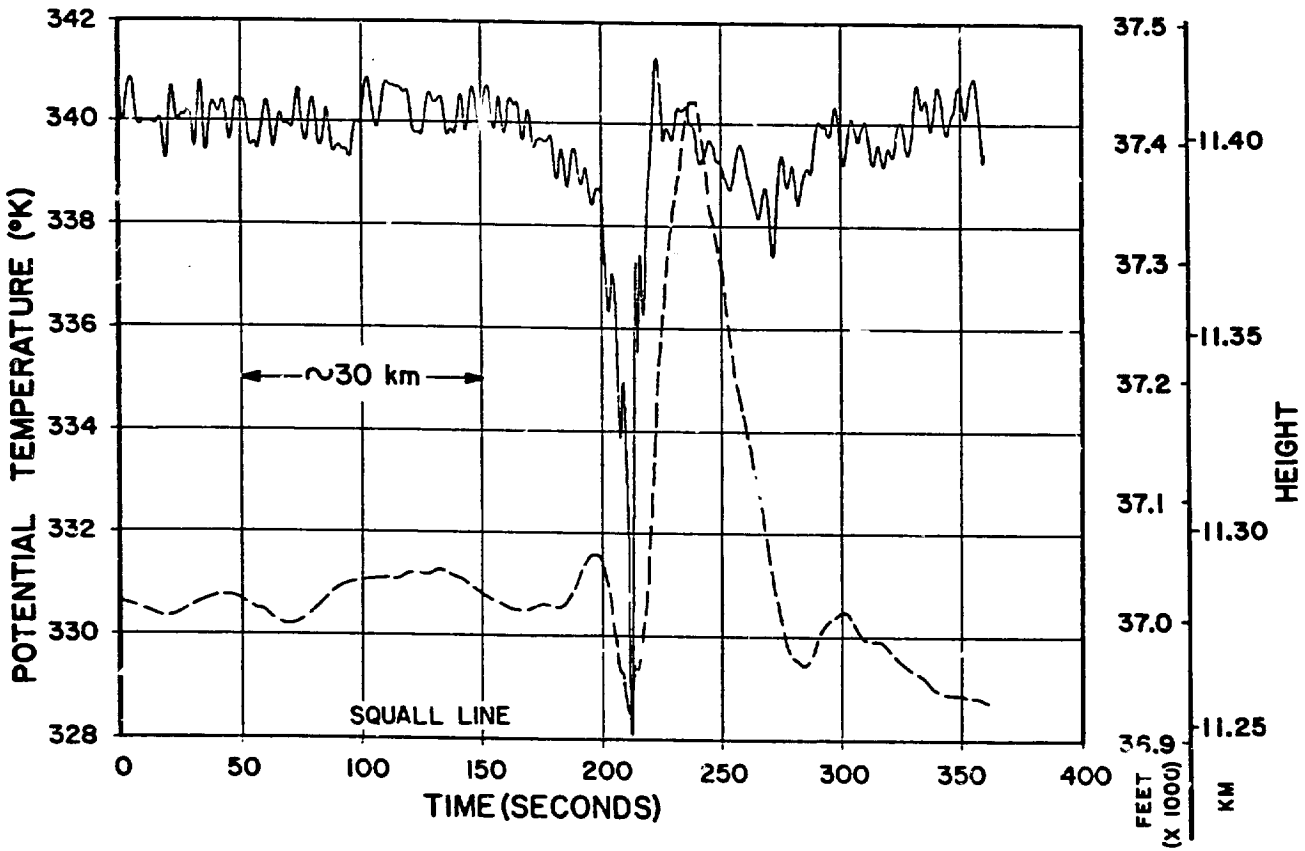

Figure 4.7 - Flight data: Potential Temperature (solid) and altitude (dashed) along the flight path for the Hannibal, MO case from 0121 to 0127 GMT on 4 April 1981. "Squall line" indicates the approximate time the squall line was passed.

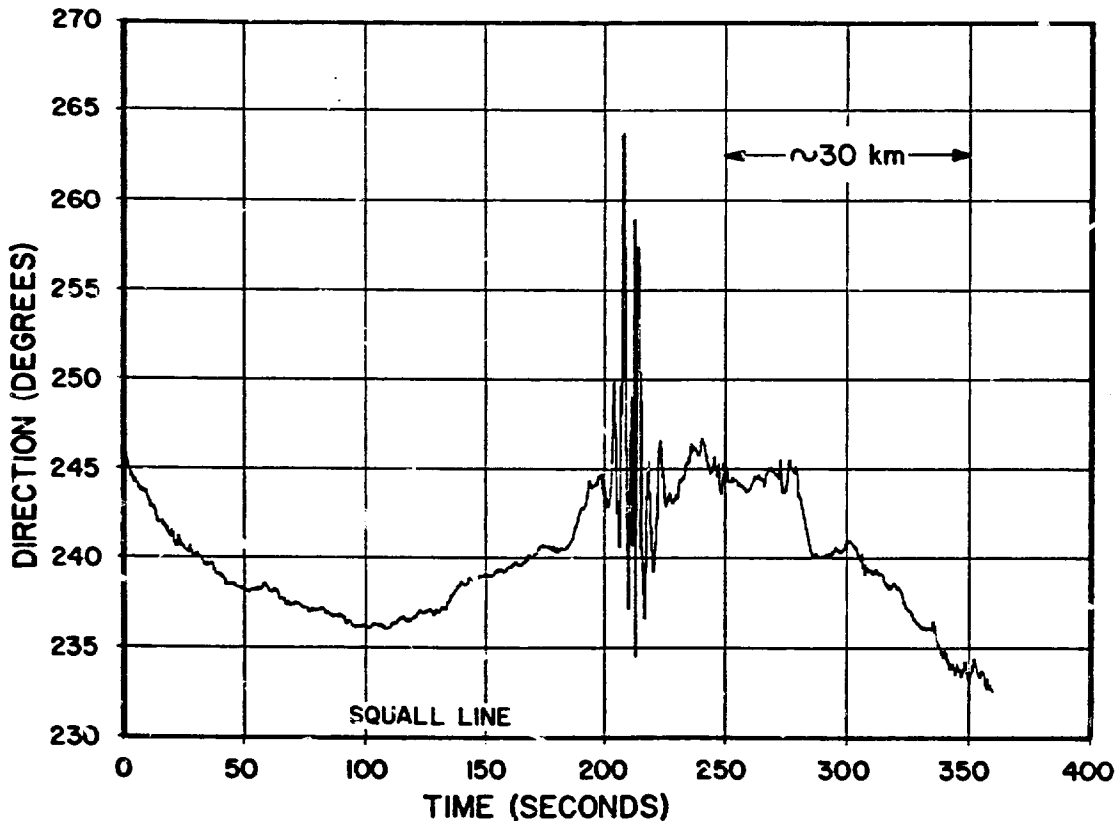

Figure 4.8 - Flight data: Horizontal wind direction along the flight path for the Hannibal, MO case from 0121 to 0127 GMT on 4 April 1981. "Squall line" indicates the approximate time the squall line was passed.

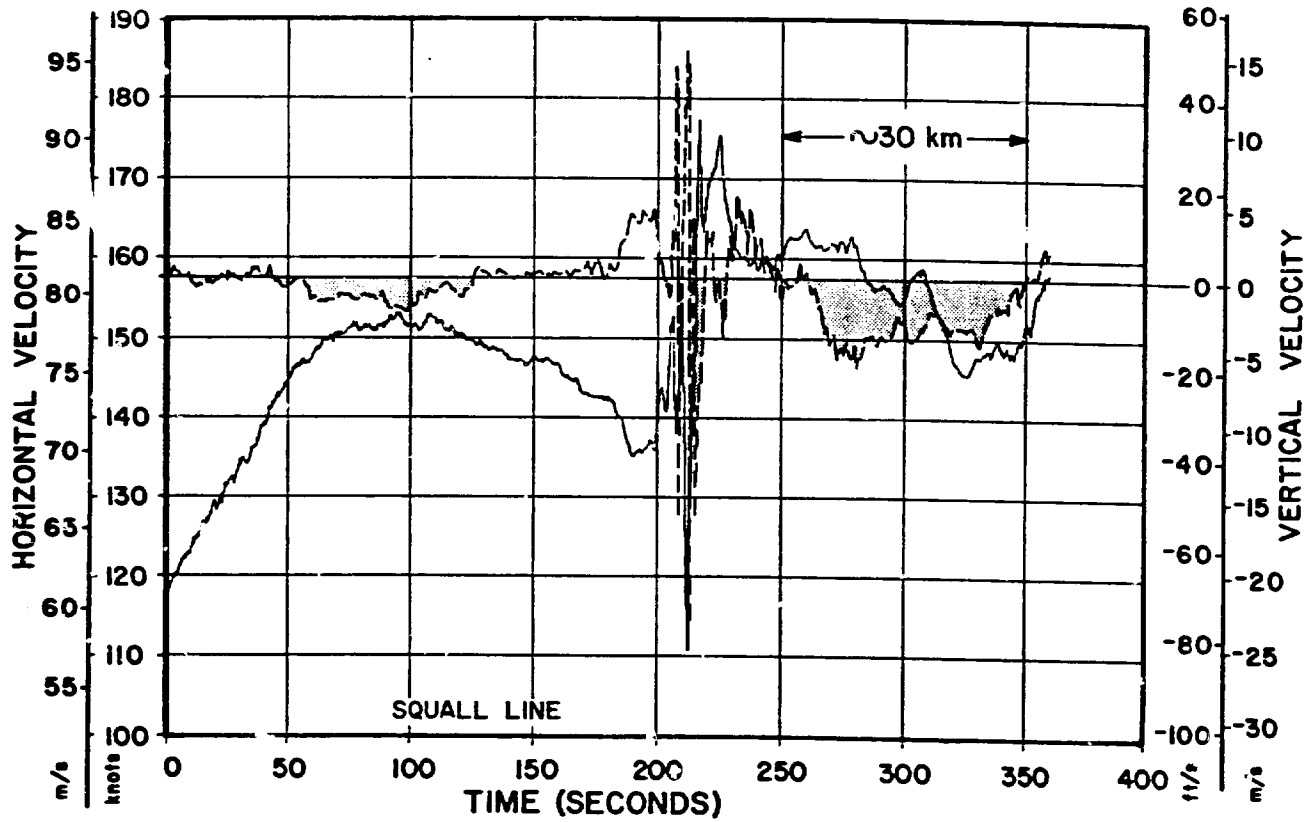

Figure 4.9 - Flight data: Horizontal wind speed (solid) and vertical velocity (dashed) along the flight path for the Hannibal, MO case from 0121 to 0127 GMT on 4 April 1981. Negative values of vertical velocity are shaded. "Squall line" indicates the approximate time the squall line was passed.

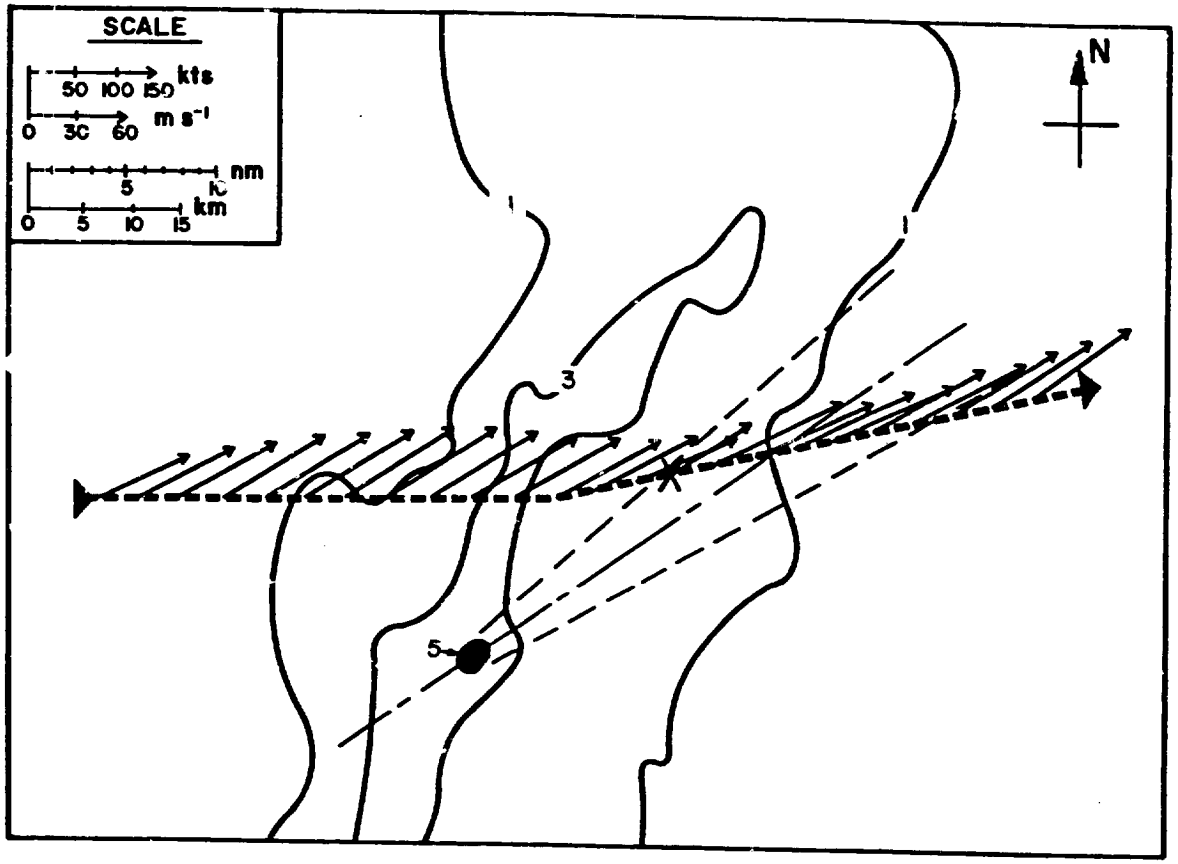

Figure 4.10 - Plan view of the Hannibal, MO case. Mean wind direction and speed are plotted at ≈ 15 s intervals along flight path. Dot-dashed line indicates mean wind direction. Dotted lines indicate apparent extent of turbulent area. DVIP levels 1 and 3 are shown by solid lines; DVIP level 5 is shown by black dot.

b. Bermuda

At 0418 GMT, 12 October 1983, an American Airlines DC-10, flying at 11.3 km, encountered severe turbulence in the vicinity of Ender Intersection (27N, 68.65W). According to the aircraft commander, the incident began with a few minutes of "light to moderate chop." Although no echoes appeared on the aircraft's radar, the aircraft "seemed to pass through the top of a cumulus cloud." Within the cloud, severe turbulence was encountered "that seemed to last for 30 seconds." As a result, twelve passengers were injured (Schweitzer, 1983).

A composite of surface and 250 mb weather patterns four hours prior to the incident is shown in Figure 4.11. The aircraft route is shown and the location of the turbulence incident (Ender Intersection) is indicated with an "X". Since no ATC radar data were available for this case, all position information is based on the reported flight path and is considered approximate.

Figure 4.11 shows that the track intersects an upper level anticyclone which dominates the area with reported winds generally less than 30 knots at 250 mb.

Satellite imagery near the time of the accident is shown in Figure 4.12. An area of apparent convective activity (cellular cloud features with cold tops) extends from Ender Intersection, along the flight path to about

30N, 70W. A comparison of the infrared imagery temperatures with a distant upper air sounding (Nassau, Bermuda, 12 October 1983, 1100 GMT) indicate that the maximum height of the cloud tops is about 12.8 km, i.e., 1.5 km above flight level. Surface ship reports (not shown) verify the presence of cumulonimbus clouds in the area.

Given the large-scale synoptic conditions (Figure 4.11), the presence of an area of intense convective activity is unexpected. It is suspected that a series of upper level disturbances are rotating clockwise around the periphery of the anticyclone.

As noted earlier, several pieces of information necessary for a complete analysis were not available for the current case. These include ATC radar data, weather radar information, and radiosonde observations. The Bermuda upper air station for example, was nearly 800 km away and the sounding was taken almost 7 hours after the accident. Thus, exact details of the aircraft position relative to the nearby thunderstorms and horizontal details of the wind and temperature fields cannot be deduced from the data presented here.

As discussed in Chapter 3, a series of experiments were carried out in an attempt to determine the horizontal wind field along the aircraft track. Despite a large number of tests, results were not conclusive, precluding the presentation of horizontal wind estimates.

There are, however, several useful parameters derived from DFDR data which are not dependent on the accuracy of horizontal position determinations and which may thus be interpreted with some confidence. For example, vertical acceleration and aircraft altitude records for a six minute (about 90 km) segment of the track centered near Ender Intersection are shown in Figure 4.13. The DC-10 encountered its most significant vertical acceleration (-1.5 g deviation from normal gravity) at 0418 GMT which corresponds with approximately 225 s elapsed time in Figure 4.13. The total extent of light or greater turbulence (magnitudes of deviations $\geq$ 0.15 g) was about 87 s or about 22 km along the flight track. In that region, aircraft altitude variations of up to 91 m occurred.

The potential temperature record along the flight track is presented in Figure 4.14. The altitude of the aircraft is also given in the figure for reference. Except for the very large deviations near the turbulence region, potential temperature shows a decreasing trend of about 1 K from the south (left) to the north (right) end of the track.

There are two other notable features when the records are compared. At about 185 s elapsed time, the aircraft ascends and θ <u>decreases</u>, while at about 210 s, the aircraft again ascends, but here θ <u>increases</u>. These sequential out-of-phase and in-phase relationships require careful

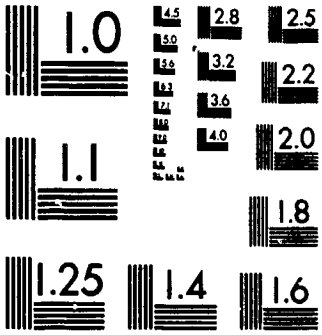

MICROCOPY RESOLUTION TEST CHART
NATIONAL BUREAU OF STANDARDS-1963-A

interpretation since, as pointed out in the last case, vertical and horizontal gradients are not easily differentiated along the aircraft track. For example, at 185 s two interpretations are possible: either the aircraft was climbing in an unstable air mass ($\partial\theta/\partial z < 0$), or the aircraft was flying into a new (cooler) air mass ($\partial\theta/\partial x < 0$). Similarly, in the latter case (at 210 s) the aircraft was either climbing in a stable air mass ($\partial\theta/\partial z > 0$) or was flying into a new (warmer) air mass ($\partial\theta/\partial x > 0$). Recall the latter region is where the aircraft was in cloud and the severe turbulence was encountered.

An examination of composite vertical velocity and potential temperature records along the aircraft track (Figure 4.15) helps to clarify the patterns in Figure 4.14. The phase of the potential temperature minimum near 185 s lags slightly a vertical velocity maximum ($w_z \approx 10\ ms^{-1}$) near 175 s. This pattern is strongly suggestive of what would be expected when traversing a gravity wave of about 10 km in length. If the slope of the aircraft track is less than the isentropes in the wave, then the aircraft would encounter relatively high values of θ with little vertical velocity in a wave trough, lower values of θ and large upward vertical velocities at the downstream inflection point, and finally low values of θ with near zero vertical velocities in the wave crest.

The potential temperature and vertical velocity patterns in the region of intense turbulence near 210 s ($w_z \approx 25\ ms^{-1}$), however, do not show an obvious phase lag. This pattern corresponds more closely with flight through convection, i.e., with strong upward heat flux.

A third feature, not as obvious in the previous figure (θ) is also noted in Figure 4.15. A series of small amplitude sinusoidal fluctuations are evident in the vertical velocity field after abut 230 s elapsed time. Upon close inspection, the same wave-type fluctuations are also found in the θ record. In both cases the wave periods are about 10 seconds; this value corresponds with a wave length of 2.5 km at an airspeed of 250 ms^{-1}. Although the asymmetry of the θ record does not allow a conclusive statement about the phase relationship between θ and w_z, the occurrence of similar wave patterns in the records of two independently determined parameters offers strong evidence that the waves are real, and, in fact, gravity waves.

The interpretations above suggest the following: the aircraft was flying in a generally stable environment. Initially it flew through a gravity wave of 10 km in length with moderate turbulence in the updraft region just outside of the convection. The aircraft then encountered the convective cloud, very likely a thunderstorm, which extended well above flight level. Severe convective turbulence was experienced. As the aircraft exited the cloud, the flight

traversed a train of shorter (2.5 km wavelength) gravity waves which produced only light turbulence. It is possible that the gravity waves encountered by the aircraft both before and after the severe turbulence were excited by the convection.

Another possibility is that the aircraft intersected a thunderstorm anvil downwind of the major thunderstorm activity. As discussed in Chapter 2 and as noted by Lilly (1986), when turbulent air and water vapor pass out of the top of a thunderstorm, the outflow collapses. Internally, the collapse relates to a decay and transformation of the turbulence into three components: a horizontal part such as two-dimensional turbulence and a tilted part such as gravity waves. This result is further complicated by turbulent entrainment of environmental air and the generation of new turbulence by shear occurring at the same time as the outflow collapse. Whether or not the turbulence located in this area is strong enough to cause the intensities experienced in this case is not known.

As in the Hannibal case, these preliminary interpretations are two-dimensional. The influence of rapidly-growing convective towers, and their three-dimensional interaction with the horizontal flow field are unknown.

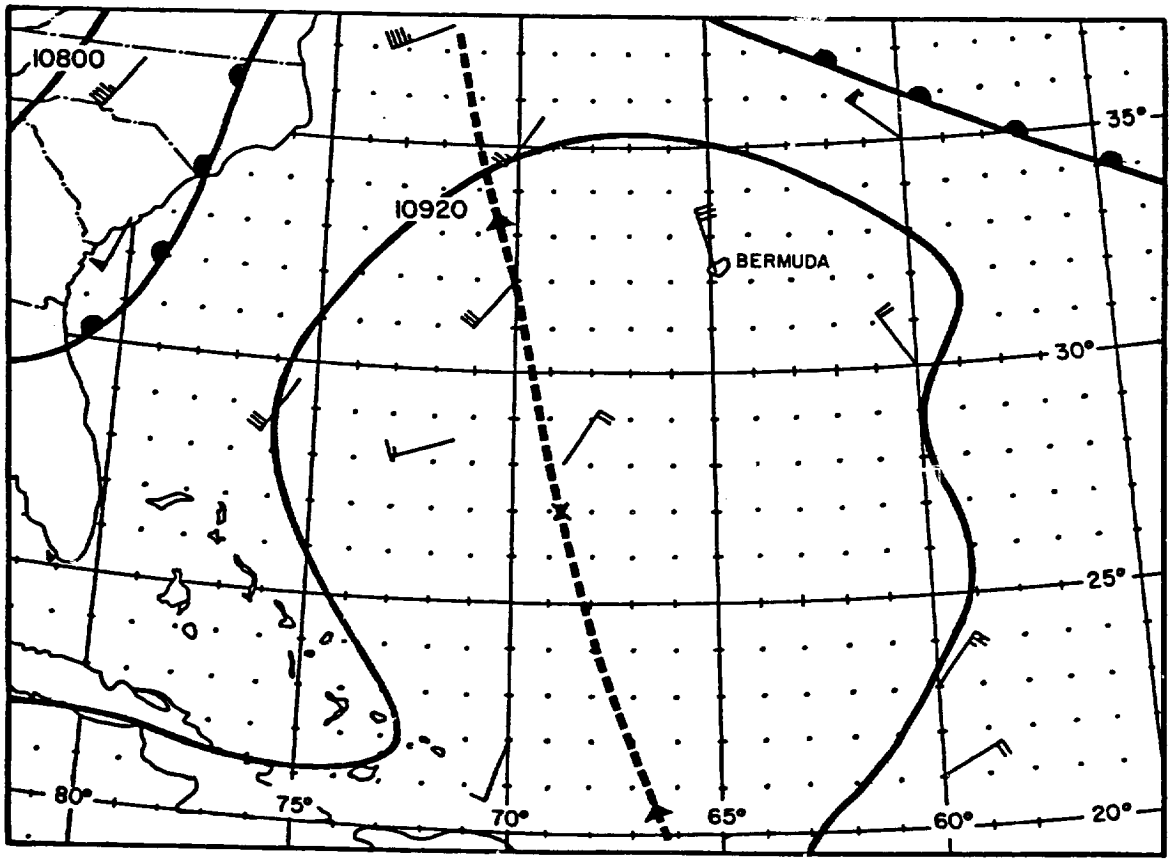

Figure 4.11 - Large-scale view of meteorological conditions in the vicinity of the Bermuda case on 12 October 1983. NMC Surface frontal positions for 0600 GMT are superimposed with NMC 250 mb winds and contour lines for 0000 GMT. The dashed line shows the approximate flight path. The X indicates Ender intersection, i.e., the approximate site of the severe turbulence incident.

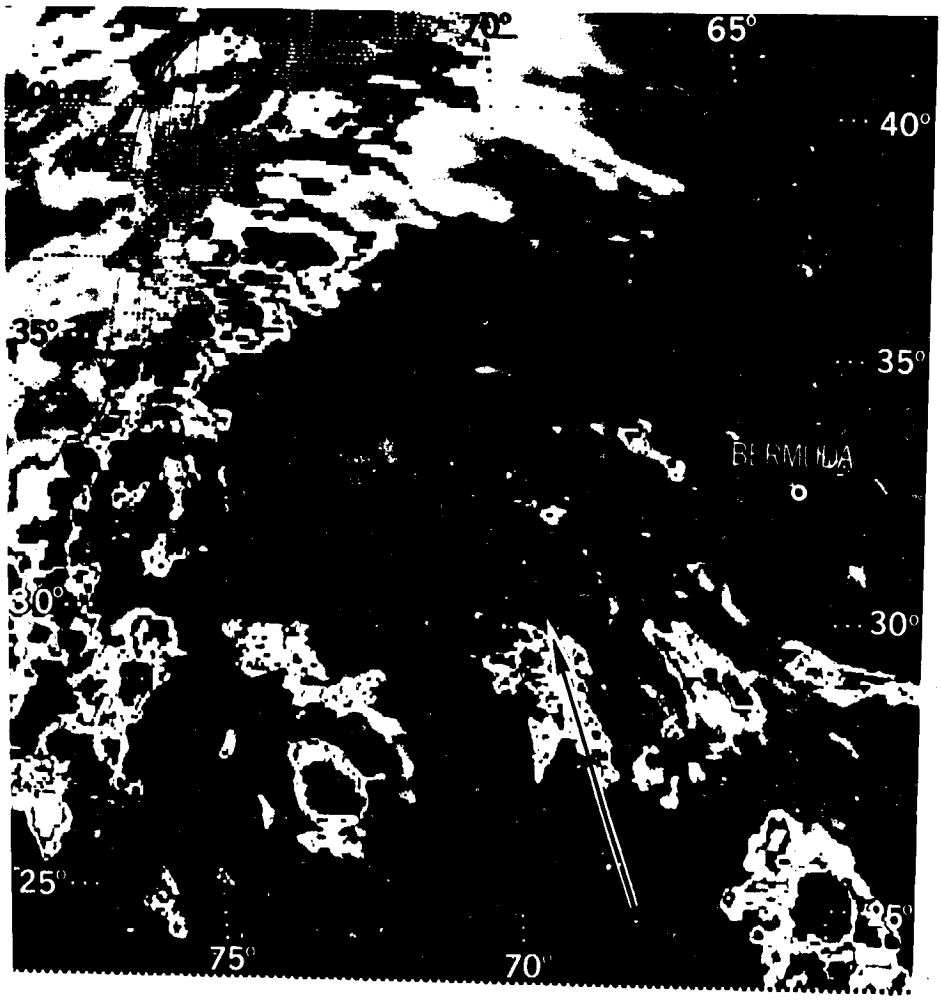

Figure 4.12 - Enhanced IR satellite image for the Bermuda case valid at 0400 GMT on 12 October 1983. The black and white line shows the approximate flight path. The "X" indicates Ender Intersection, i.e., the approximate severe turbulence location. The enhancement is curve MB with gray scale temperatures within the image: black-to-white (>-32°C), medium gray (-32 to -41°C), light gray (-41 to -52°C), dark gray (-52 to -58°C), black (-58 to -62°C).

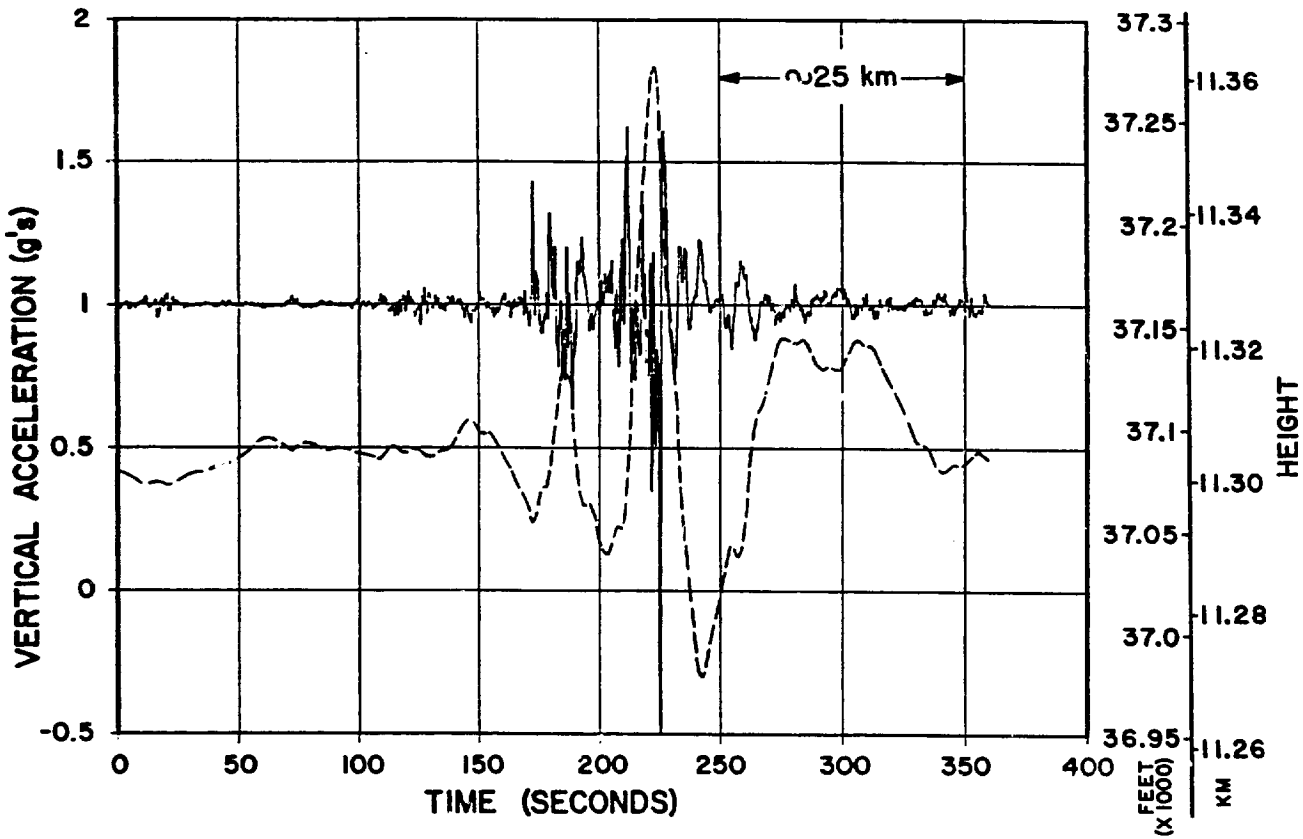

Figure 4.13 - Flight data: Vertical acceleration (solid) and altitude (dasned) along the flight path for the Bermuda case from 0415 to 0421 GMT on 12 October 1983.

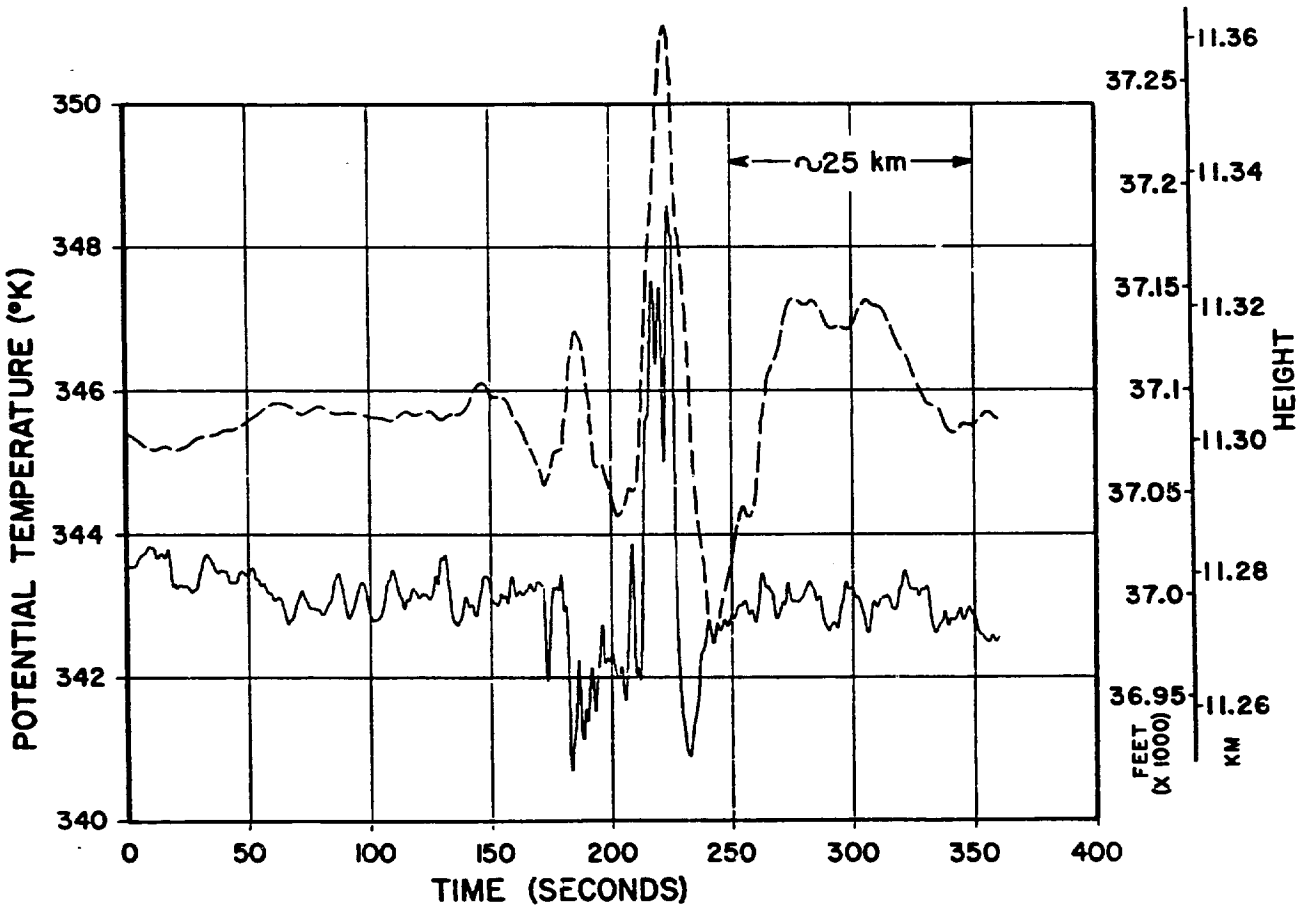

Figure 4.14 - Flight data: Potential Temperature (solid) and altitude (dashed) along the flight path for the Bermuda case from 0415 to 0421 GMT on 12 October 1983.

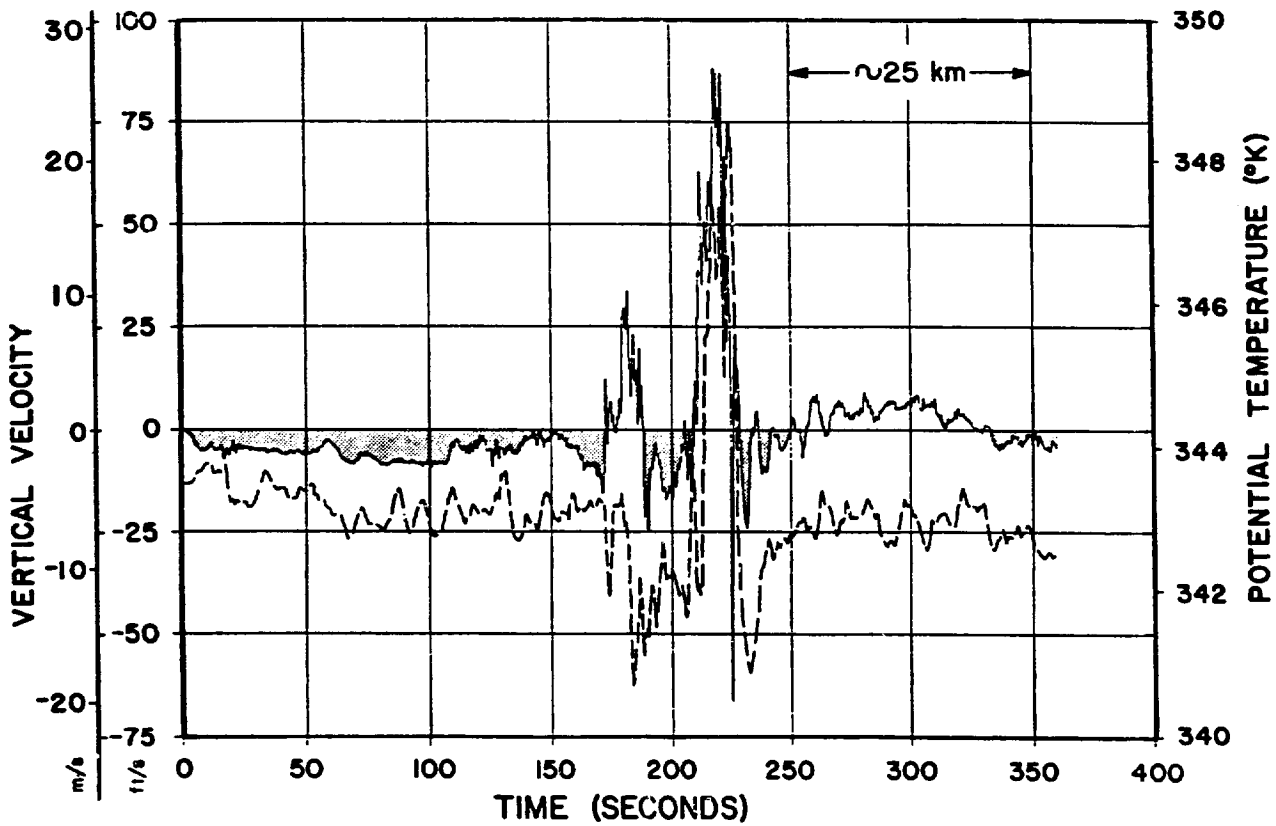

Figure 4.15 - Flight data: Vertical velocity (solid) and potential temperature (dashed) along the flight path for the Bermuda case from 0415 to 0421 GMT on 12 October 1983. Negative values of vertical velocity are shaded.

c. South Carolina

At 0026 GMT on 25 November 1983, an Air Canada L-1011 en route from Trinidad to Toronto experienced severe turbulence while flying at an altitude of 11.3 km, 110 km from the coast of South Carolina (33.2N, 77.8W). The aircraft had been flying a more westerly course when it was diverted northward at approximately 0020 GMT. According to the flight crew incident reports, the aircraft was in "upper cloud" just east of a line of weak radar returns which could only be seen when the on-board radar "was tilted downward two degrees." Shortly after the turn, light to moderate chop began and continued for several minutes. Subsequently, the aircraft experienced "two brief, severe jolts" about a minute apart. Approximately one minute later, the turbulence ended and conditions were smooth. The incident resulted in twenty-four injuries to passengers and crew (Dell, 1983; Fox, 1983; Frerichs, 1983; NTSB, 1984).

Large-scale weather conditions over the southeastern United States and the eastern Atlantic for 25 November 1983 at 0000 GMT are illustrated in Figure 4.16. As with previous cases, the important surface and 250 mb features have been composited. Winds at 250 mb are southwesterly at about 80 knots near the incident site. The core of a strong jet stream and an associated surface cold front is located to the northwest. Two squall lines precede the

cold front: one over Florida and one just off the Carolina Coast (the latter is intersected by the flight path near the turbulence site).

Enhanced IR GOES satellite images obtained just before and just after the turbulence incident are presented in Figure 4.17. The cold front seen in Figure 4.16 is covered by a broad band of baroclinic cirrus bordering the anticyclonic side of the jet stream. The nearly circular cloud mass near "X" in 4.17 is associated with the northern squall line in Figure 4.16.

A comparison of temperatures determined from the enhanced IR image in Figure 4.17b with those from the nearest sounding (Charleston, SC, CHS, Figure 4.18) indicates that cloud tops reach an altitude of at least 12.2 km, i.e., just below the tropopause and about 1 km above flight level.

The distribution of radar echoes observed at 0026 GMT by the weather radar at Wilmington, NC (ILM) is presented in Figure 4.19. The area of coverage is that within the rectangle in Figure 4.16. The aircraft track and site of the turbulence incident (white dot) are also indicated. Note that the incident occurred east of a line of intense (DVIP $\geq$ 5) radar echoes (compare with Figure 4.16). Maximum tops of echoes in the area were 11.0 km at 2335 GMT but had grown to 13.1 km by 0035 GMT, exceeding the CHS tropopause height (Figure 4.18). A superposition (not shown) of

the circular cirrus sheet identified in Figure 4.17b places the cirrus over the radar echoes of Figure 4.19 and downwind of the echoes. The circular cloud is clearly the anvil associated with the line of thunderstorms. Therefore, at 0026 GMT when the accident occurred, the aircraft (at 11.3 km) was downwind of, and below the level of the highest tops of the line of thunderstorms. Furthermore, the flight was below the tropopause and in the cirrus anvil (in agreement with pilot's statements).

Details of the DFDR records for a six minute segment of the flight centered on the turbulence incident are shown in Figures 4.20 through 4.24. In Figure 4.20, two distinct turbulence bursts are apparent. The first occurred at 26 min, 8.75 s after 0000 GMT (158.75 s into the record), with a maximum deviation from normal acceleration of -2.01 g. The second burst occurred 41 s later (about 10 km) with a maximum acceleration (deviation from normal) of +1.09 g. The corresponding effects on the aircraft altitude show a decrease of 120-150 m immediately followed each turbulent incident; The aircraft returned to its assigned altitude within a minute after the second encounter.

The aircraft altitude is superimposed on the potential temperature record in Figure 4.21. Potential temperature has been subjected to a low pass filter to eliminate contamination due to high frequency noise in the raw static temperature record. The smoothed version shows ± 3-4 K

variations in θ beginning prior to the two turbulence bursts documented in Figure 4.20. No clear relation is seen between θ and aircraft altitude, although it is noted that the range of θ variations corresponds well with θ values within several 100 m below the tropopause in the CHS sounding (Figure 4.18).

Potential temperature and vertical velocity are presented in Figure 4.22. In the turbulence regions, vertical velocities range from nearly $-30\ ms^{-1}$ to about $+33\ ms^{-1}$. As in the previous figure (and in contrast with the previous cases) there is no clear relationship between θ and w_z.

Figures 4.20-4.22 have shown that the turbulence occurred in two distinct bursts prior to the intersection of the flight path and the squall line. The lack of an obvious correlation between altitude and θ or vertical velocity and θ may be related to the large angles between the flight path, the squall line, and the wind direction and/or the three-dimensionality of the turbulence. Some additional information is found in Figures 4.23 (wind direction) and 4.24 (wind speed). High frequency variations due to noise in the static temperature are also apparent in the wind records, however, that contamination was not significant in the wind computation and so was not removed by filtering.

Following procedures used in the previous cases, the wind and potential temperature records (Figure 4.22) were combined to determine stability, shear, and Ri. Initial

calculations of stability produced scattered results, likely due to an inability to separate horizontal and vertical gradients in regions of large altitude fluctuations. If, in areas where there was both an altitude change and a relatively smooth temperature change, it was assumed that only vertical gradients were measured, then the results indicate strong stability ($\partial\theta/\partial z \approx 21.5$ Kkm^{-1}). This computed stability value is much greater than that indicated in the upstream sounding at the same height (CHS, Figure 4.18). Such a deviation may have been due to a significant modification of the stability structure as the upper tropospheric/lower stratospheric airflow was disturbed by the squall line. A similar stability variation was seen in the Hannibal case. Calculations of shear, $\partial v/\partial z$, yielded values of 0.03-0.04 s^{-1}. When these results were combined to calculate Ri, values ranged from 0.4-0.7.

Wind speeds (Figure 4.24) decrease by about 25% at both turbulence locations. Wind direction variations at those locations, however, are different. Directions veer along the flight track near the earlier turbulence burst, but back near the second. This behavior suggests a coherent horizontal wind fluctuation with a period of 50 s (a horizontal scale of about 12.5 km). A clearer understanding of the cause of this horizontal disturbance is found in Figure 4.25, which is a plan view of the flight track contained within the small rectangle of Figure 4.19.

Fifteen second mean horizontal winds have been plotted along the path. Radar echoes in the immediate vicinity of the turbulence are also shown. The general wind direction is 225°, placing the aircraft slightly downwind of a broken line of thunderstorms. Additional winds are plotted in the vicinity of both severe CAT bursts; a sharp variation in the direction and/or speed is noted at those points. In this case, as also seen in the Hannibal, MO case, there appears to be a wake region, defined by the location of the turbulent areas and an isolated, but rapidly growing upstream thunderstorm echo at location "A" in Figure 4.25. The wedge angle in this case is 11-12°, i.e., within the range found by Gjevik and Marthinsen (1978) for diverging type ship waves. On the basis of high stability and low Richardson number determinations, atmospheric conditions downwind of the highest tops of the line of thunderstorms support the existence of a three-dimensional wake. It appears that TNTT was likely the result of overturning near the edges of the wake.

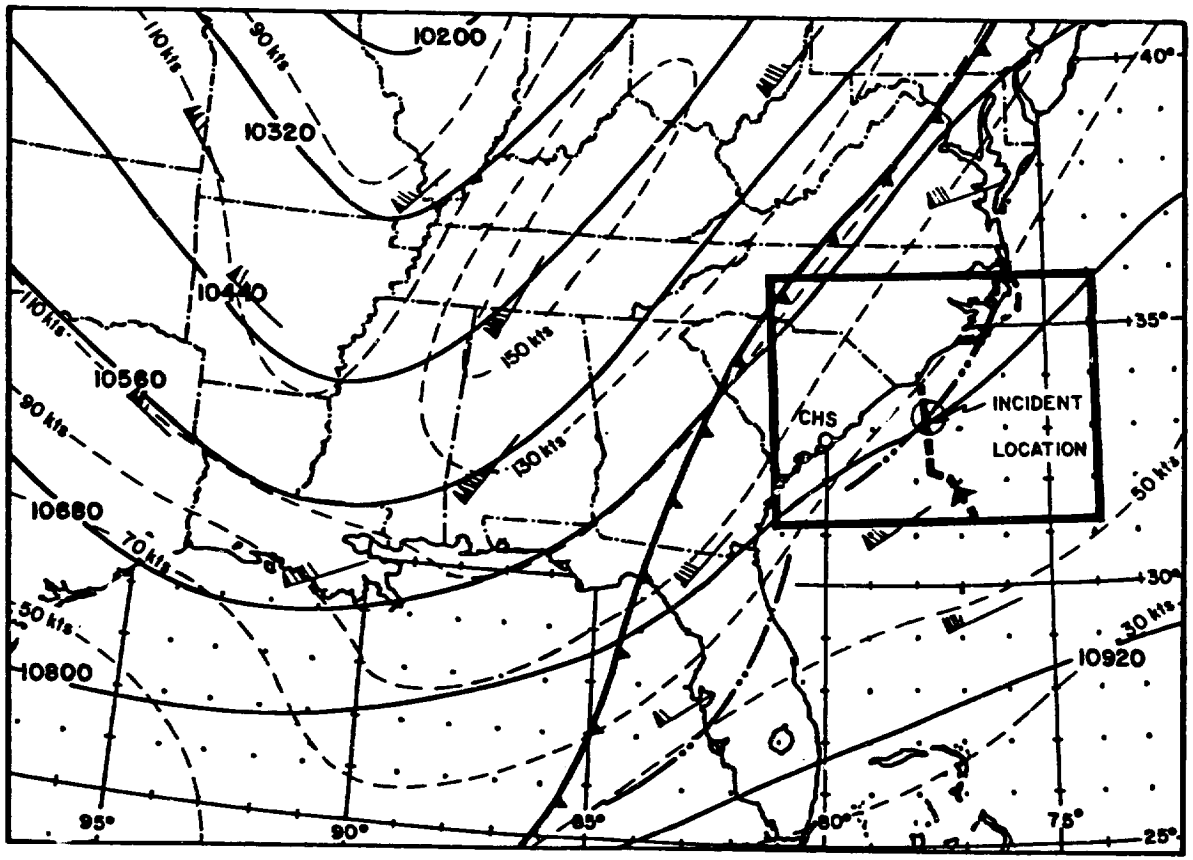

Figure 4.16 - Large-scale view of meteorological conditions near Charleston, SC on 25 November 1983. NMC Surface frontal positions for 0000 GMT are superimposed with NMC 250 mb winds, isotachs, and contour lines. The dashed line within the rectangle shows the flight path. The circle indicates the severe turbulence incident location. The two dot-dot-dash lines are squall lines.

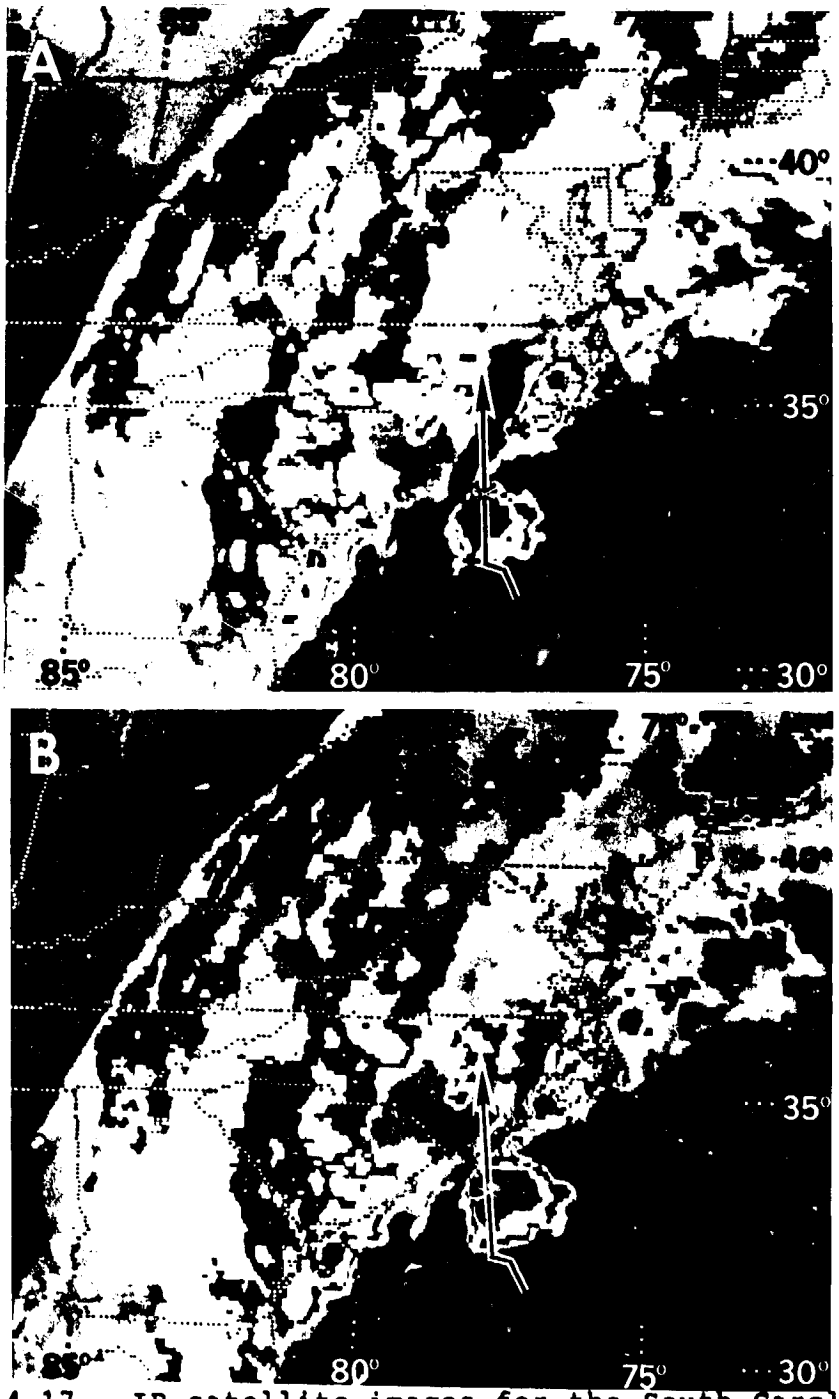

Figure 4.17 - IR satellite images for the South Carolina case of 25 November 1983. (A) Enhanced IR at 0000 GMT. (B) Enhanced IR at 0030 GMT. The black and white line and the "X" indicate the flight track and the turbulence incident location, respectively. The enhancement is curve MB (see Figure 4.12 for gray scale temperatures).

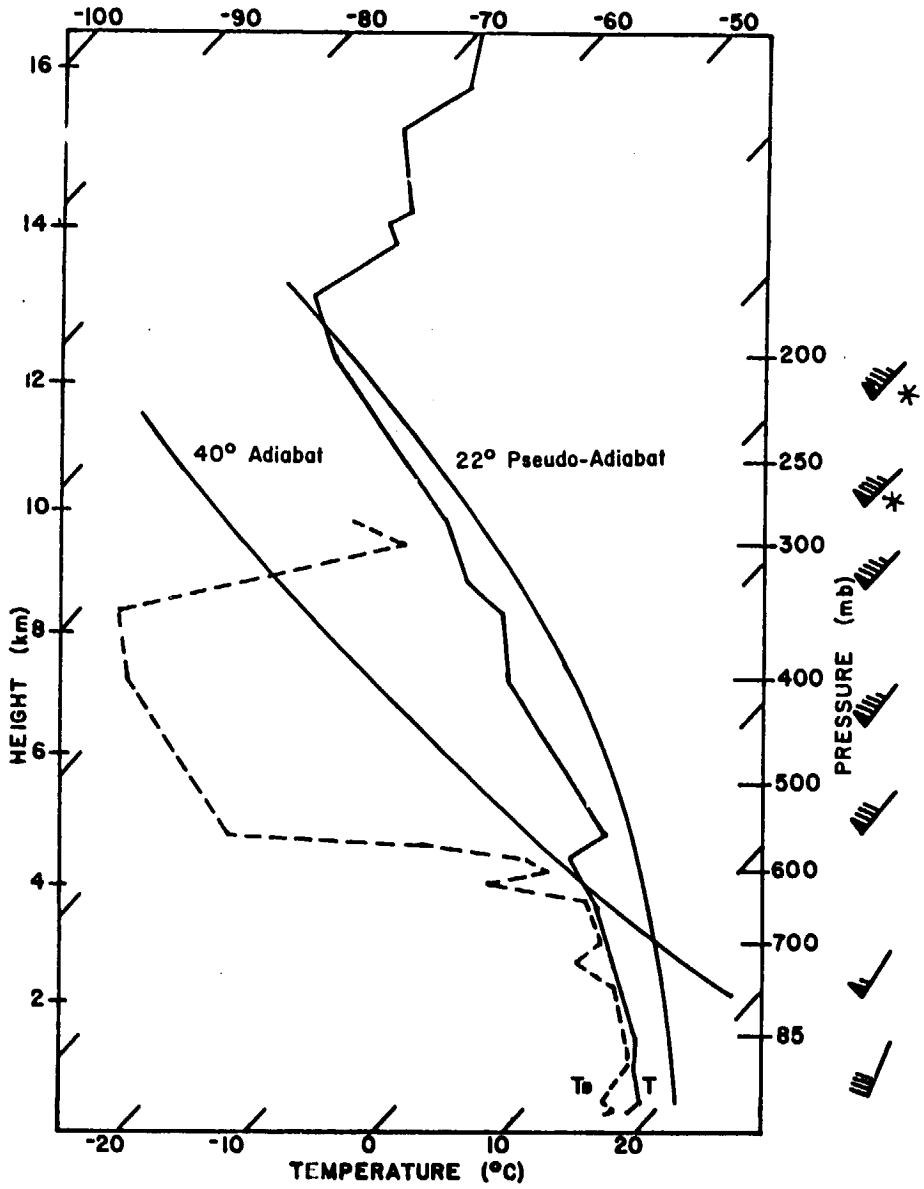

Figure 4.18 - Sounding plot for Charleston, SC at 2300 GMT on 24 November 1983. Height scale is based on reported height surfaces in geopotential meters. Gradient winds (highlighted with *) replace missing sounding winds at 200 and 250 mb.

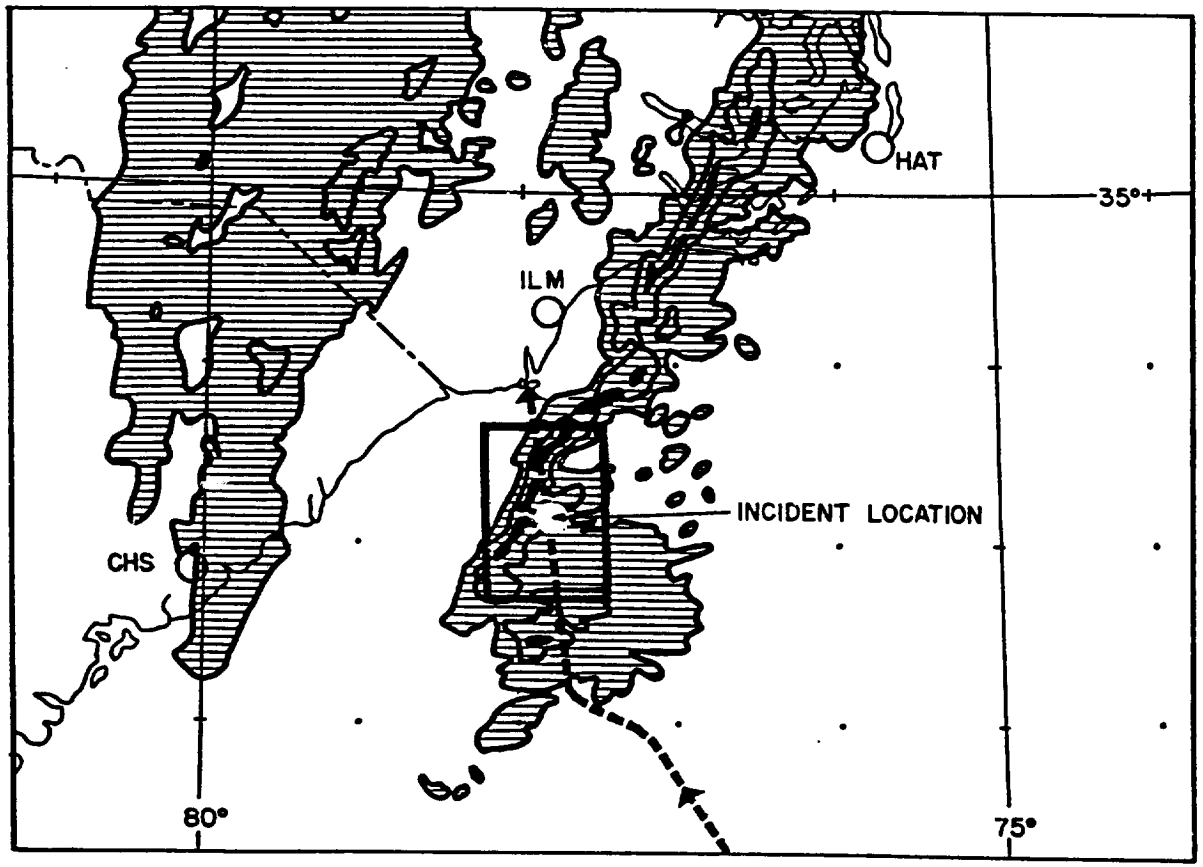

Figure 4.19 - Distribution of radar echoes at 0026 GMT on 25 November 1983. The IMN radar returns are shown for the region enclosed by the rectangle in figure 4.18. DVIP 1 and 3 levels are hatched, DVIP 5 levels are solid. A dashed line and white dot indicate the flight path and incident location, respectively.

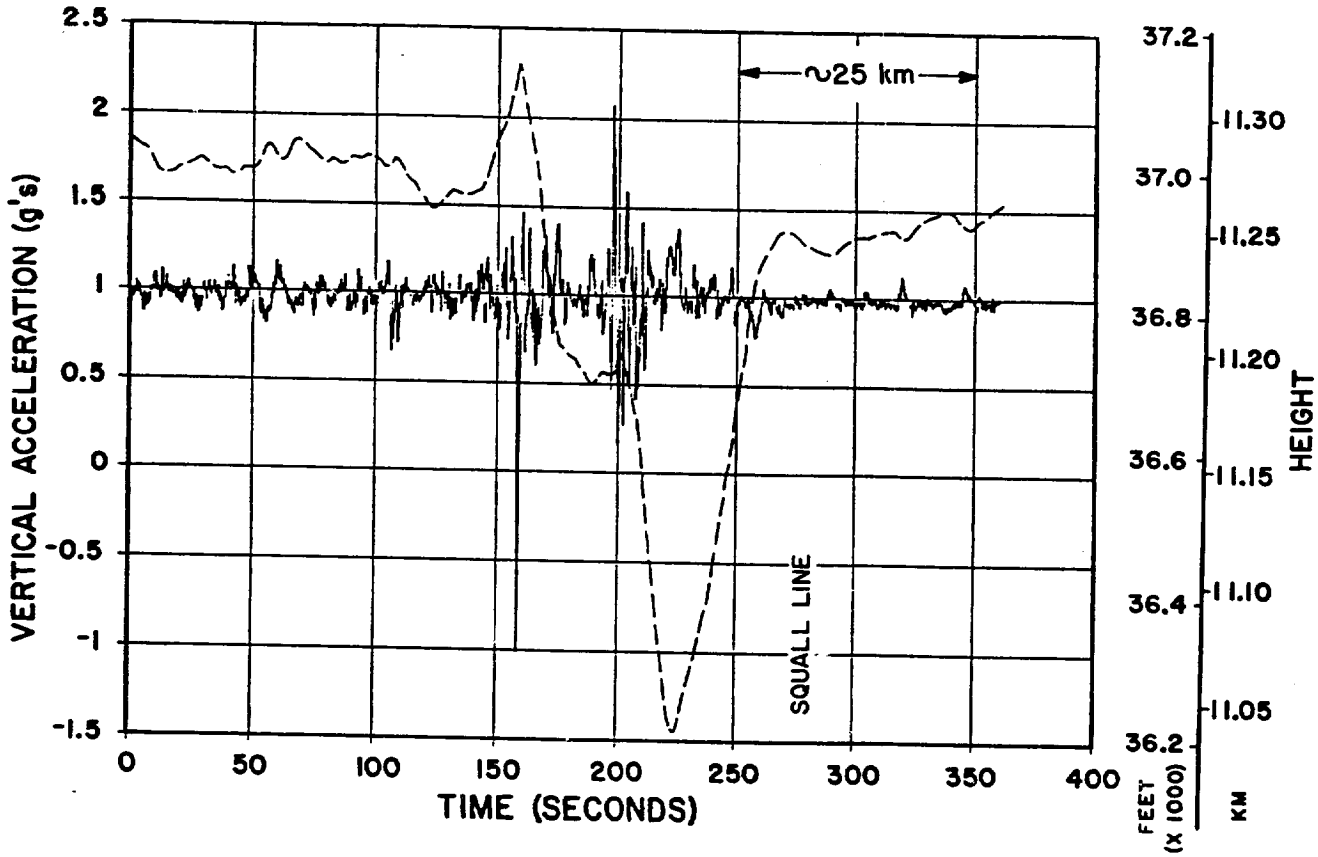

Figure 4.20 - Flight data: Vertical acceleration (solid) and altitude (dashed) along the flight path for the South Carolina case from 0023.5 to 0029.5 GMT on 25 November 1983. "Squall line" indicates the approximate time the squall line was passed.

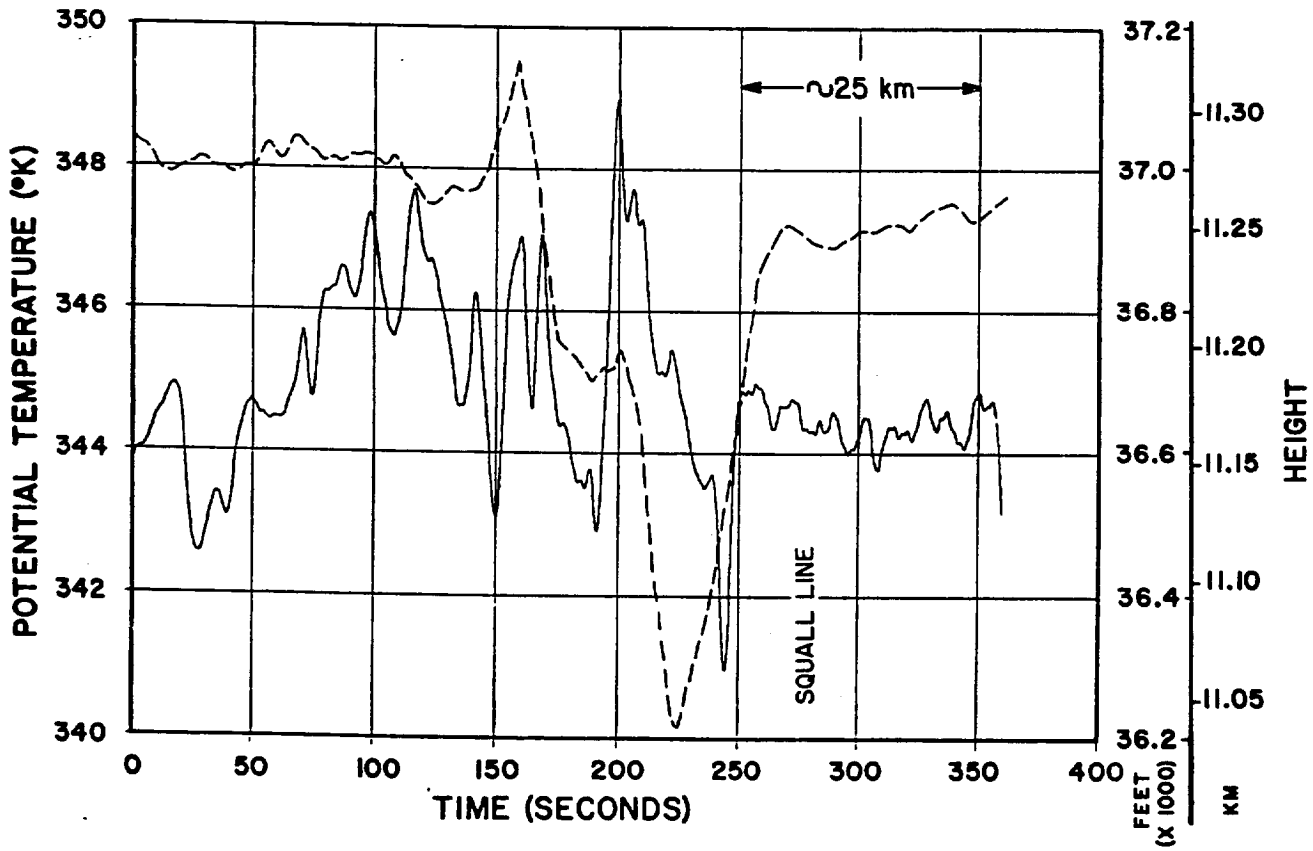

Figure 4.21 - Flight data: Potential temperature (solid) and altitude (dashed) along the flight path for the South Carolina case from 0023.5 to 0029.5 GMT on 25 November 1983. "Squall line" indicates the approximate time the squall line was passed.

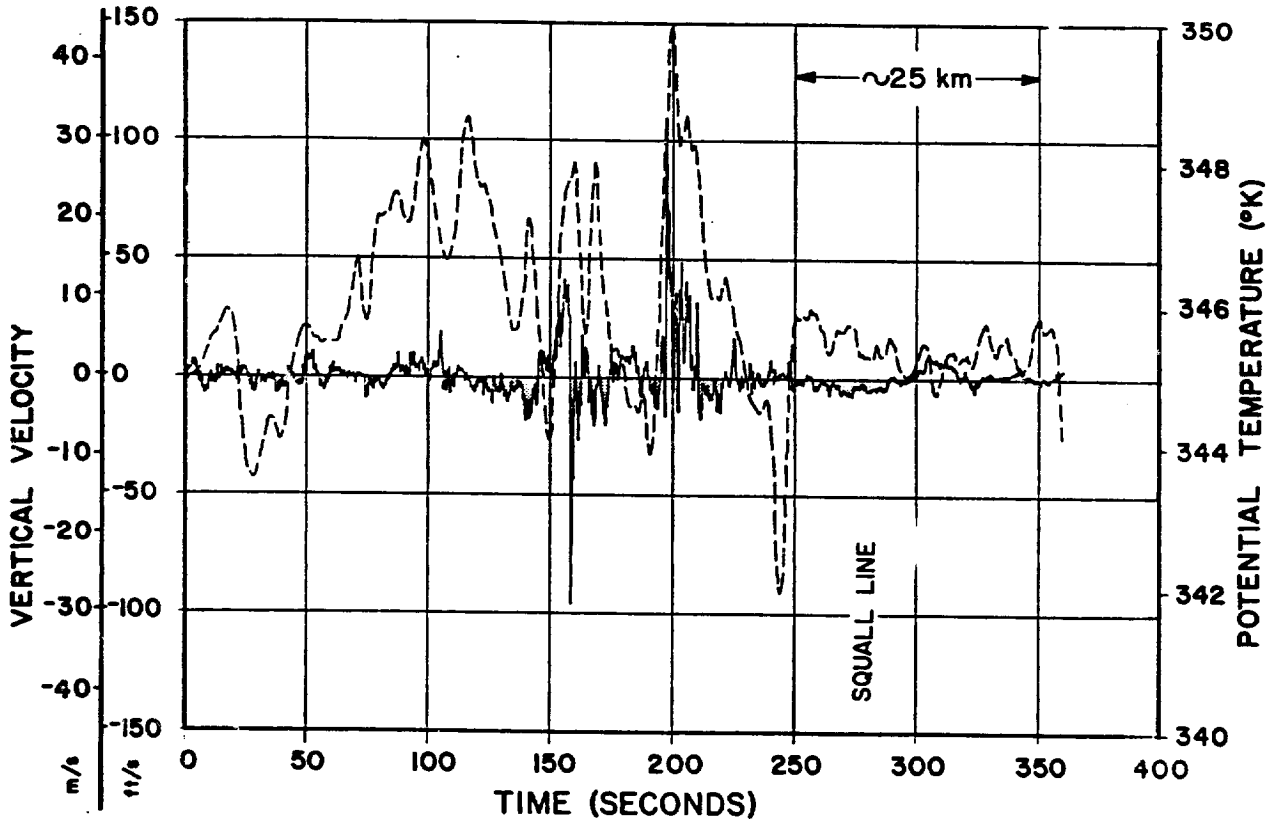

Figure 4.22 - Flight data: Vertical velocity (solid) and potential temperature (dashed) along the flight path for the South Carolina case from 0023.5 to 0029.5 GMT on 25 November 1983. Negative values of vertical velocity are shaded. "Squall line" indicates the approximate time the squall line was passed.

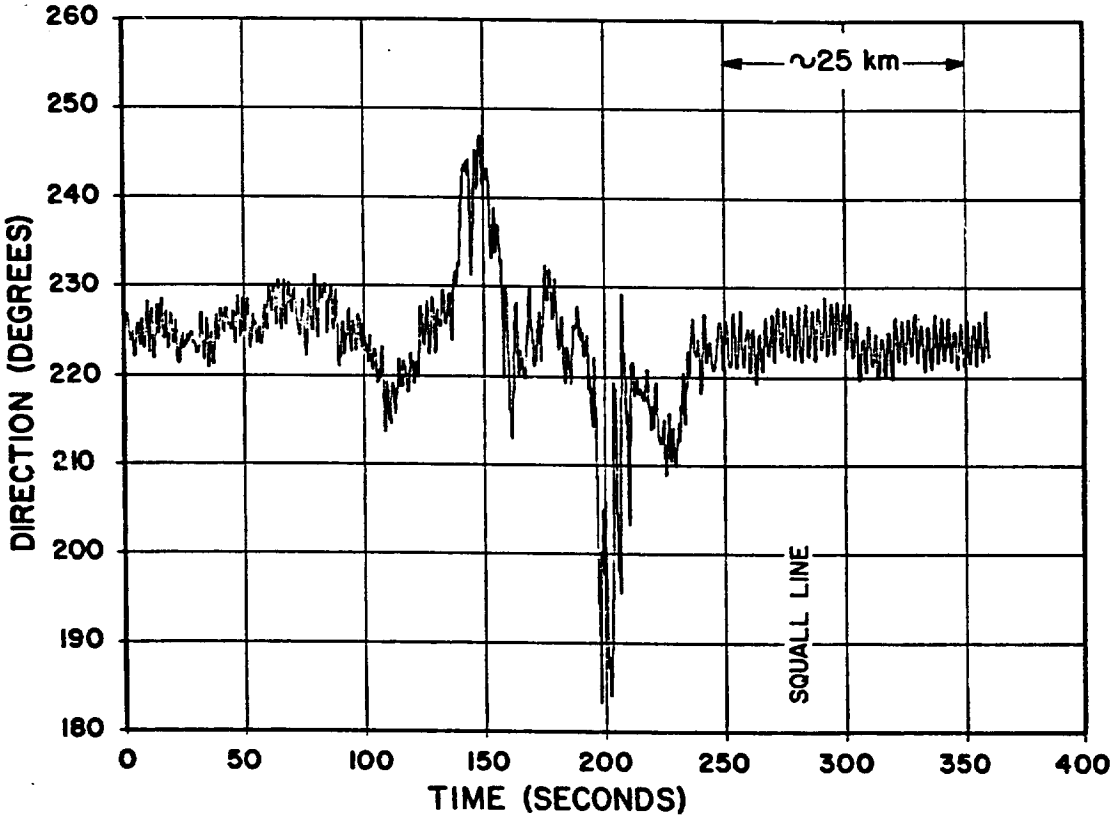

Figure 4.23 - Flight data: Horizontal wind direction along the flight path for the South Carolina case from 0023.5 to 0029.5 GMT on 25 November 1983. "Squall line" indicates the approximate time the squall line was passed.

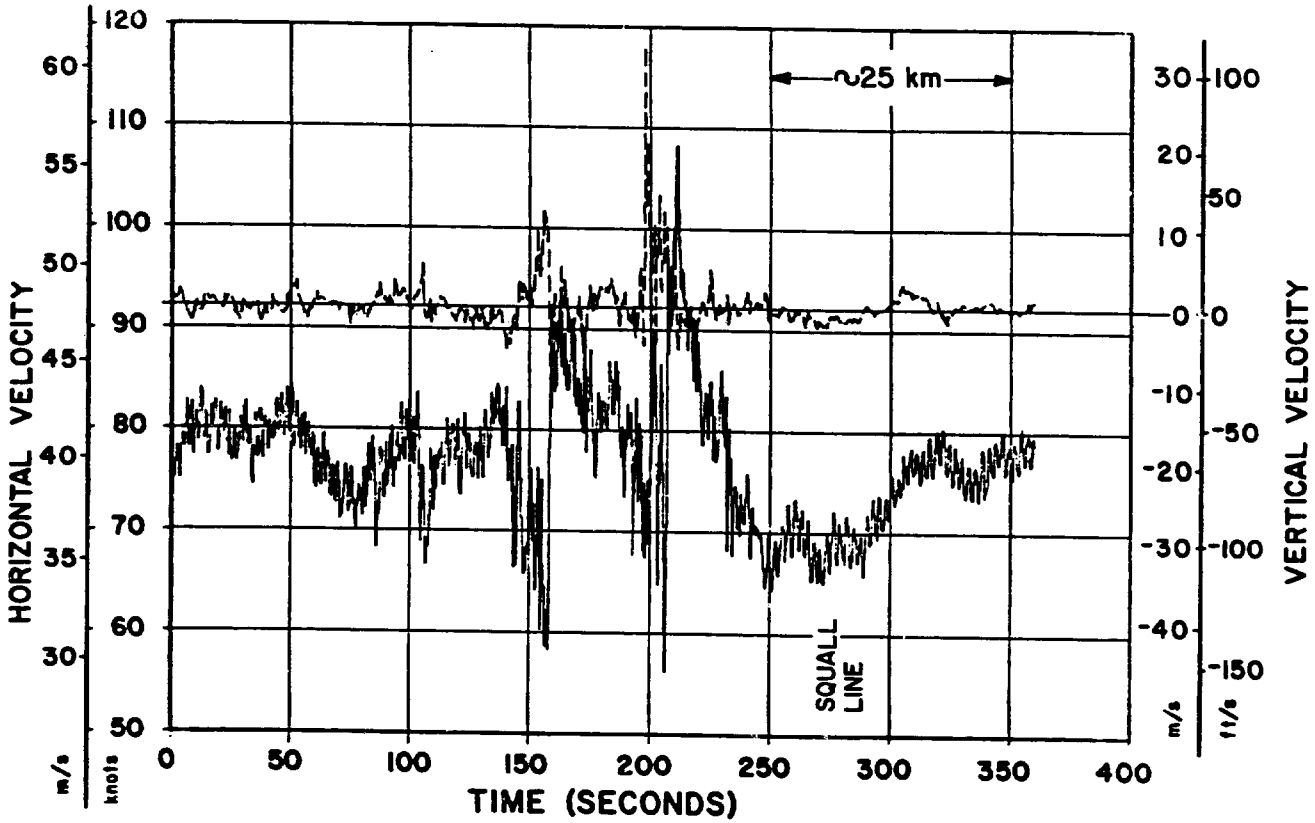

Figure 4.24 - Flight data: Horizontal wind speed (solid) and vertical velocity (dashed) along the flight path for the South Carolina case from 0023.5 to 0029.5 GMT on 25 November 1983. Negative values of vertical velocity are shaded. "Squall line" indicates the approximate time the squall line was passed.

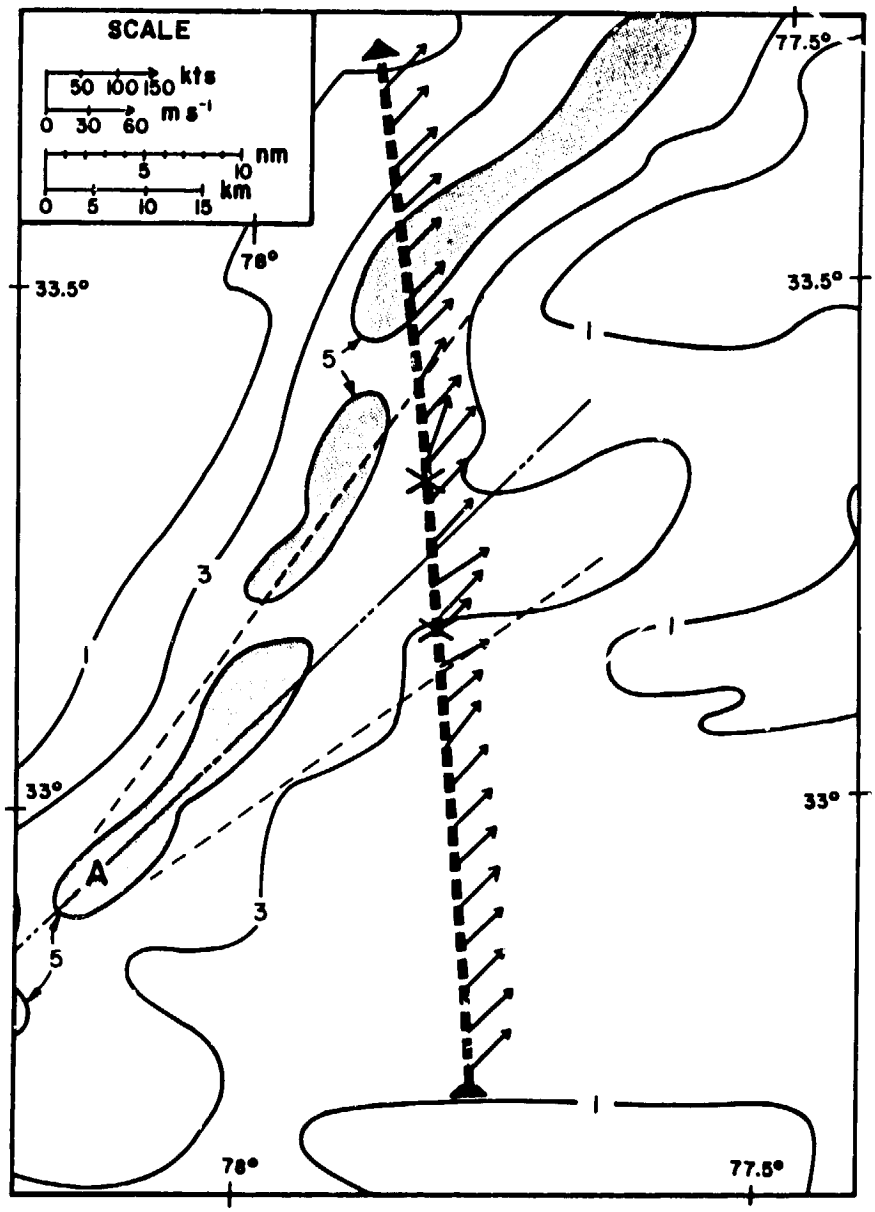

Figure 4.25 - Plan view of the South Carolina case. Mean wind direction and speed are plotted at ≈ 15 s intervals along the flight path. Dot-dashed line indicates mean wind direction. Thin dotted lines indicate apparent extent of turbulent area. "A" indicates the thunderstorm acting as an obstacle. DVIP levels 1 and 3 are shown by solid lines; DVIP levels 5 are shown by shading.

d. Case Comparison

Table 4.1 summarizes the general flight characteristics of each case as well as the properties of the meteorological environment. For convenience, some information has been repeated from Table 3.1. Altitudes for all cases were identical, and, at least for the Hannibal and South Carolina cases, they were at or just below the tropopause. Potential temperature ranges for the three cases are in agreement with this interpretation.

Wind velocities varied widely from case-to-case, with a very high tail wind in the Hannibal case, a moderate crosswind for South Carolina, and a variable wind (probably a 180° shift) in the Bermuda case. It should be noted that although horizontal wind directions could not be computed with confidence in the Bermuda case due to uncertainties in aircraft position, the calculations of wind vectors

Table 4.1 - Aircraft track and mean meteorological conditions.

CASE	HANNIBAL	BERMUDA	SOUTH CAROLINA
Flight Altitude (m ASL)	11.3	11.3	11.3
Aircraft Heading (True)	ENE	NNW	NNW
Tropopause Height (km ASL)	11.3-12.0	?	12.5
Mean Potential Temperature (K)	338.2	343.2	345.2
Vector Mean Wind Speed (ms^{-1})	80.1	5.1	40.8
Prevailing Wind Direction	SW	variable	SW

relative to each other are assumed to be valid. Results of those and several other wind related computations not sensitive to position errors are presented for that case in Table 4.1 and in some of the following tables for comparison purposes.

Any "mean" values ($\bar{\ }$) presented in Table 4.1-4.4 are averages through the turbulent portions of the six minute flight segments presented in the previous sections. "Turbulent" refers to those flight segments where vertical accelerations (deviations from normal) were greater than or equal to 0.15 g (i.e., light turbulence or greater).

Turbulence statistics based on the vertical acceleration records of the three cases are presented in Table 4.2.

Table 4.2 - Turbulence statistics.

CASE	HANNIBAL	BERMUDA	SOUTH CAROLINA
Turbulence Period (seconds)	43.75	86.50	82.00
Vertical Extreme Accelerations (g')	-1.91, +0.82	-1.50, +0.62	-2.01, +1.08
Aircraft Height Change with Turbulence (m)	+156	-92	-138, -163*
Total Injuries	29	12	24
Percent** of Time:			
Light or Greater	42	32	40
Light	31	28	34
Moderate	10	3	5
Severe or Greater	1	1	1

*Two well-defined turbulent patches.
**Percentages have been rounded to whole numbers.

Moderate and severe turbulence categories were specified using World Meteorological Organization (WMO) criteria (moderate turbulence: $0.5\ g \leq g' < 1.0\ g$, and severe or greater: $g' \geq 1.0\ g$, where g' is the deviation from normal gravitational acceleration).

The Hannibal case had the shortest turbulence period, likely due to its downwind track and the large angle at which it intersected the squall line. In terms of extreme deviations (g'), Hannibal and South Carolina were the most violent turbulence encounters and, as might be expected, produced the greater numbers of passenger and crew injuries.

The largest changes of the aircraft altitudes in the turbulence regions (Table 4.2) also give a rough indication of the intensity of the turbulence. The major difference between cases is the contrast between the altitude gain in the Hannibal incident, and the altitude losses in the latter cases. It is conceivable that downwind flight into a strong "lee wave" updraft is the cause of the Hannibal altitude change, but it must be kept in mind that the altitude changes are due in part to aircraft response and in part to pilot input.

The stratification of vertical accelerations into the various turbulent categories (Table 4.2) show that the turbulent patches were highly intermittent, i.e., light or greater turbulence was experienced only 42% (or less) of

the turbulence periods. Furthermore, severe or greater turbulence was experienced only one percent (or less) of the time in all three cases.

Another statistical measure of turbulence intensity which is more closely related to the physics of the problem is the mean turbulent kinetic energy per unit mass ($\overline{TKE}$), given in Table 3.4. Table 4.3 shows a comparison of $\overline{TKE}$ for the three cases. Interestingly, $\overline{TKE}$ in the Bermuda case is nearly equivalent to that in the South Carolina incident. The ratio of the vertical component of turbulent kinetic energy ($\overline{TKE}_{w_z}$) to the total ($\overline{TKE}$) is also shown in Table 4.3. The greater importance of the contribution of vertical component in the Bermuda case is clearly seen.

Table 4.3 - Turbulent Kinetic Energy ($\overline{TKE}$).

CASE	HANNIBAL	BERMUDA	SOUTH CAROLINA
$\overline{TKE}$ (m^2/s^2)	51	60	61
($\overline{TKE}_{w_z}/\overline{TKE}$)	0.30	0.48	0.24

The difference between the $\overline{TKE}$ characteristics of the Bermuda case and the other cases emphasizes the variation of the character of TNTT depending on the location of flight relative to the thunderstorm top, tropopause and the wind direction. Data listed in Table 4.1 and Table 4.4 illustrate these differences.

Table 4.4 - Mesoscale conditions.

CASE	HANNIBAL	BERMUDA	SOUTH CAROLINA
Squall Line Orientation	SSW-NNE	-	SSW-NNE
Height of Thunderstorm Tops Above Flight Level (m)	100-400	1500	900
Distance of Turbulence From Thunderstorms (km)	24-50	0	7-24
Wedge Angle (°)	6-7	-	11-12
Richardson Number	0.4	?	0.4-0.7

The aircraft in the Hannibal and South Carolina cases were clearly in the lee of the prominent thunderstorms. A viable explanation of the turbulence is that the aircraft in those two cases intersected thunderstorm wakes composed of either lee waves or horizontal eddies, both of which may enhance vertical shears, thus producing smaller scale KHI and related turbulence. Low Richardson numbers (also shown in Table 4.4) support the maintenance of turbulent wakes, although those calculated Ri values should be interpreted with caution since it was not possible to differentiate between vertical and horizontal gradients in regions of large and sudden altitude changes. In any case, overturning was evidently occurring in both instances.

In the Hannibal and the South Carolina cases, the turbulence appeared to be confined within an apparent wedge angle which was smaller for the case with the strongest winds (Hannibal), in agreement with wake theory (Gjevik and

Marthensen, 1978) suggesting that if the wakes were indeed "lee waves" as suggested by Keller et al (1983), they were most likely three-dimensional waves rather than two-dimensional waves as suggested by that study.

Although the lack of ATC radar fixes and weather radar data in the Bermuda case did not allow a direct determination of the location of the aircraft track relative to any thunderstorms, several pieces of information give strong evidence that the aircraft flew through the upper part of a thunderstorm: (i) the height of the cloud top above flight level (about 1500 m), (ii) the correlation between warm temperatures and strong upward vertical velocity in the main turbulent region, and (iii) the pilot's comments that the aircraft "seemed to pass through the top of a cumulus cloud" where the turbulence occurred. Initially, the latter comments were not given much weight because thunderstorm activity was not reported as in the other cases and available large-scale analyses did not appear to support thunderstorm activity. Additional evidence of convective turbulence in the Bermuda case, are (iv) the absence of strong winds aloft and (v) the large ratio of the vertical component of $\overline{TKE}$ to the horizontal component (versus the other cases).

Chapter 5

SUMMARY, CONCLUSIONS, AND RECOMMENDATIONS

A better understanding of turbulence near thunderstorm tops (TNTT) is needed by pilots and forecasters to ensure passenger, crew, and aircraft safety during flights in those areas. The present study has attempted to update that understanding via a comprehensive literature review of theoretical, observational, numerical, and laboratory studies related to TNTT. Furthermore, three case studies were carried out to investigate the feasibility of using DFDR data from commercial aircraft as a quantitative source of more and better information about TNTT.

The literature review revealed that thunderstorms commonly act as obstacles to the environmental flow, especially when they penetrate regions of strong winds, usually near the tropopause. A variety of mesoscale circulations may be produced under the latter conditions. The characteristics of those circulations depend on the direction and strength of the environmental winds, stability, shear, and thunderstorm growth and topography. The circulations include two- and three-dimensional "lee waves" and rotors caused when the flow of stable air is displaced vertically by a thunderstorm, and horizontal eddies due to flow around the thunderstorm. While very large amplitude lee waves and overturning in rotors are possible sources of turbulence

for aircraft, lee waves and horizontal eddies also may enhance vertical shears leading to the production of secondary instabilities, i.e., unstable K-H waves.

The case study analyses combined DFDR data with available meteorological information to isolate two cases (Hannibal and South Carolina) of turbulence in the wakes of thunderstorms that were growing into strong winds at and above flight level. The Bermuda case contrasted clearly with the other two. Although gravity wave activity outside the thunderstorm probably accounted for some light and moderate turbulence, the severe turbulence was most likely due to flight through an active thunderstorm updraft. It should also be noted that in all three cases, flight procedures contradicted common practices of safe flight near or downwind of thunderstorm tops.

The DFDR data in the three cases were very useful in discriminating between turbulence most likely associated with mesoscale waves and turbulence associated with convection. Unquestionably, the DFDR data add a new dimension to the investigation of turbulence (not only TNTT) encounters by commercial aircraft. The objective DFDR turbulence measurements, especially when combined with conventional surface, upper air, radar, and satellite data, offer a unique opportunity for more complete and revealing analyses.

Recommendations for further study include:

(1) The current, rather small DFDR data case archive should be enhanced with data from turbulent, non-injury incidents. These data could be made available in a cooperative effort between research laboratories and commercial airlines.

(2) The study of the cases investigated here should be expanded to include time series and energy budget analyses using DFDR data. It is clear from the current study that more information may be found when the DFDR records are analyzed in more detail than by simple inspection. For example, spectrum analysis could be used to determine the significant scales of the wake circulations. Also, an energy budget analysis (even if not complete) would quantitatively illuminate physical processes responsible for the production and redistribution of turbulence in thunderstorm wakes. Furthermore, the larger scale significance of such interactions between thunderstorms and their environments could be studied.

(3) Flight procedures in the vicinity of thunderstorms, including ATC vectoring of aircraft, should be examined. In all three cases studied here the on-board radar failed to indicate the presence of dangerous convective activity. In addition, in one case (South Carolina), the aircraft was vectored into the turbulent thunderstorm region by ATC.

REFERENCES

Alaka, M. A., Ed., 1960: The airflow over mountains, WMO TN No. 34, Geneva, 115 pp.

Atkinson, B. W., 1981: Mesoscale Atmospheric Circulations. Academic Press, 495 pp.

Atlas, D., J. I. Metcalf, J. H. Richter, and E. E. Gossard, 1970: The birth of "CAT" and microscale turbulence. J. Atmos. Sci., 27, 903-913.

Bach, R. E., Jr. and E. K. Parks, 1987: Angle-of-attack estimation for analysis of wind shear encounters. J. Aircraft, 24, 789-792.

_____ and _____, 1985: Applications of state estimation in aircraft flight-data analysis. J. Aircraft, 22, 547-554.

_____ and _____, 1986: Personal communication.

Bailey, M., 1970: Mountain lee-wave incidents in Scotland. Meteor. Mag., 99, 110-118.

Balachandran, N. K., 1980: Gravity waves from thunderstorms. Mon. Wea. Rev., 108, 804-816.

Bekofske, K. and V. C. Liu, 1972: Internal gravity wave -- atmospheric wind interaction: a cause of clear air turbulence. Science, 178, 1089-1092.

Beran, D. W., W. H. Hooke, and S. F. Clifford, 1973: Acoustic echo-sounding techniques and their application to gravity-wave, turbulence, and stability studies. Bound.-Layer Meteor., 4, 133-153.

Bosart, L. F. and J. P. Cussen, Jr., 1973: Gravity wave phenomena accompanying east coast cyclogenesis. Mon. Wea. Rev., 101, 446-454.

Bradbury, T. A. M., 1973: Glider flight in the lower stratosphere above cumulonimbus clouds. Meteor. Mag., 102, 110-120.

Brandes, E. A., R. P. Davies-Jones, and B. C. Johnson, 1986: Vorticity distribution effects on supercell thunderstorms. Preprints, Joint Sessions, 23rd Conference on Radar Meteorology and Conference on Cloud Physics, Snowmass, CO, Amer. Meteor. Soc., J69-J72.

Brewster, K. A. and D. S. Zrnic, 1986: Kinetic energy evolution in a developing severe thunderstorm. Preprints, Joint Sessions, 23rd Conference on Radar Meteorology and Conference on Cloud Physics, Snowmass, CO, Amer. Meteor. Soc., J38-J41.

Brighton, P. W. M., 1978: Strongly stratified flow past three-dimensional obstacles. Quart. J. Roy. Meteor. Soc., **104**, 289-307.

Browning, K. A., 1971: Structure of the atmosphere in the vicinity of large-amplitude Kelvin-Helmholtz billows. Quart. J. Roy. Meteor. Soc., **97**, 283-299.

_____, G. W. Bryant, J. R. Starr, and D. N. Axford, 1973: Air motion within Kelvin-Helmholtz billows determined from simultaneous Doppler radar and aircraft measurements. Quart. J. Roy. Meteor. Soc., **99**, 608-618.

_____, and F. H. Ludlam, 1962: Airflow in convective storms. Quart. J. Roy. Meteor. Soc., **88**, 117-135.

_____ and C. D. Watkins, 1970a: Observations of clear air turbulence by high power radar. Nature, **227**, 260-263.

_____ and _____, 1970b: Structure of the atmosphere in the vicinity of large-amplitude Kelvin-Helmholtz billows. Preprints, 14th Radar Meteorology Conference, Tucson, AZ, Amer. Meteor. Soc., 95-100.

_____, _____, J. R. Starr, and A. McPherson, 1970: Simultaneous measurements of clear air turbulence at the tropopause by high-power radar and instrumented aircraft. Nature, **228**, 1065-1067.

Brunk, I. W., 1949: The pressure pulsations of April 11, 1944. J. Meteor., **6**, 181-187.

Burnham, J., 1970: Atmospheric gusts -- a review of the results of some recent research at the Royal Aircraft Establishment. Mon. Wea. Rev., **98**, 723-734.

Burns, A., 1972: On the nature of large clear air gusts near storm tops, R. Aircr. Establ. TR 72036, 37 pp.

_____ and T. W. Harrold, 1966: An atmospheric disturbance encountered by a Canberra aircraft over storms at Oklahoma on 27th May, 1965, R. Aircr. Establ. TR 66241, 20 pp.

Byers, H. R. and R. R. Braham, 1949: The Thunderstorm. Government Printing Office, 287 pp.

Camp, D. W. and W. Frost, 1987: Atmospheric turbulence relative to aviation, missile, and space programs. NASA CP-2468, 258 pp.

Chandler, C. L., 1987: Turbulence forecasting. From NASA CP-2468, D. W. Camp and W. Frost, Eds., 137-154.

Chopra, K. P. and L. F. Hubert, 1965: Mesoscale eddies in wake of islands. J. Atmos. Sci., 22, 652-657.

Clark, T. L. and W. R. Peltier, 1977: On the evolution and stability of finite amplitude mountain waves. J. Atmos. Sci., 34, 1715-1730.

Collis, R. T. H., F. G. Fernald, and J. E. Adler, 1968: Lidar observations of Sierra-wave conditions. J. Appl. Meteor., 7, 227-233.

Cornford, S. G., 1973: Flight in turbulence, AGARD CP No. 140, 14 pp.

Corby, G. A., 1957: A preliminary study of atmospheric waves using radiosonde data. Quart. J. Roy. Meteor. Soc., 83, 49-60.

Cunning, J. B., Jr., 1974: The analysis of surface pressure perturbations within the mesoscale range. J. Appl. Meteor., 13, 325-330.

Curry, M. J. and R. C. Murty, 1974: Thunderstorm-generated gravity waves. J. Atmos. Sci., 31, 1402-1408.

Davies, K. and J. E. Jones, 1971: Ionospheric disturbances in the F2 region associated with severe thunderstorms. J. Atmos. Sci., 28, 254-262.

Delay, R. D. and J. A. Dutton, 1971: An analysis of conditions associated with an occurrence of stratospheric CAT. J. Atmos. Sci., 28, 1272-1279.

Daley, V., 1981: Turbulence encounter statement. Obtained from NTSB, 1 pp.

Dell, G. I., 1983: Incident report. Obtained from NTSB, 3 pp.

Detwiler, A. and A. J. Heymsfield, 1987: Air motion characteristics in an anvil of a severe thunderstorm during CCOPE. J. Atmos. Sci., 44, 1899-1911.

Durran, D. R., 1986: Mountain Waves. Mesoscale Meteorology and Forecasting, Amer. Meteor. Soc., Boston, 472-492.

Dutton, J. A., 1969: An energy budget for a layer of stratospheric CAT. Radio Sci., 4, 1137-1142.

_____, 1971: Clear-air turbulence, aviation, and atmospheric science. Rev. Geophys. Space Phys., 9, 613-657.

Endlich, R. M., 1964: The mesoscale structure of some regions of clear-air turbulence. J. Appl. Meteor., 3, 261-276.

Erickson, C. O. and L. F. Whitney, Jr., 1973: Picture of the month -- Gravity waves following severe thunderstorms. Mon. Wea. Rev., 101, 708-711.

FAA, 1975: Aviation Weather for Pilots and Flight Operations Personnel, Department of Trans., 114-115.

_____, 1977: Aviation Weather Services, Department of Trans., 112-113.

Fankhauser, J. C., 1971: Thunderstorm-environment interactions determined from aircraft and radar observations. Mon. Wea. Rev., 99, 171-192.

Foldvik, A., 1962: Two-dimensional mountain waves -- a method for the rapid computation of lee wavelengths and vertical velocities. Quart. J. Roy. Meteor. Soc., 88, 271-285.

Fox, R. J., 1983: Severe Turbulence Encounter Flt 965/24. Incident Report, obtained from NTSB, 4 pp.

Fraser, A. B., 1968: The white box: the mean mechanics of the cumulus cycle. Quart. J. Roy. Meteor. Soc., 94, 71-87.

Frerichs, R. D., 1983: Severe turbulence. Incident report, obtained from NTSB, 3 pp.

Fujita, T. T., 1978: Manual of downburst identification for project NIMROD. SMRP 156, University of Chicago, 104 pp.

_____ and H. Grandoso, 1968: Split of a thunderstorm into anticyclonic and cyclonic storms and their motion as determined from numerical model experiments. J. Atmos. Sci., 25, 416-439.

Gjevik, B. and T. Marthinsen, 1978: Three-dimensional lee-wave pattern. Quart. J. Roy. Meteor. Soc., 104, 947-957.

Gossard, E. E. and W. H. Hooke, 1975: Waves in the Atmosphere, Elsevier Scientific, 456 pp.

_____, J. H. Richter, and D. Atlas, 1970: Internal waves in the atmosphere from high-resolution radar measurements. J. Geophys. Res., 75, 3523-3536.

Hardy, K. R. and R. J. Reed, 1972: Wave patterns and clear air turbulence. Preprints, 15th Radar Meteorology Conference, Champaign-Urbana, IL, Amer. Meteor. Soc., 262-267.

_____, _____, and G. K. Mather, 1973: Observation of Kelvin-Helmholtz billows and their mesoscale environment by radar, instrumented aircraft, and a dense radiosonde network. Quart. J. Roy. Meteor. Soc., 99, 279-293.

Heymsfield, G. M., R. H. Blackmer, Jr., and S. Schotz, 1983a: Upper-level structure of Oklahoma tornadic storms on 2 May 1979: Part I. J. Atmos. Sci., 40, 1740-1755.

_____, R. Fulton, G. Szejwach, and J. D. Spinhirne, 1986: Structure of an Oklahoma storm top from high-altitude remote measurements. Preprints, Joint Sessions, 23rd Conference on Radar Meteorology and Conference on Cloud Physics, Snowmass, CO, Amer. Meteor. Soc., J57-J60.

_____ and S. Schotz, 1986: Thunderstorm anvil dynamics for the 1 August 1981 case. Preprints, Joint Sessions, 23rd Conference on Radar Meteorology and Conference on Cloud Physics, Snowmass, CO, Amer. Meteor. Soc., J53-J56.

_____, G. Szejwach, and R. H. Blackmer, Jr., 1983b: Upper-level structure of Oklahoma tornadic storms on 2 May 1979: Part II. J. Atmos. Sci., 40, 1756-1767.

Hicks, J. J., 1968: Radar observations of gravitational waves in a clear atmosphere. 13th Radar Meteorology Conference, Proceedings, Montreal, Amer. Meteor. Soc., 258-261.

_____ and J. K. Angell, 1968: Radar observations of breaking gravitational waves in the visually clear atmosphere. J. Appl. Meteor., 7, 114-121.

Holcomb, M. C., 1976: Jet stream analysis and turbulence forecasting. AFGWC TM 76-1, ADA062344, 101 pp.

Hooke, W. H. and K. R. Hardy, 1975: Further study of the atmospheric gravity waves over the eastern seaboard on 18 March 1969. J. Appl. Meteor., 14, 31-38.

Hubert, L. F. and A. F. Krueger, 1962: Satellite pictures of mesoscale eddies. Mon. Wea. Rev., 90, 457-463.

Jaeckisch, H., 1970: Waveflow above convective streets. Aero-Revue, 45, 150-152.

James, P. K. and K. A. Browning, 1981: An observational study of primary and secondary billows in the free atmosphere. Quart. J. Roy. Meteor. Soc., 107, 351-365.

Jessup, E. A., 1972: Interpretations of chaff trajectories near a severe thunderstorm. Mon. Wea. Rev., 100, 653-661.

Johnson, B. C. and E. A. Brandes, 1986: A study of barrier effects and shed eddy phenomena associated with supercells. Preprints, Joint Sessions, 23rd Conference on Radar Meteorology and Conference on Cloud Physics, Snowmass, CO, Amer. Meteor. Soc., J65-J68.

Keller, T. L., 1975: Prediction and monitoring of clear-air turbulence: An evaluation of the applicability of the rawinsonde system. J. Appl. Meteor., 20, 686-692.

_____, 1985: Clear turbulence forecasting: towards a union of art and science. Paper AIAA-85-0014, AIAA 23rd Aerospace Sciences Meeting, Reno, Amer. Inst. Aeronautics and Astronautics, 8 pp.

_____, L. Ehernberger, and M. Wurtele, 1983: Numerical simulation of the atmosphere during a CAT encounter, Proceedings, 9th Conference on Aerospace and Aeronautical Meteorology, Kansas City, MO, Amer. Meteor. Soc., 316-319.

Kessler, E., ed., 1981: Thunderstorms: A Social, Scientific, and Technological Documentary. Volume 1 -- The Thunderstorm in Human Affairs. U.S. Dept. of Comm., 206 pp.

_____, 1982: Thunderstorms: A Social, Scientific, and Technological Documentary. Volume 2 -- Thunderstorm Morphology and Dynamics. U.S. Dept. of Comm., 603 pp.

Klaassen, G. P. and W. R. Peltier, 1985: The onset of turbulence in finite-amplitude Kelvin-Helmholtz billows. J. Fluid Mech., 155, 1-35.

Klemp, J. B. and D. K. Lilly, 1975: The dynamics of wave-induced downslope winds. J. Atmos. Sci., 32, 320-329.

Kuettner, J. P., 1958: The rotor flow in the lee of mountains. Aero-Revue, 33, 208-215.

_____, 1972: Thermal wave soaring. Aero-Revue, 47, 394-396.

_____, P. A. Hildebrand, and T. L. Clark, 1987: Convection waves: observations of gravity wave systems over convectively active boundary layers. Quart. J. Roy. Meteor. Soc., 113, 445-467.

_____ and D. K. Lilly, 1968: Lee waves in the Colorado Rockies. Weatherwise, 21, 180-185.

Lemon, L. R., 1976: Wake vortex structure and aerodynamic origin in severe thunderstorms. J. Atmos. Sci., 33, 678-685.

Lester, P. F., 1972: Some physical and statistical aspects of clear air turbulence. Dept. of Atmos. Sci. Paper No. 165, Colorado State University, 154 pp.

_____, 1988: Personal communication.

_____ and R. E. Bach, Jr., 1986: An extreme clear air turbulence incident associated with a strong downslope windstorm. Paper AIAA-86-0329, AIAA 24th Aerospace Sciences Meeting, Reno, Amer. Inst. Aeronautics and Astronautics, 7 pp.

_____ and M. Burton, 1988: Development of low level turbulence (LLT) forecasting methodologies. Report, prepared under contract DAAL 3-86-001, US Army Atmos. Sci. Lab., White Sands Missile Range, NM, 81 pp.

_____ and W. A. Fingerhut, 1974: Lower turbulent zones associated with mountain lee waves. J. Appl. Meteor., 13, 54-61.

_____, O. Sen, and R. E. Bach, Jr., 1988: The use of DFDR information in the analysis of a turbulence incident over Greenland. Mon. Wea. Rev., to b published.

Ley, B. E. and W. R. Peltier, 1981: Propagating mesoscale cloud bands. J. Atmos. Sci., 38, 1206-1219.

Lilly, D. K., 1978: A severe downslope windstorm and aircraft turbulence event induced by a mountain wave. J. Atmos. Sci., 35, 59-77.

_____, 1983: Stratified turbulence and the mesoscale variability of the atmosphere. J. Atmos. Sci., 40, 749-761.

_____, 1986: Turbulent transfer in thunderstorm outflows and thick cirrus sheets. Seminar given at MIT.

_____ and E. L. Petersen, 1983: Aircraft measurements of atmospheric kinetic energy spectra. Tellus, 35A, 379-382.

Lin, Y.-L., 1986: Calculation of airflow over an elevated heat source with application to the dynamics of V-shaped clouds. Preprints, Joint Sessions, 23rd Conference on Radar Meteorology and Conference on Cloud Physics, Snowmass, CO, Amer. Meteor. Soc., JP138-JP141.

Lindzen, R. S., 1974: Wave-CISK in the tropics. J. Atmos. Sci., 31, 156-179.

_____ and K. K. Tung, 1976: Banded convective activity and ducted gravity waves. Mon. Wea. Rev., 104, 1602-1617.

Lu, D., T. E. Van Zandt, and W. L. Clark, 1984: VHF Doppler radar observations of buoyancy waves associated with thunderstorms. J. Atmos. Sci., 41, 272-282.

Ludlam, F. H., 1967: Characteristics of billow clouds and their relation to clear-air turbulence. Quart. J. Roy. Meteor. Soc., 93, 419-435.

Lyons, W. A. and T. Fujita, 1968: Mesoscale motions in oceanic stratus as revealed by satellite data. Mon. Wea. Rev., 96, 304-314.

McCann, D. W., 1981: The enhanced-v, a satellite observable severe storm signature. NOAA Tech. Memo, NWS NSSFC-4, 31 pp.

Mason, P. J. and R. I. Sykes, 1979a: Separation effects in Ekman layer flow over ridges. Quart. J. Roy. Meteor. Soc., 105, 129-146.

_____ and _____, 1979b: Flow over an isolated hill of moderate slope. Quart. J. Roy. Meteor. Soc., 105, 383-395.

Mather, G. K. and K. R. Hardy, 1970: Instrumented aircraft measurements in the vicinity of clear air radar structures. Preprints, 14th Radar Meteorology Conference, Tucson, AZ, Amer. Meteor. Soc., 49-52.

Mehta, R. S., 1984: Modeling clear-air turbulence with vortices parameter-identification techniques. AIAA Paper 84-2083-CP, AIAA 11th Atmospheric Flight Mechanics Conference, Seattle, Amer. Inst. Aeronautics and Astronautics, 8 pp.

Miller, A., J. C. Thompson, R. E. Peterson, and D. R. Haragan, 1983: Elements of Meteorology. Charles E. Merrill, 417 pp.

Miller, L. J. and J. C. Fankhauser, 1983: Radar echo structure, air motion, and hail formation in a large stationary multicellular thunderstorm. J. Atmos. Sci., **40**, 2399-2418.

Mills, P. B. and E. G. Astling, 1977: Detection of tropopause penetrations by intense convection with GOES enhanced infrared imagery. Preprints, 10th Conference on Severe Local Storms, Omaha, NE, Amer. Meteor. Soc., 61-64.

Mumford, J. C., 1982: The structure of the large eddies in fully developed turbulent shear flows. Part 1. The plane jet. J. Fluid Mech., **118**, 241-268.

_____, 1983: The structure of the large eddies in fully developed turbulent shear flows. Part 2. The plane wake. J. Fluid Mech., **137**, 447-456.

Nastrom, G. D. and K. S. Gage, 1983: A first look at wave number spectra from GASP data. Tellus, **35A**, 383-388.

Newton, C. W. and H. R. Newton, 1959: Dynamical interactions between large convective clouds and environment with vertical shear. J. Meteor., **16**, 483-496.

Nicholls, J. M., 1973: The airflow over mountains: research 1958-1972. WMO TN No. 127, 73 pp.

NOAA, 1979: Introduction to Weather Radar. U.S. Dept. of Comm., 70 pp.

NTSB, 1981: Meteorological Summary. CHI 81 DA 042, Hannibal, Missouri, April 3, 1981, DC 10-10, N1809U, United Airlines Inc. Flight 12, 7 pp.

_____, 1984: Aircraft accident report - Air Canada, Lockheed L-1011, C-FTNJ, near Charleston, South Carolina, November 24, 1983. NTSB/AAR-84/13, 35 pp.

NWA, 1986: Technical attachment 77-G4, displacement error of satellite cloud tops. Satellite Imagery Interpretation for Forecasters. P. S. Parke, Ed., National Weather Association, 3 pp.

NWS, 1974: Severe Weather Avoidance, Western Region Technical Attachment #74-9, 4 pp.

Palmén, E. and C. W. Newton, 1969: Atmospheric Circulation Systems. Their Structure and Physical Interpretation. Academic Press, 586 pp.

Paluch, I. R., 1979: The entrainment mechanism in Colorado cumuli. J. Atmos. Sci., 36, 2467-2478.

Panofsky, H. A. and J. A. Dutton, 1984: Atmospheric Turbulence Models and Methods for Engineering Applications. John Wiley & Sons, 397 pp.

Parks, E. K., R. E. Bach, Jr., and R. C. Wingrove, 1982: Analysis of the nature and cause of turbulence upset using airline flight records. Paper presented at Symposium of the Society of Flight Test Engineers, New York, 8 pp.

_____, R. C. Wingrove, R. E. Bach, Jr., and R. S. Mehta, 1984: Identification of vortex-induced clear air turbulence using airline flight records. Paper AIAA-84-0270, AIAA 22th Aerospace Sciences Meeting, Reno, NV, 8 pp.

Pierce, A. D. and S. C. Coroniti, 1966: A mechanism for the generation of acoustic-gravity waves during thunderstorm formation. Nature, 210, 1209-1210.

Pinus, N. Z., 1962: Atmospheric Turbulence Affecting Aircraft Flight, Foreign Tech. Div., Wright Patterson AFB, OH, 167 pp.

Poellot, M. R. and G. M. Heymsfield, 1986: Structure of an Oklahoma storm top from in-situ measurements. Preprints, Joint Sessions, 23rd Conference on Radar Meteorology and Conference on Cloud Physics, Snowmass, CO, Amer. Meteor. Soc., J61-J64.

Pratt, K. G. and W. G. Walker, 1954: A revised gust load formula and reevaluation of V-G data taken on civil transport airlines from 1933-1950. NACA Report 1206, 10 pp.

Prophet, D. T., 1970: Vertical extent of turbulence in clear air above the tops of thunderstorms. J. Appl. Meteor., **9**, 320-321.

Raymond, D. J. and M. H. Wilkening, 1982: Flow and mixing in New Mexico mountain cumuli. J. Atmos. Sci., **39**, 2211-2228.

Reed, R. J. and K. R. Hardy, 1972: A case study of persistent, intense, clear air turbulence in an upper level frontal zone. J. Appl. Meteor., **11**, 541-549.

Reiss, N. M. and T. J. Corona, 1977: An investigation of a Kelvin-Helmholtz billow cloud. Bull. Amer. Meteor. Soc., **58**, 159-162.

Reiter, E. R., 1963: Jet Stream Meteorology. Univ. of Chicago Press, 431 pp.

_____ and P. F. Lester, 1968: Richardson's number in the free atmosphere. Archiv. Meteor. Geophys. Bioklim. Sec. A., **17**, 1-7.

Reynolds, R. D., R. L. Lambert, and M. G. Wurtele, 1968: Investigation of a complex mountain wave situation. J. Appl. Meteor., **7**, 353-358.

Roach, W. T., 1967: On the nature of the summit areas of severe storms in Oklahoma. Quart. J. Roy. Meteor. Soc., **93**, 318-336.

_____, 1969: Some aircraft reports of high-level turbulence. Meteor. Mag., **98**, 65-78.

Rossiter, W. W., 1981: Turbulence encounter statement, obtained from NTSB, 1 pp.

Rotunno, R. and J. B. Klemp, 1982: The influence of shear-induced pressure gradient on thunderstorm motion. Mon. Wea. Rev., **110**, 136-151.

Schweitzer, D. T., 1983: Turbulence encounter statement, obtained from NTSB, 1 pp.

Scorer, R. S., 1971: The origins and forms of dynamic instability in clear air at high altitude. AGARD CP No. 48, Paper No. 2, 12 pp.

_____, 1978: Environmental Aerodynamics. Wiley, 488 pp.

Seitter, K. L. and H.-L. Kuo, 1983: The dynamical structure of squall-line type thunderstorms. J. Atmos. Sci., 40, 2831-2854.

Sharman, R. D. and M. G. Wurtele, 1983: Ship wakes and lee waves. J. Atmos. Sci., 40, 396-427.

Starr, J. R. and K. A. Browning, 1972a: Observations of lee waves by high-power radar. Quart. J. Roy. Meteor. Soc., 98, 73-85.

_____ and _____, 1972b: Doppler radar measurements of clear air turbulence. Preprints, 15th Radar Meteorology Conference, Champaign-Urbana, IL, Amer. Meteor. Soc., 248-251.

Stobie, J. G., F. Einaudi, and L. W. Uccellini, 1983: A case study of gravity waves-convective storms interaction: 9 May 1979. J. Atmos. Sci., 40, 2804-2830.

Stull, R. B., 1976: Internal gravity waves generated by penetrative convection. J. Atmos. Sci., 33, 1279-1286.

Taylor, P. A., 1983: On wakes and the net forces produced by surface-mounted obstacles in neutrally stratified atmospheric boundary layers. Bound.-Layer Meteor., 27, 393-412.

Taylor, R. C., 1981: Turbulence encounter statement, obtained from NTSB, 1 pp.

Telford, J. W. and P. B. Wagner, 1974: The measurement of horizontal air motion near clouds from aircraft. J. Atmos. Sci., 31, 2066-2080.

_____ and _____, 1980: The dynamical and liquid water structure of the small cumulus as determined from its environment. Pure Appl. Geophys., 118, 935-952.

Thorpe, S. A., 1973: Turbulence in stably stratified fluids: A review of laboratory experiments. Bound.-Layer Meteor., 5, 95-119.

_____, 1983: Experiments on instability and turbulence in a stratified shear flow. J. Fluid Mech., 61, 731-751.

Townsend, A. A., 1966: Internal waves produced by a convective layer. J. Fluid Mech., 24, part 2, 307-319.

Tsuchiya, K., 1969: The clouds with the shape of Karman vortex street in the wake of Cheju Island, Korea. J. Meteor. Soc. Japan, **47**, 457-465.

Uccellini, L. W., 1975: A case study of apparent gravity wave initiation of severe convective storms. Mon. Wea. Rev., **103**, 497-513.

USA, 1982: Meteorology for Army Aviators. FM 1-230, 12-17--12-20.

USAF, 1981: Weather for Aircrews. Vol 2. AFM51-12V2, 5-1--5-14.

_____, 1982: Weather for Aircrews. Vol 1. AFM51-12V1, 13-7--13-13.

Vergeiner, I. and D. K. Lilly, 1970: The dynamic structure of lee wave flow as obtained from balloon and airplane observations. Mon. Wea. Rev., **98**, 220-232.

Vinnichenko, N. K., N. Z. Pinus, S. M. Shmeter, and G. N. Shur, 1980: Turbulence in the Free Atmosphere, Second Edition. Consultants Bureau, 310 pp.

Wallace, J. M. and P. V. Hobbs, 1977: Atmospheric Science, An Introductory Survey. Academic Press, 467 pp.

Wingrove, R. C. and R. E. Bach, Jr., 1986: Analysis of atmospheric waves and severe turbulence from wide-body airline flight data. Paper AIAA-86-0257, AIAA 24th Aerospace Sciences Meeting, Reno, Amer. Inst. Aeronautics and Astronautics, 9 pp.

Zimmerman, L. I., 1969: Atmospheric wake phenomena near the Canary Islands. J. Appl. Meteor., **8**, 896-907.

APPENDIX A.1

Typical scales of motion observed in the atmosphere associated with gravity waves (including mountain lee waves).

REFERENCE	λ(km)	AMPLITUDE (m)	LIFETIME (min)	PHASE SPEED (ms^{-1})	WIND SHEAR ($ms^{-1}(200m)^{-1}$)	VERTICAL VELOCITY (ms^{-1})	Ri	TURBC REPORTED
Bailey, 1970	24				0.6-1.0	1.5-2.0		
	17				0	2.0		
Beran et al, 1973	5-10		360	10				
	4.3		180	7				
	14		60	12				
	0.9		60	2				
Bosart & Cussen, 1973	55-60		900	10-13				
Browning, 1971	15-30	100-300			0.2			
Collis et al, 1968	6	300			0.2			
	17.5	500			0.2			
	21	500						
Corby, 1957	10.8*					5.1(max)		
Cunning, 1974	160			30				
	116			31				
	52			27				
Foldvik, 1962	28					7		
	31					2		
	20					3.5		
	15					2-3		
Gossard et al, 1970	5.5	120	30	14				
	2.5	100	30	8				
	7.1	60	40	13				
	3.4	200	30	7				
Hooke & Hardy, 1975	12-14	680		40-50	2.8	2		
Kuettner & Lilly, 1968	15	400						LGT
	16	2000						MDT-SVR
	15	600						MDT
	45	1000						LGT**
Reed & Hardy, 1972	17	600		67	2.4		1.0	LGT-MDT
	30	1500-1800		44	4-6		0.25	MDT-SVR
Reynolds et al, 1968	11.3	300			0.4	1.0		
	9.8	580			0.4	2.9		
	9.4	580			0.4	2.9		
	11.3	1165			0.4	5.0		
Starr & Browning, 1972a	20-25	300-400		18-20	0.5			
	16	700	120		0.7			
	8-10	200						
	20	800-1000			1.4			
Vergeiner & Lilly, 1970	6.8				1	1		
	8.5	200			1	0.6		
	10	400				1		
	20	800			3.6	3		
	20	1100			1.2	3.5		
	20	1200			2.4	4		
	10.4	800			1.8	5		
	10.4	1100			1.8	7		
	11	600			0.6	3		
	12	1200			1	5.5		
	12	1000			2.4	4		
	11.5	600			1	3.5		
	14	700			2.6	3		
	13.5	600			2.4	3		
	17	500			3	2		

* 26 Case average

** MDT in rotors

APPENDIX A.2

Typical scales of motion observed in the atmosphere associated with Kelvin-Helmholtz waves.

REFERENCE	λ(km)	AMP(m)	LIFETIME (min)	$\Delta\theta/\Delta z$ $(K(200m)^{-1})$	WIND SHEAR $(ms^{-1}(200m)^{-1})$	VERTICAL VELOCITY (ms^{-1})	Ri	TURBC REPORTED
Atlas et al, 1970	0.23	200		10	1.4			
Browning, 1971[1]	1.5	400-500	>240[2]	2.7	9-10		0.1-0.3	MDT[3]
	4	400	10-15	4	10		<0.3	
	2	240	9	1.3	5		0.25-0.5	
	0.8	300	<2	3.5	5		0.7	
	2	220	13	1	7		0.1-0.2	
	1.5	400	16	0.8	5		0.1-0.3	
	1	380	11	1.2	4.5		0.25	
	1.5	400	12	0.7	4		0.2	
	2.5	430	<2	2-4	9		0.25-0.3	
	0.8	300	8	3.5-5	6		0.6	
	2	300	4	4-6	9		0.2-0.3	
	1	220	<2	1-1.5	3-4		0.5	
	1.5	400	<2	2	4-6		0.28-1.0	
	3.5	340	5	1.5	5.5		0.25	
	2	430	18	1	6		0.2-0.3	
	0.8	400	3	1	4.5		0.3	
Browning et al, 1973	1.3-2.4	230-450			7.5[4]		≤0.3	
Hardy et al, 1973[5]	2.7-3.0	500	21	2	5-9	0.5-1	0.2	MDT
Hicks & Angell, 1968[6]	1.4	300		0.6	1.1			
	1.9	500		1.6	0.5			
	1.8	300		0.7	1.6			
	1.5	500		0.8	0.8			
	0.9	300		0.9	2.4			
	1.4	300		1.7	1.4			
	2.2	300		0.6	1			
	1.5	400		1.6	1.6			
	1.4	300		1.2	1.4			
James & Browning, 1981	4.2	340	15	1.5	5	0.5	0.25	
	0.35[7]		15	1.5	5	1-2[8]	0.25	
Ludlam, 1967	1.3		30	2	1		<1	
	3			1.6	3.5		0.35	
	6.2	800-1000	30	1.6	2-4		0.25	
	1.5-2			1.5	3-4		0.25-0.3	
	1.1-3.5			1.3	3		0.65	
Reed & Hardy, 1972	1.6	200			2.4		0.25	MDT-SVR
Starr & Browning, 1972b	1.5	500	8		2-7		≤0.25	
Thorpe, 1973[9]	1.5	400	20				0.15	

[1] Supplemented by Browning et al, 1970; Browning and Watkins, 1970a,b; Starr and Browning, 1972b
[2] Series of waves in same location
[3] ≤0.65g
[4] >12 in "roll up" portion
[5] Supplemented by Hardy and Reed, 1972; Mather and Hardy, 1970
[6] Supplemented by Hicks, 1968
[7] Secondary billow which developed within upslope portion of primary billow when latter attained largest observed amplitude
[8] Resulting effect of secondary billow: $\pm 1.5ms^{-1}$ and embedded in primary billow, therefore, up portion $>2ms^{-1}$, down portion $>1ms^{-1}$
[9] Average values for atmosphere